

IN VIVO EFFECTS OF FTORAFUR AND FLUOROURACIL ON
MAMMARY TUMORS AND SMALL INTESTINE IN MICE

by

Maria Georgina Pallavicini

A dissertation submitted to the faculty of the
University of Utah in partial fulfillment of the requirements
for the degree of

Doctor of Philosophy

Department of Pharmacology

University of Utah

August 1977

THE UNIVERSITY OF UTAH GRADUATE SCHOOL

SUPERVISORY COMMITTEE APPROVAL


of a dissertation submitted by

Maria Georgina Pallavici

I have read this dissertation and have found it to be of satisfactory quality for a doctoral degree.

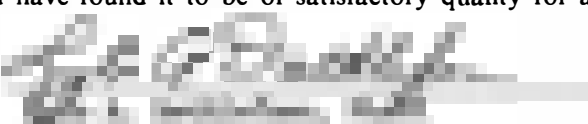
August 12, 1977

Date


Arthur M. Cohen, Ph.D.
Chairman, Supervisory Committee

I have read this dissertation and have found it to be of satisfactory quality for a doctoral degree.

August 12, 1977


Member, Supervisory Committee

I have read this dissertation and have found it to be of satisfactory quality for a doctoral degree.

August 12, 1977

Date


Louis S. Goodman, M.D., Ph.D.
Member, Supervisory Committee

I have read this dissertation and have found it to be of satisfactory quality for a doctoral degree.

August 12, 1977

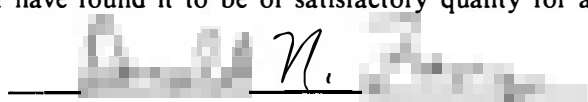
Date


Arthur D. Broom, Ph.D.
Member, Supervisory Committee

I have read this dissertation and have found it to be of satisfactory quality for a doctoral degree.

August 12, 1977

Date


Donald N. Franz, Ph.D.
Member, Supervisory Committee

UNIVERSITY OF UTAH GRADUATE SCHOOL

FINAL READING APPROVAL

To the Graduate Council of the University of Utah:

I have read the thesis of Maria Georgina Pallavicini in its final form and have found that (1) its format, citations, and bibliographic style are consistent and acceptable; (2) its illustrative materials including figures, tables, and charts are in place; and (3) the final manuscript is satisfactory to the Supervisory Committee and is ready for submission to the Graduate School.

August 12, 1977

Date



Robert M. Cohen, Ph.D.

Member, Supervisory Committee


Approved for the Major Department


Chairman/Dean

Approved for the Graduate Council


McMurrin, Ph.D.

ABSTRACT

The in vivo effects of Ftorafur (FT) and 5-fluorouracil (FU) were evaluated at several different organizational levels within the same animal model. On a molar basis, FU was found to be two to three times more potent than FT with respect to growth inhibition of murine mammary adenocarcinomas. However, administration of FT produced less host toxicity at a dose level which resulted in similar antitumor activity. Drug-induced perturbations in cell cycle phase distributions were analyzed by the flow cytometer (FCM). Although FCM analysis is limited by the lack of information on the extent of dead and dying cells, data obtained with both drugs were consistent with the possibility of S phase cytotoxicity and drug-induced G₁/S block or delay. Changes in the age distribution of perturbed tumor cells, as detected by FCM analysis, correlated with ³H-TdR autoradiography and with ³²P incorporation into DNA but not with ³H-deoxyuridine incorporation into DNA. Both drugs depressed ³H-deoxyuridine incorporation into DNA; however, incorporation in both the tumor and small intestine returned to control levels earlier with FT than

with an equimolar dose of FU. However, both drugs produced similar patterns of ^3H -deoxyuridine incorporation when FT was administered at three times the molar equivalent dose of FU. The results of these studies also suggest that deoxyuridine incorporation primarily reflects drug effects on thymidylate synthetase and not necessarily the overall rate of DNA synthesis.

This study also involved the development of techniques for the dispersal of solid tumors and intestinal lining epithelium into single cell suspensions for FCM analysis. Tetraphenylboron (TPB) was utilized as an aid to solid tumor dispersal. TPB-dispersed tumors yielded DNA distributions with minimal cell clumping and low levels of cellular debris. Fluorescent enzyme histochemistry with subsequent FCM analysis was utilized to separate dispersed epithelial cells of the small intestine into crypt and villus subpopulations. When fully optimized, the epithelial cell separation should offer a rapid method by which perturbations in the age distribution of crypt cells can easily be evaluated by FCM.

ACKNOWLEDGEMENTS

Many people have helped to make my graduate education both rewarding and enjoyable. I wish to thank Dr. Dixon M. Woodbury and all of the faculty in the Department of Pharmacology for making this experience possible. I am grateful to Dr. William K. Nichols, advisor of my first research rotation, who introduced me to both the problems and promises of doing scientific research.

Appreciation is expressed to the members of my supervisory committee, Drs. Arthur M. Cohen, Lyle A. Dethlefsen, Louis S. Goodman, Arthur D. Broom, and Donald N. Franz, for their constructive criticism and support. I am indebted to my Chairman, Dr. Arthur M. Cohen, for his help and guidance during the last three years. Words cannot express my gratitude to Dr. Lyle A. Dethlefsen of the Radiology Department, who introduced me to the area of cell kinetics and whose advice and encouragement were invaluable during all of my pursuits.

I also wish to thank Dr. Joe W. Gray at Lawrence Livermore Laboratory for his help and patience in developing my ideas and without whom this project would not have been possible. In addition, I wish to thank Dr. Donald C. Peters at Lawrence Livermore Laboratory for his effort and suggestions on various aspects of this project.

I am grateful for the friendship and technical assistance of Reba M. Riley, Judith Iwamoto, and Yolanda S. George.

I am particularly grateful to my very best friend, Jitendra P. Singh, whose love and encouragement has sustained me through four years of graduate school.

Finally, I would like to dedicate this thesis to my parents, whose love, support, and understanding have meant everything to me.

This work was supported by USPHS Pharmacology Training Grant GM 00153 and N.C.I. Grant CA 14165 (Dr. Lyle A. Dethlefsen).

TABLE OF CONTENTS

	Page
ABSTRACT	iv
ACKNOWLEDGEMENTS	vi
LIST OF TABLES	x
INTRODUCTION	1
MATERIALS AND METHODS	14
Mice and Tumors	14
Drugs	15
Radioisotopically-Labeled Precursor Incorporation Studies	15
Deoxyuridine incorporation Into Deoxyribose Nucleic Acid (DNA)	15
Phosphorus Incorporation Into DNA	17
Thymidine Incorporation Into DNA	18
Autoradiography	19
Tumor Cell Dispersal	20
Intestinal Epithelial Cell Isolation	21
Intestinal Cell Dispersal	22
Enzyme Histochemical Reaction	23
Cell Staining for FCM Analysis	24
Tumor Cells	24

	Page
Intestinal Epithelial Cells.	24
Flow Cytometer	26
Tumor DNA Distributions.	26
Intestinal Epithelial Cell Analysis.	27
RESULTS.	28
Comparison of Drug Effects at Whole Animal and Organ Level.	28
Comparison of Drug Effects at the Cellular Level.	33
Development of Tumor Dispersal Technique	33
FCM Analysis of Perturbed Sl02F Tumors	38
Drug Effects at the Molecular Level: Tumor and Small Intestine.	45
Intestinal Epithelial Cells: Isolation, Dispersal, and Separation.	48
DISCUSSION	57
REFERENCES	71
FIGURES.	84
VITA	140

LIST OF TABLES

	Page
1 FCM ANALYSIS OF UNPERTURBED S102F TUMORS . .	35
2 LABELING INDICES IN TUMOR SECTIONS AND SINGLE CELL SUSPENSIONS.	37
3 FCM ANALYSIS OF DNA CONTENT OF PERTURBED S102F TUMORS	39
4 FCM ANALYSIS OF DNA CONTENT OF PERTURBED S102F TUMORS	40
5 FCM ANALYSIS OF DNA CONTENT OF PERTURBED S102F TUMORS	42
6 AUTORADIOGRAPHY: S102F TISSUE SECTIONS. . .	44
7 ³² P INCORPORATION INTO DNA OF S102F TUMOR. .	49
8 INCORPORATION OF ³ H-TdR INTO DNA OF INTESTINAL EPITHELIAL CELLS.	51

INTRODUCTION

5-Fluorouracil (FU) is a fluorinated pyrimidine antimetabolite which has been used in the treatment of both experimental animal tumors and human malignant disease (1-8). FU has been widely employed in the treatment of metastatic colorectal cancer (8, 9) and is currently a component of several combination therapeutic schedules for treatment of metastatic carcinoma of the breast (10, 11, 12) and gastrointestinal cancer (13). The rationale for the development of fluorinated pyrimidines as chemotherapeutic agents arose from the observation that a chemically-induced rat hepatoma utilized uracil for nucleic acid biosynthesis to a greater extent than did normal rat liver (14). FU was synthesized (15) as an antimetabolite which closely resembled uracil in structure but differed in the substitution of a stable fluorine atom for a hydrogen atom at carbon-5 of the pyrimidine ring. It was thought that FU might be preferentially utilized by tumors and, therefore, exert a specific antitumor effect. Although absolute specificity has not been achieved, it was later shown that FU and other fluorinated pyrimidines, e.g., 5-fluorouridine (FUR),

5-fluoro-2'-deoxyuridine (FUdR), do have clinically useful antitumor activity (1).

Several laboratories have investigated the biochemical and pharmacological effects of the fluorinated pyrimidines (1, 3, 16, 17, 18). Pyrimidine analogs are transformed to the nucleotide stage via pyrophosphorylase or phosphorylase plus kinase reactions. They are then substituted for normal pyrimidines in the various metabolic reactions of the cell. As illustrated in the diagram in Figure 1, the biochemical effects of FU in the anabolic pathway are three-fold. First, FU inhibits the incorporation of uracil and orotic acid into RNA (19, 20). Second, FU can be metabolized to the nucleoside triphosphate level and then be incorporated into fraudulent RNA (19, 20, 21). It has been suggested that incorporation of fluorinated pyrimidines into RNA may result in mispairing or miscoding, thus producing "phenotypic mutations" (22). Third, the active metabolite of FU, 5-fluoro-2'-deoxyuridine-5'-monophosphate (FdUMP), inhibits DNA synthesis by blocking thymidylate synthetase (17, 19, 23), the enzyme which catalyzes the formation of thymidylate from deoxyuridylate. Neither FU or its metabolites are incorporated into DNA (24). Although recent studies have indicated that FU and its metabolites may also affect other aspects of nucleic

acid biosynthesis, such as inhibition of ribosomal RNA maturation (25, 26), the inhibition of thymidylate synthetase is believed to be the major locus of the anti-tumor activity of FU (27, 28).

The excretion, distribution, and metabolism of radioactively-labeled FU have been extensively studied in both animals and human patients (20, 21, 29, 30, 31). The initial steps of FU degradation, i.e., the conversion to dihydrofluorouracil, α -fluoro- β -ureidopropionic acid, α -fluoro- β -alanine, α -fluoro- β -guanidopropionic acid and CO_2 are exactly analogous to those for uracil (32). In addition, FU is extensively converted to urea in human patients (29). These degradative products lack antitumor activity (31). The liver, which is the principal site of FU catabolism (29), will catabolize FU up to a threshold dose, above which anabolism proceeds. In humans, approximately 60-80% of an intravenous dose of FU is excreted as respiratory CO_2 in 8-12 hours (31), and approximately 15% is excreted in the urine in 6 hours as unchanged drug (30). Therefore, only a small percent of the administered dose follows the anabolic pathway.

The goal of most treatment schedules is to destroy the tumor population without causing irreversible damage to the normal proliferating cells. In addition

to biochemical factors, the effectiveness of many of the antitumor agents may be influenced by the proliferating status of the tumor versus normal cell populations. Knowledge of the cell kinetics of the tumor, in conjunction with information about the cell-killing characteristics of the antitumor agent, can be used to design effective drug combinations and treatment schedules. For example, an agent that may selectively kill cells in the DNA synthetic phase of the cell cycle could be combined with a treatment modality that is more cytotoxic for cells in other phases of the cycle. This approach was successfully utilized by Nitze et al. in human solid tumors (33). Treatments based on cell cycle kinetic principles have been particularly useful in patients with acute lymphoblastic leukemia (34, 35, 36).

Cell cycle studies originated with the work of Howard and Pelc in 1951 (37), which documented the presence of a DNA synthesis period (S phase) in the growth cycle of cells. The cell cycle can be divided into discrete phases: G_1 , S, G_2 , and mitosis (M), the duration of which can be determined by the percent labeled mitosis of Quastler and Sherman (38). These phases are characterized by specific biochemical and molecular events. RNA and protein synthesis are necessary for cell progress through the G_1 period (39, 40).

The levels of specific enzymes necessary for DNA replication, such as thymidine kinase, have been shown to increase during G_1 phase (41). There is evidence that regulation of cell proliferation in a particular tissue is governed by lengthening or shortening the G_1 period (42). The G_1 to S phase transition is probably brought about by an initiator protein whose production is regulated by RNA synthesis (43). S phase is the period of DNA replication. Ribonucleotide reductase activity rises at the beginning of S phase, whereas other enzymes involved in pyrimidine deoxyribonucleotide synthesis increase later in S (44). The G_2 period, which is relatively short compared to other phase durations, is usually assumed to be necessary for chromosome condensation and mitotic assembly. During M the parent cell divides to produce daughter cells. There is a decrease in protein synthesis (45) and cessation of RNA synthesis during mitoses (45, 46).

In the majority of tissues, certain cell subpopulations exist in a "resting" or quiescent stage in which they retain their proliferative capacity but do not actually replicate. The growth fraction of a tissue, such as a tumor, is a term introduced by Mendelsohn (47) to describe the fraction of proliferating cells in the population. The drug sensitivity of quiescent cells may

be different than that for rapidly proliferating cells. Investigations with the model of Bruce et al. (48) with haematopoietic stem cells have indicated that resting cells are less sensitive to cytotoxic agents than are cycling cells (18, 49). Although a reverse relationship has been observed with particular drugs, e.g., bleomycin and BCNU, in other model systems it is generally believed that a low growth fraction of a tumor may influence the apparent effectiveness of an antitumor agent. Another important cell kinetic parameter which may be utilized in designing chemotherapy schedules is that of recruitment, a term used to designate the induction of resting cells into the proliferating cycle. Recruitment can result from depletion or killing of the proliferating population of a tumor, such as occurs with radiation (50) and chemotherapy (51, 52). Schabel (53) successfully utilized low-dose therapy in a solid tumor to kill proliferating cells and recruit the resting population for subsequent chemotherapy. Therefore, information about the cell killing characteristics of a particular agent can potentially be utilized to predict optimal drug combination and schedules for maximum anti-tumor activity.

Chemotherapeutic agents can be subdivided into two general categories based on their cytotoxic characteristics. The cell cycle stage specific agents (CCSS)

kill cells only when they are present during the sensitive phase of the cycle. Drugs, such as vinblastine, amethopterin, and azaserine, are included in this class (54). The cell cycle stage nonspecific drugs (CCSN) kill cells in all phases of the cycle to a similar extent and are less cytotoxic for cells in a nonproliferating state. These drugs include actinomycin D, nitrogen mustard, and cyclophosphamide (54). Although FU is generally believed to be a CCSN agent (54, 55), there is evidence that its metabolites, FUR and FUdR may be CCSS. Several investigators (54, 56) have reported that FU is equally cytotoxic in all parts of the cycle and that the sensitivity of the cell population depends strongly upon the fraction of the population in the proliferative state (54). In vitro studies of Bhuyan et al. (56) indicated that FUdR kills cells preferentially in S phase, whereas Lozzio (57) found that it was cytotoxic to cells in both G₁ and S. Cells in M were relatively insensitive to FUdR (57). The majority of these studies on the cell cycle stage specificity of FU and its metabolites were done with in vitro model systems. The effect of FU on mammalian cell cycle kinetics has not been extensively investigated with in vivo animal models. Information obtained from such studies could be useful in the

planning of rational therapeutic regimens which might be more effective than currently used protocols.

FU, like most of the clinically useful anti-tumor agents, has a low therapeutic index. Toxicity to normal tissues, such as the bone marrow and gastrointestinal tract, is the major limiting factor in the clinical usefulness of FU. Stomatitis, nausea, vomiting, diarrhea, and leukopenia are common side effects of FU therapy (58-62). As a result, much effort has been spent in the development of chemotherapeutic analogs of FU which, hopefully, would display improved therapeutic indices. Ftorafur ([5-fluoro-1-(tetrahydro-2-furyl)uracil] [FT]), a tetrahydrofuran-containing pseudonucleoside analog of FU, was synthesized in the Soviet Union in 1965 (63) as part of a program designed to study the antitumor activity of nucleosides containing a variety of sugar and heterocyclic moieties. Subsequent studies on the pharmacological activity of FT indicated that it was less toxic and possessed equal or greater antitumor activity than FU (64-67). Initially, limited quantities of FT in the United States restricted investigation of its properties in this country. However, in 1972, Earl and Townsend (68) at the University of Utah developed a rapid and efficient method for the synthesis of FT and, consequently, large quantities of drug became available for basic and clinical studies in this country.

The principal advantage of FT, as compared to FU, was reported to be lower toxicity, with retention of the same antineoplastic effect. Hrsak et al. (69) reported that mice treated with FT showed less reduction and faster recovery of haematopoietic stem cells than after a comparable dose of FU. In recent studies, FT, as a single treatment in mice, was half as toxic as FU on an mg/kg basis but not on a molar basis (70). FT was less suppressive to both cell-mediated and humoral immunity than was FU (970). A number of clinical trials have also suggested that FT was less myelosuppressive than FU, yet was still effective against solid tumors (65, 68). Clinically, FT, like FU, appears most effective against breast (64, 65, 71-73) and gastrointestinal cancer (64, 74, 75). Recent reports on experimental tumor models have indicated that FT and FU may have slightly different antitumor spectra (76).

Biochemical and pharmacological studies with FT suggested that it acted as a depot form of FU and must be metabolically activated (77, 78). FT is metabolized in vivo to FU and other known fluorinated pyrimidine metabolites (77, 79-82). It is fairly evenly distributed to liver, small intestine, kidney, spleen, and brain (79). The liver contains the highest initial proportions of FU and its metabolites and may be the

primary site at which FU is released in vivo. In rats, the half-life of FT in plasma was estimated to be approximately 5-6 hours, whereas the half-life of FU was between 10 and 30 minutes (79).

The studies reported in the following sections are a comparison of the in vivo effects of FU and FT in tumors and in normal proliferating tissue of mice. Drug effects were examined at the whole animal, tissue, cellular, and molecular levels. Varying doses and treatment protocols were utilized to obtain information about the efficacy of FT versus FU with respect to growth inhibition of murine mammary adenocarcinomas. Changes in mouse body weight were also monitored during each therapeutic regimen in an effort to compare the extent of host toxicity produced by each drug.

Although FU has been used clinically for several years, its in vivo effects on mammalian cell cycle kinetics have not been clearly documented. Since FT is a relatively new drug, there are even fewer detailed studies on its in vivo effects, and no information is available on drug-induced cell cycle perturbations. As seen from the previous discussion on cell kinetics, such information should be potentially useful in planning effective treatments.

In this study, drug-induced cell cycle perturbations were examined by standard autoradiographic procedures and by the flow cytometer (FCM). The FCM is an instrument which rapidly determines the distribution of cells throughout the cell cycle by measuring the DNA content of individual cells. Cells in suspension are stained with a fluorescent dye such as acriflavin or chromomycin. The amount of fluorescence in an individual cell is directly proportional to its DNA content. The FCM will detect and analyze the DNA-specific fluorescence and display the cell cycle phase distribution of the population in the form of a histogram. The fraction of the cell population in G_1 , S and $G_2 + M$ can then be calculated. The advantage of the FCM over standard autoradiographic procedures lies in the rapid analysis of cell cycle phase distributions. Since as many as a million cells can easily be analyzed within a few minutes, data obtained by FCM are more statistically reliable than those obtained by autoradiography. In addition, unlike autoradiography, FCM analysis yields direct information about cell phase distributions, even in the presence of agents which interfere with DNA synthesis.

FCM analysis of drug-induced cell cycle changes can easily be performed on in vitro cell cultures (83, 84). These single cell suspensions contain negligible

amounts of cellular debris and provide DNA distributions which can readily be analyzed as a result of the low level of background fluorescence. However, it is advantageous to evaluate drug effects on animal tumors in vivo, which more closely approximate the clinical situation and, thus, may be more appropriate models for studying the cell cycle effects of chemotherapeutic agents. FCM analysis of DNA distributions of cells obtained from solid tissues necessitates the development of cell dispersal, separation, and isolation procedures. In the present study, sodium tetraphenylboran (TPB), a potassium-complexing reagent reported to aid in the dispersal of liver cells (85), was used successfully with solid tumors (86).

Since many of the clinically useful cancer chemotherapeutic agents exert effects on both tumor and normal tissue, it is desirable to evaluate drug-induced cell cycle changes in both types of tissue. Drug toxicity in the small intestine is one of the major limiting factors in therapeutic protocols. Cell cycle perturbations in the proliferating cells of the small intestine, the crypts, are usually studied with tedious and time-consuming autoradiographic techniques. In order to utilize FCM for analysis of the age distribution of the proliferating cells of the small intestine, it would

be necessary to obtain a suspension of pure crypt cells. Most of the presently available procedures for obtaining so-called "crypt" preparations yielded mixed populations of both crypt and villus epithelial cells. Therefore, a method to separate crypt and villus cells with the FCM on the basis of fluorescent enzyme histochemistry was developed.

In vivo effects of FU and FT were also examined at the molecular level by monitoring the incorporation of tritiated deoxyuridine and $\text{Na}_2\text{H}^{32}\text{PO}_4$ incorporation into DNA. These data were correlated with those obtained at the tissue and cellular levels in the hope that such information will prove useful clinically in planning and evaluating effective chemotherapeutic regimens with these agents.

MATERIALS AND METHODS

Mice and Tumors

C3H mice of both sexes, 8-12 weeks old, were utilized in all studies. Mammary tumors from the established S102F and Slow lines were used (87, 88). These lines were developed from adenocarcinomas which arose spontaneously in breeding female C3H mice. The S102F tumor has a doubling time of approximately 2 days, a growth fraction of 55%, and a generation time of 17 hours (87). The Slow tumor has a doubling time of 5-6 days, a growth fraction of 25%, and a generation time of 33 hours (87). The lines were maintained by subcutaneous trocar transplants of 1-2 mm pieces of tumor into both flanks of ether-anesthetized animals. Tumor growth was followed serially by caliper measurements in three dimensions. Tumor volume was estimated by a hemi-ellipsoid approximation with a correction for skin thickness (89).

Drugs

FU (Sigma) and FT (prepared in the laboratory of Dr. L.B. Townsend) were administered by intraperitoneal injection into unanesthetized mice between 7:00 and 9:00 a.m. All drug solutions were freshly prepared immediately before use and were injected in a volume of 0.01 ml/gm body weight. FU was dissolved in 0.9% NaCl solution. FT was dissolved in either 0.9% NaCl solution for the 100 mg/kg dose or with slight heating in 0.2 M sodium carbonate buffer, pH 9.4 for the 300 mg/kg dose. Sterile 0.9% NaCl solution or carbonate buffer was injected into control animals. All drug treatment studies were begun when the tumor volume was approximately 200 $\mu\ell$ (\pm 50 $\mu\ell$). Body weight was monitored daily.

Radioisotopically-Labeled Precursor Incorporation Studies

Deoxyuridine Incorporation Into Deoxyribose Nucleic Acid (DNA)

Deoxyuridine [6-³H] (³H-UdR New England Nuclear: 100 $\mu\text{Ci}/\text{kg}$, S.A. 21 $\mu\text{Ci}/\mu\text{mole}$) was administered by intraperitoneal injection at 1-96 hours after drug treatment. Mice were killed 30 minutes thereafter by cervical dislocation and tumors and small intestine were quickly

removed. The tumors and small intestine were rinsed with 0.9% NaCl solution, frozen between two blocks of dry ice and stored at -20°C for subsequent analysis. Nucleic acids were extracted according to the phenol procedure of Morley and Kingdon (90). Briefly, the tissue was homogenized on ice in either 7 ml (tumor) or 15 ml (intestine) of 1% 8-anilino-1-naphthalene-sulfonic acid sodium salt (tech.) (Eastman Kodak) dissolved in 0.2 M acetate buffer, pH 7.0. Five ml of the homogenate was mixed with 5 ml of 88% (w/v) liquified phenol (Mallinckrodt) and centrifuged at $18,000 \times g$ for 20 minutes. The clear supernatant was removed, and the nucleic acids were precipitated by the addition of 1.5 volumes of absolute ethanol. The resulting strands were washed once with ice-cold 10% trichloroacetic acid (TCA) and once with absolute ethanol. The precipitate was then dissolved in 0.5 N perchloric acid (PCA) and the nucleic acids were hydrolyzed by heating at 90°C for 10 minutes. An aliquot was removed for radioactivity determination and the remainder was utilized for DNA-deoxyribose determination by means of the diphenylamine reaction of Burton (91). Deoxyadenosine served as a standard. Radioactivity was measured in a Packard scintillation spectrometer. The efficiency of the Triton X-100 scintillation counting mixture was

estimated by internal standardization and was approximately 25% (\pm 5%). Data are expressed as dpm/ μ mole deoxyribose or as percent of control.

Phosphorus Incorporation
Into DNA

$\text{Na}_2\text{H}^{32}\text{PO}_4$ (New England Nuclear: carrier free, 20 μ Ci/mouse) was administered intraperitoneally at specific intervals after drug treatment. Thirty minutes were allowed for metabolic utilization of the labeled precursor. The mice were then killed by cervical dislocation, and the excised tissues were rinsed with 0.9% NaCl solution and frozen on dry ice. Nucleic acids were isolated according to the procedure described above. However, since ^{32}P can be incorporated into both ribonucleic acids (RNA) and DNA, the RNA was separated from DNA by base-catalyzed hydrolysis (92) as follows: the washed nucleic acid precipitate was dissolved in 0.3 N KOH at 37°C for 2 hours. Ice-cold 1.2 N PCA was then added to precipitate potassium perchlorate and the unhydrolyzed DNA. The precipitate was washed with 0.2 N PCA and the DNA hydrolyzed by heating at 70°C for 20 minutes in 0.5 N PCA. DNA-deoxyribose was measured by the diphenylamine procedure (91), and radioactivity was determined by liquid scintillation counting, as described above. The counts per minute were

corrected for ^{32}P decay such that all data were related to the original dose of administered ^{32}P . Data are expressed as counts per minute (cpm) per μmole deoxyribose. Measurements of the amount of RNA present in the DNA fraction by the orcinol reaction (92) indicated that there was less than 7% contamination of the DNA fraction with RNA.

Thymidine Incorporation Into DNA

Thymidine [methyl- ^3H] (^3H -TdR) was utilized for both autoradiographic studies and for radioactivity determination by liquid scintillation counting. For autoradiography, mice were injected intraperitoneally with ^3H -TdR (New England Nuclear: 20 $\mu\text{Ci}/\text{mouse}$, specific activity 6.7 Ci/mmole) and killed at specified intervals after injection. Criteria for determining labeling indices are described in the next section. In experiments in which radioactivity was determined by scintillation counting, ^3H -TdR (New England Nuclear: 100 $\mu\text{Ci}/\text{mouse}$, specific activity 40 $\mu\text{Ci}/\mu\text{mole}$) was administered intraperitoneally at specified intervals prior to sacrifice. The specific activity of the radioactively-labeled DNA was determined by the procedures described above. Results were recorded as DPM per μmole deoxyribose.

Autoradiography

Tumors were removed, rinsed with 0.9% NaCl solution and fixed in 10% buffered formalin. Duodenums were flushed with isotonic saline prior to fixation in a formalin solution (20% v/v formaldehyde, 70% ethanol, glacial acetic acid; 2:20:1, v/v/v). Formalin-fixed tumors and duodenums were embedded in Paraplast (Sherwood Medical Industries, Inc.) and sectioned at 2-3 μ m. In experiments with single cell preparations, the suspensions were placed on glass slides, air-dried and fixed in Carnoy's fluid (absolute ethanol, glacial acetic acid; 3:1, v/v). The slides were dipped in Kodak NTB3 liquid emulsion and exposed for 6-60 days, developed with Kodak D19 developer and stained with hematoxylin and eosin. To minimize observer bias, the slides were coded with random numbers before cells were scored as labeled or nonlabeled. A minimum of 200 labeled cells were counted. The background averaged less than one grain per cell; therefore, cells with three or more grains were considered as being labeled.

Tumor Cell Dispersal

The TPB dispersal technique has previously been published (86). A schematic of the TPB dispersal procedure is shown in Figure 2. Tumors with a volume of less than 200 μl contain minimal amounts of necrotic debris and were routinely used to prepare cell suspensions. After the tumor was removed from the mouse and halved, any grossly necrotic material was scraped off with a glass rod. The tumor was minced in 0.9% NaCl solution with a sharp scalpel or scissors and the minced tissue transferred to a flask containing 7 ml 3 mM sodium tetraphenylboron (J.T. Baker), 0.05 M sucrose, 0.005 M Na_2HPO_4 , and 0.14 M NaCl. The minced tissue was incubated at 37°C with gentle shaking in a reciprocating water bath for one minute. Cell debris was often found in the incubation fluid after the one minute incubation. Therefore, the initial incubation medium was removed and fresh solution added to the tumor fragments; this mixture was incubated for 30 minutes. The suspension was then passed through a plastic syringe (10-15 times) to completely disperse the remaining tissue fragments. After an additional 30 minutes of incubation, the cell suspension was filtered through 37 μm nylon mesh to remove residual clumped cells, and washed three

times with 0.14 M NaCl solution. The washed cells were then fixed in 10% buffered formalin and stained by an acriflavin-Feulgen technique (93) for FCM analysis. If ^3H -TdR autoradiography was also done, drops of unstained single cell suspensions were placed on glass slides and air-dried in preparation for dipping in photographic emulsion.

Intestinal Epithelial Cell Isolation

Intestinal epithelial cells were isolated from C3H mice by the Weiser (94) procedure with the following modifications. The entire small intestine was removed and flushed with phosphate-buffered saline (PBS: 0.96 M Na_2HPO_4 , 0.29 M NaCl, 0.38 M KH_2PO_4 , pH 7.2) containing 1.5 mM dithiothreitol (Sigma). It was then filled with a solution containing 1.5 mM KCl, 27 mM sodium citrate, 96 mM NaCl, 8 mM KH_2PO_4 , 5.6 mM Na_2HPO_4 , pH 7.3 (Solution A) and each end was tied off with surgical thread. The filled intestine was then placed in 0.3 M sucrose and incubated at 37°C with gentle agitation for 15 minutes in a reciprocating shaker. Solution A was then removed and replaced by Solution B (1.5 mM [ethylenedinitrilo]-tetraacetic acid disodium salt [EDTA], 0.5 mM dithiothreitol dissolved in PBS). The filled intestine was then incubated for 25 minutes, during which time the

villus epithelium became detached from the basement membrane and underlying lamina propria. The villus fraction was then collected by flushing the gut with Solution B. Fresh Solution B was then added and an enriched crypt fraction, containing varying amounts of villus cells, was removed during a subsequent 50 minute incubation. In later experiments, it was found that a higher cell yield could be obtained by everting the intestines prior to incubation in Solution A.

Intestinal Cell Dispersal

The crypt fraction obtained by the previously discussed isolation procedure consists of single crypt and villus cells, with some clumping due to undispersed epithelial fragments and to contaminating mucus which tends to aggregate the single cells. Cell clumps were separated by passing the suspension 15 times through a 15 g needle, 5 times through a 22 g needle, and subsequent filtration through 37 μ m nylon mesh. The cells were then washed twice with 30 ml of PBS and resuspended in the same solution.

Mucus was removed by incubating washed epithelial cells in 2 mg/ml ascorbic acid, 1% hydrogen peroxide, and 0.001 M $\text{CuSO}_4 \cdot 5\text{H}_2\text{O}$, pH 7.2, for 20 minutes at 37°C (95). The cells were then centrifuged at 500 \times g; mucus

was found in the supernatant and along the sides of the test tube. The suspension was washed once with PBS to remove traces of the mucolytic incubation fluid and the cells were resuspended in PBS.

Enzyme Histochemical Reaction

A simultaneous-coupling procedure was used for the leucine aminopeptidase reaction (96). The epithelial cell suspension was diluted with PBS to a final concentration of approximately 10^7 cells/ml. The enzyme substrate, L-leucyl-4-methoxy- β -naphthylamide-HCl (Sigma) was initially dissolved in 1-2 drops of dimethylformamide (DMF: Eastman Organic Chemicals) and then diluted with 0.2 M morpholinethane sulfonic acid (MES: Sigma), pH 6.3, to a final concentration of 0.5 mg/ml. Nitro-salicylaldehyde (NSA: Eastman Organic Chemicals) was prepared in 50% DMF at a concentration of 10 mg/ml. The final concentration of NSA in the enzyme incubation mixture was 10 μ g/ml. The NSA solution was freshly prepared immediately before use. One-quarter ml of the cell suspension was incubated with 2 ml of the incubation mixture (substrate plus NSA) for 30 minutes at 37°C with occasional shaking. The cells were then washed once with 0.2 M MES at 4°C. Every effort was made to analyze the enzymatically-stained cells as soon as possible after

the enzyme reaction. The samples were maintained at 4°C prior to FCM analysis.

Cell Staining for FCM Analysis

Tumor Cells

After fixation (at least 24 hours) in 10% buffered formalin, TPB-dispersed tumor cells were stained by the acriflavin-Feulgen technique (93) for FCM analysis. The staining protocol is represented in a flow diagram (Figure 3). All centrifuging was done at 500 xg for 5 minutes and supernatants were removed by aspiration. Five mls of each reagent was added to the tube with vortexing. Acriflavin (Gurrs) (4×10^{-4} M) was dissolved in 1 part 0.5 N HCl and 9 parts glass-distilled water. Acid alcohol was prepared by a 1:100 dilution of concentrated HCl with 70% ethanol.

Intestinal Epithelial Cells

Fluorescent enzyme histochemical staining procedures are discussed in a previous section. DNA distributions of mixed epithelial cell populations were obtained by staining either with acriflavin (as described previously, chromomycin, or Hoechst 33258.

Chromomycin. Chromomycin staining (97) was done on cells fixed in ice-cold 70% ethanol for at least 30

minutes. The ethanol-fixed cells were then centrifuged at 500 xg for 5 minutes. The supernatant was removed by aspiration and the cells were resuspended in 5 ml of chromomycin staining solution. The chromomycin staining solution consists of 10 mg chromomycin A₃ (Calbiochem), 1.5 g MgCl₂·6H₂O and 500 ml cold distilled water. After staining, the cells were placed in the dark for 20 minutes at room temperature prior to FCM analysis.

Hoechst 33258 staining. A modification of the Hoechst 33258 staining protocol described by Latt et al. (98) was utilized. The modification included a marked reduction in the dye concentration in order to obtain nuclear fluorescence with minimal cytoplasmic fluorescence. Epithelial cells were fixed in 70% ethanol for at least 30 minutes. The cells were then centrifuged and resuspended in 2 ml of 0.005 M HEPES (N-2-Hydroxyethylpiperazine-N'-2-ethane sulfonic acid), 0.15 M NaCl, pH 7.0 buffer. One-tenth ml of Hoechst 33258 (Dr. H. Loewe, Frankfurt, Germany) (0.01 mg/ml dye in Hepes buffer) was then added. The final dye concentration was 5×10^{-7} M. The cells were allowed to stand at room temperature in the dark for at least 15 minutes prior to FCM analysis. In experiments in which samples dually-stained for leucine aminopeptidase activity and

for DNA were needed, the Hoechst staining was performed after the enzymatic staining reaction.

Flow Cytometer

Tumor DNA Distributions

The FCM used in these studies has been previously described (99) and, therefore, will not be discussed in detail. The FCM was equipped with a 4-watt (all-lines) argon ion laser (Spectra Physics Model 164-05) adjusted to emit 1.0 W at 488 nm. Briefly, acriflavin-stained cells were passed through a beam of laser light and excited at a wavelength of 488 nm, and the resulting fluorescence was collected perpendicular to both laser beam and flow axis. The fluorescence, which was proportional to DNA content, was projected through a Corning 3-69 color filter (50 percent transmission at 525 nm) onto an RCA 7164 R photomultiplier tube. After the photomultiplier output was integrated, amplified, and digitized, the data were transferred to magnetic tape or computer disc for subsequent analysis. The stability of the overall system was repeatedly checked by running 1.75 μm fluorescent microspheres (Polysciences, California). DNA distributions were analyzed according to the method of Dean et al. (100).

Intestinal Epithelial Cell Analysis

The Lawrence Livermore Laboratory flow sorter (99), a modified Becton-Dickinson FACS-II model, was utilized in the analysis of the chromomycin-stained intestinal epithelial cells. The sorter was equipped with a 4-watt (all-lines) argon ion laser (Spectra Physics Model 171-03) which was adjusted to emit 200 mw at 457 nm. The cells emerged from a 100 μ m diameter nozzle and intersected the laser beam at 90°. Fluorescence was collected perpendicular to both flow axis and laser beam and was projected through a filter (Corning 3-71) transmitting light above 480 nm (50 percent transmission point) onto a photomultiplier tube (RCA 8575). The pulse processing and storage were the same as described above for the FCM.

For Hoechst 33258-stained cells, the argon ion laser was adjusted to emit 300 mw at the 351-364 nm doublet. Logarithmic amplification of fluorescence and low-angle (0-7°) forward scatter was utilized in the two-variable analysis. A dual parameter multichannel pulse height analyzer was utilized for displaying three-dimensional pulse amplitude distributions of enzymatically-stained cells. The fluorescence of preparations stained for leucine aminopeptidase activity was excited at either 457 nm or at the 351-364 nm doublet, as specified.

RESULTS

Comparison of Drug Effects at Whole Animal and Organ Level

The S102F and Slow murine adenocarcinomas were utilized to compare the efficacy of FT and FU. Both single dose and multiple dose regimens were examined.

The multiple dose treatment protocol consisted of ten consecutive daily injections of FT (100 mg/kg) or FU (20 mg/kg). An equimolar dose of FU would have been 65 mg/kg; however, preliminary studies with multiple daily injections of FU (40 and 65 mg/kg) indicated that the mice were unable to tolerate daily administration at these dose levels. Therefore, FU was administered at a maximally tolerated dose of 20 mg/kg for ten days. The growth of S102F tumors of mice treated with either FU (20 mg/kg) or FT (100 mg/kg) in a multiple dose regimen is shown in Figure 4. Day 0 represents the first day of treatment. In order to maintain uniformity in results between experiments, the first treatment day was chosen as the time at which the tumor had grown to approximately 200 μl (\pm 50 μl). S102F tumors begin to ulcerate at volumes greater than 800 μl , thus, measurements of large tumors are meaningless and were not

included in the figures. Ten daily injections of FT slowed tumor growth for the duration of the treatment schedule. Maximally tolerated doses of FU did not have a significant antitumor effect.

Changes in the body weight of the mice were monitored during all studies as part of an effort to compare drug toxicity to the host. Body weight changes as a function of time after the first drug injection are shown in Figure 5. At the start of treatment, the mice weighed between 23 and 28 g. Control mice injected with 0.9% NaCl solution gained about 1 g during the course of treatment. With both multiple dose drug treatments, the mice lost approximately 3-4 g. The body weight of animals which received daily injections of FT returned to pretreatment levels between 18 and 24 days after the initial injection. In contrast, FU-treated animals remained at 2-3 g below pretreatment levels for the duration of the study (approximately 25 days).

A similar study was performed on animals bearing the Slow tumor. Groups of tumor-bearing mice received either FU (20 mg/kg) or FT (100 mg/kg) for ten consecutive days. Drug effects on the growth of the Slow tumor are presented in Figure 6. FT exhibited antitumor activity, resulting in a slowing of tumor growth for the first 4-8

days of treatment, after which the rate of growth approximated that of control tumors. A less pronounced effect was observed with a maximally tolerated regimen of FU. As shown in Figure 7, the FT and FU treatment protocols were more toxic to animals bearing the Slow tumor as compared to those bearing the S102F tumor (see Figure 5). With both drugs, tumor-bearing animals lost between 5 and 7 g of weight. Although not shown, FT-treated animals regained their weight to original levels on days 15-20 after the initial injection, whereas FU-treated mice maintained their weight at 3-4 g below control animals for the duration of the study.

Although antitumor agents are usually administered clinically in multiple dose regimens, it is initially essential to study and evaluate biochemical and cellular drug-induced perturbations in the simplest situation following a single dose, before attempting to study the more complex conditions following multiple dose therapy. Therefore, the effects of large, single doses of FT (300 mg/kg) and FU (65 mg/kg) were examined in the S102F and Slow tumors. Figure 8 illustrates the effect of these drug treatments on the growth of the S102F tumor. Tumor growth was slowed for 3-4 days after treatment with either drug. Partial regression was observed 1-3 days after FT or FU treatment in some tumors.

Data regarding drug toxicity to animals bearing the Sl02F tumor are shown in Figure 9. Animals which received FT (300 mg/kg) lost approximately 1 g within 2 days after treatment. During the subsequent 3 days, their body weight returned to the pretreatment level. Mice treated with a single injection of FU (65 mg/kg) had an initial weight loss of 2-3 g. This weight loss was maintained for 10-12 days after the initial injection.

The antitumor effect of single, large doses of FU and FT was also studied in animals bearing the Slow tumor, as shown in Figure 10. In this study, day 0 represents the first day of tumor measurement rather than the day of the first injection. In animals which received FT (300 mg/kg) on day 8, tumor growth was dramatically slowed for 4-5 days. In some tumors, partial regression was observed 1-3 days after treatment. Mice treated with FU (65 mg/kg) also showed a decrease in the rate of tumor growth for 4-5 days after treatment. With both drugs, the rate of tumor growth approximated that of controls within 6-8 days after drug injection. However, even though both drugs exhibited similar antitumor activity against the Slow tumor, a dramatic difference in host toxicity was observed. Figure 11 indicates that animals bearing the Slow tumor, which received a single injection of FT (300 mg/kg), lost approximately 2-3 g

of weight and maintained this weight loss for the duration of the study. Mice treated with FU (65 mg/kg) showed a steady weight loss for 10-12 days after drug injection. A maximum weight loss of approximately 8-9 g was observed. Animals regained about 50% of their weight loss on days 18-20 after the injection. However, despite this large weight loss, none of the FU-treated animals died.

Since the marked antitumor effects observed with large, single injections of either FT or FU were accompanied by a marked weight loss, a study was undertaken to evaluate the effect of body weight loss per se on the rate of tumor growth. Tumor-bearing mice were allowed water ad libitum, while food was withheld until the desired weight loss was achieved. This procedure was originally designed to induce approximately the same degree of weight loss (8-9 g) as was observed in FU-treated mice. However, mice bearing the Slow tumor were not able to tolerate a weight loss of more than 6-7 g. Therefore, groups of 8-10 mice were forced to lose 5-6 g of weight, which usually occurred in 2-3 days. Tumors were measured throughout the duration of the study. The effect of this procedure on the growth rate of Slow tumors is shown in Figure 12. It is evident that a body weight loss of this magnitude did not directly affect

tumor growth. Similar results were obtained in animals bearing the S102F tumor (data not shown).

Comparison of Drug Effects at the Cellular Level

Development of Tumor Dispersal Technique

A procedure to prepare single cell suspensions from the solid tumors for FCM analysis was developed. A schematic of the TPB dispersal procedure is shown in Figure 2 and is discussed in detail in the Methods section. Figure 13a shows a hematoxylin and eosin-stained histological section of the solid S102F tumor. Connective tissue and alveolar ducts containing some pyknotic cells are clearly visible. A cell suspension of the tumor prepared by the TPB procedure is shown in Figure 13b. Hematoxylin and eosin-stained cells show a high nuclear to cytoplasmic ratio. Although the cells were nonviable as determined either by trypan blue or eosin-y dye uptake, the preparation consisted of single cells with minimal nuclear and cytoplasmic debris. Since the acriflavin staining is performed on formalin-fixed cells, cell viability was unimportant for FCM analysis of DNA distributions.

An uncorrected DNA distribution of acriflavin-stained TPB-dispersed S102F cells is shown in Figure 14. As evidenced from this histogram, the level of background

fluorescence noise was negligible. The distribution was characterized by a small peak at low fluorescence values due to normal diploid cells and by a bimodal distribution due to near-tetraploid tumor cells. The coefficient of variation of the G_1 peak was routinely between 4% and 6%. The TPB technique was also used to disperse Slow tumors (data not shown). Although the Slow tumor suspensions appeared to contain more residual debris than the S102F, DNA histograms were still superior to those obtained by a mechanical dispersal procedure (105).

Computer analysis of the areas under G_1 , $G_2 + M$ and S phase portions of the histogram is illustrated in Figure 15. A Gaussian distribution was used to fit the G_1 and $G_2 + M$ peaks and a second-order polynomial equation was utilized to fit the S phase portion of the histogram (100). Computer analysis of the DNA distribution of several individual S102F tumors is shown in Table 1. The standard error of the mean of the fraction of the tumor cell population in G_1 , S and $G_2 + M$ phase demonstrates the small inter-tumor variation in these data.

In order to ascertain if the TPB dispersal procedure was yielding cell suspensions which were representative of the in situ tumor, labeling indices were determined on histological sections and single cell

TABLE 1
FCM ANALYSIS OF UNPERTURBED S102F TUMORS

Tumor	C.V. (%)	Fraction of Cells		
		G ₁	S	G ₂ + M
1	4	0.65	0.23	0.12
2	6	0.67	0.14	0.19
3	4	0.65	0.25	0.10
4	5	0.66	0.18	0.16
5	6	0.65	0.10	0.25
6	6	0.66	0.14	0.21
7	5	0.67	0.20	0.12
8	6	0.65	0.16	0.19
9	4	0.68	0.18	0.14

Mean ± S.E.		0.66 ± 0.01	0.18 ± 0.02	0.16 ± 0.02

Computer analysis of DNA distributions of TPB-dispersed S102F tumors. The values represent the fraction of cells in G₁, S, and G₂ + M phases. The coefficient of variation (C.V.) of the G₁ peak is also listed.

preparations from the same tumor. As reported previously (88), the phase durations of the S102F tumor in hours are as follows: G_1 (6.5), S (7.7), G_2 (2.5), M (0.6). Based on these kinetic parameters, three experimental protocols were utilized to evaluate the random selection of cells in various phases of the cell cycle:

- 1) $^3\text{H-TdR}$ was given to mice bearing S102F tumors to label those cells in S phase. The mice were then killed 30 minutes later, and half of the tumor was fixed for sectioning, and the remainder was utilized to prepare single cell suspensions;
- 2) the mice were killed 3 hours after the single injection of $^3\text{H-TdR}$ with the labeled cells expected to be in mid to late S, G_2 , and M phase; and,
- 3) to obtain labeled G_1 cells, mice bearing S102F tumors were given two injections of $^3\text{H-TdR}$ 6 hours apart and then killed 10 hours after the last injection. Although labeled cells will be distributed throughout G_1 phase, they will be found in other phases of the cell cycle as well. With this protocol, the labeling index was expected to be about twice that found with a 30 minute pulse. Table 2 shows autoradiographic data for both tissue sections and single cells. The labeling indices for the tumor section versus the cell suspension correlate highly in each of the the three protocols (correlation coefficient, $r = + 0.94$).

TABLE 2
 LABELING INDICES IN TUMOR SECTIONS
 AND SINGLE CELL SUSPENSIONS

Description	N	S102F Labeling Index	
		Tissue Section	Single Cells
S-Phase	4	0.15 \pm 0.02	0.17 \pm 0.03
Mid to Late S, G ₂ and M-Phase	3	0.15 \pm 0.01	0.14 \pm 0.02
G ₁ -Phase	4	0.31 \pm 0.01	0.32 \pm 0.08

The values represent the mean \pm S.E. of the mean of N samples, where N is the number of tumors analyzed per point.

These data indicate that gross preferential cell selection or elimination from a particular phase of the cell cycle does not occur with the TPB dispersal procedure.

FCM Analysis of Perturbed
S102F Tumors

The effects of FT (100 mg/kg) on the DNA distribution of S102F tumors are presented in Table 3. One and 8 hours after drug injection, there was a significant increase ($p < 0.01$ Student's t-test) in the proportion of the tumor cell population residing in G_1 phase. A corresponding decrease was observed in S and $G_2 + M$ phase. However, 24 hours after injection, the DNA distributions appear to have returned to control values.

FCM analysis of the DNA content of S102F tumors perturbed by FT (300 mg/kg) is shown in Table 4. One and 8 hours after treatment, there was an increase in the percent of cells in S phase with a corresponding decrease of the tumor cell population in $G_2 + M$ phase. By 12 hours, the percent of cells with an S phase DNA content was 1.5-fold higher than the control value. In contrast, at 24 hours after treatment, the fraction of cells in S was reduced below the control level, and the majority of the tumor cells appeared to be located in G_1 . Although the percent of the cells in G_1 decreased slightly at 28 hours, as compared to control, it returned to

TABLE 3
FCM ANALYSIS OF DNA CONTENT OF PERTURBED S102F TUMORS

Treatment	Fraction of Cells In		
	G ₁	S	G ₂ + M
Control	0.66 ± 0.00	0.18 ± 0.02	0.16 ± 0.02
Ftorafur (100 mg/kg)			
1 hour	0.72 ± 0.01 ^a	0.13 ± 0.01	0.15 ± 0.01
8 hour	0.71 ± 0.01 ^b	0.15 ± 0.02	0.14 ± 0.01
24 hour	0.66 ± 0.01	0.18 ± 0.02	0.15 ± 0.01

Each value is the mean + S.E. of 6-9 samples. The coefficients of variation of the G₁ peak were less than 5%. Control values were taken from Table 1.

^ap < 0.05 vs. control (t-test).

^bp < 0.01 vs. control (t-test).

TABLE 4

FCM ANALYSIS OF DNA CONTENT OF PERTURBED S102F TUMORS

Treatment	Fraction of Cells In		
	G ₁	S	G ₂ + M
Control	0.66 ± 0.01	0.18 ± 0.02	0.16 ± 0.02
Ftorafur (300 mg/kg)			
1 hour	0.66 ± 0.02	0.20 ± 0.02	0.14 ± 0.01
8 hour	0.66 ± 0.02	0.20 ± 0.01	0.13 ± 0.01
12 hour	0.63 ± 0.01	0.26 ± 0.02 ^b	0.11 ± 0.01
24 hour ^a	0.81 ± 0.01 ^c	0.07 ± 0.01 ^c	0.13 ± 0.01
28 hour ^a	0.73 ± 0.02 ^c	0.13 ± 0.02 ^b	0.14 ± 0.01
36 hour ^a	0.83 ± 0.01 ^c	0.08 ± 0.01 ^c	0.09 ± 0.01 ^c

Each value is the mean + S.E. of 6-9 samples. The coefficients of variation of the G₁ peak were less than 5%. Control values were taken from Table 1.

^ap < 0.01 vs. control (multivariate analysis of variance).

^bp < 0.05 vs. control (t-test).

^cp < 0.01 vs. control (t-test).

the previously high levels again at 36 hours after the injection of FT.

Table 5 represents FCM analysis of the DNA content of S102F tumors perturbed by the systemic administration of FU (65 mg/kg). The percent of the tumor cell population in $G_2 + M$ phase increased from 17% to 22% within 1 hour after drug injection. Eight hours after treatment, there was marked increase in the percent of cells in S phase and a significant decrease in the tumor cell population residing in $G_2 + M$ phase. This was followed 16 hours later (the duration of approximately one cell cycle) by an increase in cells in G_1 . The percent of the tumor cell population in G_1 phase continued to be elevated at 36 hours after treatment, whereas the percent of cells in S and $G_2 + M$ phase was drastically reduced.

Autoradiography was utilized to confirm selected portions of the data obtained by FCM analysis of perturbed S102F tumors. Specifically, changes in labeling indices at various times after drug treatment were correlated with changes in the fraction of cells in S phase as determined by FCM analysis. S102F tumor-bearing animals were treated with either FU (65 mg/kg) or FT (300 mg/kg). $^3\text{H-TdR}$ was administered at various intervals after drug injection, and the mice were killed

TABLE 5
FCM ANALYSIS OF DNA CONTENT OF PERTURBED S102F TUMORS

Treatment	Fraction of Cells In		
	G ₁	S	G ₂ + M
Control	0.66 ± 0.01	0.18 ± 0.02	0.16 ± 0.02
Fluorouracil (65 mg/kg)			
1 hour	0.64 ± 0.01	0.14 ± 0.01	0.22 ± 0.01
2 hour ^b	0.69 ± 0.03	0.25 ± 0.02 ^d	0.06 ± 0.01 ^d
8 hour ^a	0.63 ± 0.01 ^c	0.28 ± 0.01 ^d	0.10 ± 0.02 ^d
14 hour ^b	0.61 ± 0.01 ^d	0.28 ± 0.02 ^d	0.10 ± 0.01 ^d
16 hour ^a	0.65 ± 0.01	0.24 ± 0.01 ^c	0.13 ± 0.01
24 hour ^b	0.72 ± 0.01 ^d	0.14 ± 0.02	0.14 ± 0.01
28 hour ^b	0.79 ± 0.02 ^d	0.14 ± 0.03	0.08 ± 0.02 ^d
36 hour ^b	0.80 ± 0.01 ^d	0.08 ± 0.01 ^d	0.11 ± 0.01 ^c

Each value is the mean + S.E. of 6-9 samples. The coefficients of variation of the G₁ peak were less than 5%. Control values were taken from Table 1.

^ap < 0.05 vs. control (multivariate analysis of variance).

^bp < 0.01 vs. control (multivariate analysis of variance).

^cp < 0.05 vs. control (t-test).

^dp < 0.01 vs. control (t-test).

30 minutes later. Intervals were chosen such that the maximum changes in cells in S phase, as determined by FCM analysis, would also be evaluated by autoradiographic techniques. Thus, tumors prepared 8 hours and 36 hours after FU treatment, in which the percent of cells in S phase was 28 and 8, respectively, were utilized for autoradiography. In addition, autoradiographic analysis was done on FT (300 mg/kg)-treated tumors 12, 24, and 36 hours after injection in which the fraction of the tumor cell population in S phase was 26, 7, and 8%, respectively. These data are presented in Table 6. Both labeled and degenerate (pkynotic and karyorrhectic) cells were scored. Eight hours after FU treatment, the degenerate index (D.I.) was not different than control. There was a significant increase ($p < 0.01$, Student's t-test) at 36 hours after FU. In contrast, the D.I. increased at 12 and 24 hours after FT treatment and returned to control levels at 36 hours after the initial injection. The labeling indices of S102F tissue sections were observed to change in the same direction as did the fraction of the cells in S phase, as determined by FCM (Tables 4 and 5).

TABLE 6
 AUTORADIOGRAPHY: S102F TISSUE SECTIONS

Treatment: Hr Post Injection ^a	N	Labeling Index	Degenerate Index
Control	4	14.4 \pm 1.7	0.4 \pm 0.1
FU: 8 hr	4	20.6 \pm 1.5	0.4 \pm 0.1
FU: 36 hr	4	0.9 \pm 0.3 ^b	1.0 \pm 0.1 ^b
FT: 12 hr	5	20.6 \pm 1.5	0.8 \pm 0.3
FT: 24 hr	5	3.3 \pm 1.1 ^b	1.0 \pm 0.1
FT: 36 hr	3	0.5 \pm 0.2 ^b	0.4 \pm 0.1

Values represent the mean \pm S.E. of the mean, where N is the number of samples per group.

^aFU: 65 mg/kg, i.p.
 FT: 300 mg/kg, i.p.

^b $p < 0.01$ (Student's t-test) vs. control.

Drug Effects at the Molecular Level:
Tumor and Small Intestine

The incorporation of deoxyuridine into DNA relates, in part, to the activity of thymidylate synthetase and, therefore, was utilized to investigate biochemical lesions induced by FT and FU. Tumor-bearing mice received either FT, FU, or an equivalent volume of 0.9% NaCl solution. At various intervals thereafter, they were injected with $^3\text{H-UdR}$. Thirty minutes later, the mice were killed and the extent of incorporation of the labeled precursor into DNA was measured.

The effect of equimolar doses of FT and FU on $^3\text{H-UdR}$ incorporation into DNA of the S102F tumor is shown in Figure 16. Within 1 hour after administration of FT, the $^3\text{H-UdR}$ incorporation was approximately 25-30% of that observed in the tumors from control animals. $^3\text{H-UdR}$ incorporation had increased significantly at 12 hours after injection, and at 24 hours after treatment, it was not significantly different from controls. FU depressed $^3\text{H-UdR}$ incorporation to 10% of control values for at least 24 hours after drug injection. By 48 hours, it was again elevated significantly and approximated that of controls 72 hours after FU injection.

Drug-induced changes in the extent of $^3\text{H-UdR}$ incorporation into DNA of the small intestine of mice bearing the S102F tumor after systemic administration of equimolar doses of FU and FT are illustrated in Figure 17. Although both drugs depressed incorporation to approximately 10% of the control level at 1 hour after injection, the intestine of animals treated with FT recovered at a faster rate (complete recovery observed in 24 hours) than did that from FU-treated mice. In each case, however, the rate of recovery proceeded more rapidly in the small intestine than in the S102F tumor (Figure 16).

An analogous study was completed in animals bearing the Slow tumor. These results are shown in Figure 18. FT (100 mg/kg) depressed $^3\text{H-UdR}$ incorporation to approximately one-third of control levels for at least 12 hours after treatment, and by 24 hours it had exceeded control levels. However, an equimolar dose of FU depressed incorporation to approximately 15% of control levels for 48 hours after drug injection, and even at 72 hours after treatment, $^3\text{H-UdR}$ incorporation was still only about one-third of the control level. As shown in Figure 19, incorporation of $^3\text{H-UdR}$ into the DNA of the small intestine of animals bearing the Slow tumor was inhibited by about 90% at 1 hour after the injection of either drug. This low level of incorporation was

maintained for 24 hours after FU treatment, whereas the intestine of FT-treated mice returned to control levels within the same period. At 72 hours after FU treatment, $^3\text{H-UdR}$ incorporation in the small intestine of mice bearing the Slow tumor appeared to approximate that of controls. In contrast, $^3\text{H-UdR}$ incorporation in the intestine of animals bearing S102F tumors returned to control levels 48 hours after FU treatment (Figure 17). The data in Figure 20 compare the effect of FT (300 mg/kg) and FU (65 mg/kg) on $^3\text{H-UdR}$ incorporation into DNA of the S102F tumor. $^3\text{H-UdR}$ incorporation is presented as percent of control values. At 1 hour both drugs depressed $^3\text{H-UdR}$ incorporation to 10% of control levels. The rate of recovery of the tumor followed a similar pattern with both drugs.

Incorporation of $^3\text{H-UdR}$ into DNA is sometimes used as an indication of the rate of DNA synthesis (4, 107). However, data obtained by FCM analysis of perturbed S102F tumors did not correlate with the studies of $^3\text{H-UdR}$ incorporation into DNA. For example, $^3\text{H-UdR}$ incorporation into DNA of the S102F tumor after FU treatment was depressed to 10% of control levels for more than 36 hours (Figure 16). But FCM analysis of S102F tumors perturbed by the systemic administration of FU indicated that cells were moving in and out of S phase during that 36 hour

period (Table 5). Thus $\text{Na}_2\text{H}^{32}\text{PO}_4$ incorporation into DNA was utilized as an independent measure of overall DNA synthesis. S102F tumor-bearing animals were treated with FU (65 mg/kg). At 1, 8, 24, or 36 hours after drug administration, the mice were injected with ^{32}P and killed 30 minutes thereafter. The data in Table 7 show that the incorporation of ^{32}P into tumor DNA was depressed to 50% of control levels 1 hour after drug injection. However, incorporation was not significantly different ($p < 0.01$, Student's t-test) from control levels 8 hours after injection. This is in contrast to the results obtained with respect to ^3H -UdR incorporation, which was depressed for more than 48 hours after FU treatment (Figure 16). At 24 and 36 hours after FU treatment, ^{32}P incorporation was again depressed to 50% of control values.

Intestinal Epithelial Cells: Isolation,
Dispersal, and Separation

Techniques were developed to prepare single cell suspensions of intestinal crypt and villus cells for FCM analysis. A phase contrast photomicrograph of an unstained epithelial cell suspension is shown in Figure 21. Crypt cells, which tend to be smaller than villus cells, displayed a high nuclear to cytoplasmic ratio and lacked

TABLE 7
 ^{32}P INCORPORATION INTO DNA OF S102F TUMOR

Time Post Treatment ^a	N	cpm/ μ Mole Deoxyribose
Control	11	576 \pm 64
1 Hour	7	291 \pm 31 ^b
8 Hour	9	429 \pm 90
24 Hour	8	198 \pm 46 ^b
36 Hour	7	252 \pm 44 ^b

Each value represents the mean \pm S.E. of the mean of 7-11 samples.

^aFU (65 mg/kg) injected i.p. at 0 hour.

^bSignificantly different than control, $p < 0.01$ (Student's t-test).

visible microvilli. Villus cells were observed to have distinct brush borders and contained more cytoplasm than did crypt cells.

The dispersal procedure was based on incubation of the small intestine in EDTA and dithiothreitol (94). EDTA was used to dissociate the cells and dithiothreitol acted as a mucolytic agent. Cells were isolated in a sequential manner with upper villus cells being removed early during the incubation period and crypt cells at later time periods. It was necessary to determine the optimal time interval for maximum crypt cell removal. Mice received a 30 minute pulse of $^3\text{H-TdR}$ prior to sacrifice to label the proliferating crypts. Cells were then isolated at 10 minute intervals during the incubation period and radioactivity due to incorporation of the labeled precursor was determined. The results are shown in Table 8. These data demonstrated that the 20-100 minute incubation period yielded cells which had incorporated $^3\text{H-TdR}$ and, thus, were proliferating. Since villus cells are not cycling, the fraction of cells obtained during this incubation interval was utilized as an enriched crypt preparation.

Figure 22a illustrates an enzymatically-stained epithelial cell suspension, as viewed under the light microscope. A small, round crypt cell is located

TABLE 8
INCORPORATION OF ^3H -TdR INTO DNA OF
INTESTINAL EPITHELIAL CELLS

Incubation Period (min)	dpm/ μMole Deoxyribose
0- 20	4,063
20- 40	12,777
40- 50	20,861
50- 60	23,722
60-100	28,684

^3H -TdR was administered to mice 30 minutes prior to cell isolation. Cells were collected during specific intervals of the incubation period in Solution B.

between several hemi-ellipsoid villus cells in the center of the field. Figure 22b depicts the same field of cells, but with fluorescent illumination. The villus cells fluoresced brightly, whereas the crypt cell, with low enzyme activity, had minimal fluorescence. These photomicrographs demonstrate that the leucine aminopeptidase reaction was specific for villus cells.

Crypt and villus cell suspensions, incubated with the leucine aminopeptidase substrate, were analyzed by the FCM equipped with a cell sorter. The resulting histogram was displayed in three dimensions, with enzyme fluorescence viewed as a function of low-angle ($0-7^\circ$) forward scatter (related to cell size) and cell number. Linear amplification of fluorescence and low-angle forward scatter of a mixed epithelial cell preparation is shown in Figure 23 (a and b). Two distinct populations are clearly visible. Logarithmic amplification of enzyme fluorescence and small-angle scatter of the same cell suspension is shown in Figure 24 (a and b). This histogram displayed four distinct populations. Electronic sorting was done on cells comprising the various portions of the histogram. Microscopic examination of sorted cells indicated that the crypts were localized in two areas: the small peak with low fluorescence and high forward angle scatter and the peak which exhibited

relatively high enzyme fluorescence but low forward angle scatter values. The villus cells were located under the largest peak in the histogram, with high enzyme fluorescence and forward angle scatter values. The small peak with low fluorescence and forward angle scatter consisted of debris and cell fragments. Photomicrographs of the sorted crypt and villus populations are shown in Figure 25 (a and b). The amount of villus contamination based on morphological criteria in the crypt sort was less than 0.1%. No crypt cells were found in the sorted villus population.

To ascertain that the cells sorted as crypts were, indeed, the proliferating cells of the small intestine, sorting was done on epithelial cell preparations, obtained from mice who had received a 30 minute pulse of ^3H -TdR prior to cell isolation. Autoradiography was performed on both the sorted crypt and sorted villus populations. The labeling index on the sorted crypts varied from 10-12%. Labeled cells were not observed in the sorted villus fraction.

The histograms shown in Figure 24 (a and b) were obtained under less than optimal enzyme conditions. Due to insufficient amounts of NSA coupler in the original incubation medium, enzyme product produced within the villus cells diffused out into the crypts. Although the

relative position of the crypts along the y-axis of the histogram in Figure 24 indicated that they were smaller than the villus cells, their location along the x-axis indicated that they had considerable enzyme fluorescence. By increasing the amount of NSA in the incubation mixture, according to the procedure described in the Methods section, the histograms shown in Figure 26 (a and b) were obtained. As evidenced from microscopic examination, the crypts were localized along the y-axis. Villus cells, which were larger and more fluorescent than the crypts, were seen along the x-axis with high forward angle scatter values. When alkaline phosphatase, instead of leucine aminopeptidase, was utilized as the fluorescent enzyme marker, histograms similar to those seen in Figure 25 were obtained.

Restaining of the sorted crypt and villus populations with a DNA-specific dye was attempted. The emission spectra of the enzyme product-NSA complex ranges from 480-615 nm (96). The complex can be excited with wavelengths from 340-460 nm. Since the enzyme product remained in the cells indefinitely, a DNA-specific dye with a different emission maximum than the enzyme complex was needed to obtain accurate FCM analysis of DNA distributions of the sorted cells. Hoechst 33258 was chosen for this purpose. Hoechst 33258 is maximally

excited at 350 nm and has a maximum emission at 450 nm. With appropriate filters, e.g., 466 band pass, in the photomultipliers of the FCM, it was possible to block out the enzyme fluorescence and detect only the DNA-specific Hoechst fluorescence. Although many attempts were made to analyze sorted samples stained with Hoechst 33258, the DNA distributions were difficult to evaluate. The sorted villus cells yielded DNA distributions with a definite G_1 peak and a small peak probably due to cell clumps. However, the sorted crypts DNA distribution did not show either an S phase or $G_2 + M$ phase, as would be expected from a proliferating population. 3H -TdR autoradiographic studies were done to verify that the proliferating intestinal epithelial cells were removed from the small intestine during the isolation procedure. These data indicated that: 1) very few labeled cells remained in the intestine after cell isolation, and, 2) the sorted crypt population had a 10-12% labeling index. Thus, although S phase cells were present as determined by autoradiography, they were not detected by FCM analysis.

Several studies were also carried out to determine if it would be possible to simultaneously evaluate epithelial cells stained for LAP and for DNA. Such a technique would eliminate the lengthy sorting

procedure and make it possible to obtain a DNA distribution of only the proliferating crypt cells. Since Hoechst 33258 is maximally excited in the u.v. region, it was verified that u.v. excitation of LAP-stained cells yielded similar histograms as those obtained after excitation at 457 nm. For dual staining, cells were first incubated with the LAP substrate and then stained with Hoechst 33258. Microscopic examination of dually-stained cells showed a fluorescent blue nucleus and yellow cytoplasm. Through a combination of filters placed in the photomultiplier tubes of the FCM, it was possible to distinguish the Hoechst 33258 fluorescence of the proliferating crypts from the Hoechst plus enzyme fluorescence of the villus cells. However, the problem of obtaining an adequate DNA distribution of the crypts remained. Thus, even though the crypt and villus populations could be separated, further work was needed to obtain DNA distributions of the sorted samples. Several experiments are suggested and discussed in the following section.

DISCUSSION

FU and FT have antitumor activity against the S102F and Slow murine mammary tumors. Both drugs are most effective when administered as a single, large dose. Multiple injections of FT given to animals bearing the S102F tumor have somewhat greater anti-tumor effects than do maximally tolerated doses of FU (Figure 4). In animals bearing the Slow tumor, multiple injections of either drug have similar antitumor activity (Figure 6). Although FT has been reported by some investigators to have twice the therapeutic index of FU (66, 67), other reports have indicated that FT is not more effective than or even as effective as FU (76, 101, 102). Van Putten et al. (103) showed that FU, in a single dose, was two- to three-fold more potent than FT against leukemic stem cells. However, with multiple dose treatment, FU was much more potent than FT. Results presented in this study demonstrate that FU is two to three times more potent than FT on a molar basis. Single or multiple dose treatments do not seem to affect this ratio. However, similar anti-tumor effects can be achieved with larger doses of FT.

The advantage of FT over FU lies in the decreased host toxicity at a dose which results in similar antitumor activity. In all cases, animals which received FT recovered from drug-induced toxicity at a faster rate than did FU-treated mice (Figures 5, 7, 9, 11). In fact, mice bearing the Slow tumor did not completely recover from the toxic effects of FU given either as a single injection or in a multiple injection regimen. Moreover, host toxicity persisted beyond the period of effective antitumor activity. Based on these results, it may be concluded that FT is less toxic to the host than FU when the two drugs are administered at equally effective tumor doses (Figures 8 and 9).

The decreased toxicity of FT might be due to a variety of factors. Van Putten et al. and others (103) reported that FU was two to three times more potent than FT in killing hematopoietic stem cells. Moderate leukopenia and thrombocytopenia were observed following administration of FT (133 mg/kg) and FU (23 mg/kg) for six days by Hrsak et al. (69). However, the decrease in the total number of colony forming units (CFUS) following FT administration was less than that observed after treatment with FU. In addition, subsequent recovery of CFUS in the marrow was more rapid after FT. Clinical trials have also indicated that FT is less

myelosuppressive than conventional FU therapy (65, 68, 71-75, 104). Variances in the physiologic disposition and metabolism of FT may also contribute to its decreased toxicity compared to FU (79).

Another major part of this study was to compare the cell cycle perturbations induced by FT and FU. FCM analysis of DNA distributions of cells in suspension is a rapid method by which cell cycle perturbations can be examined. However, FCM analysis of the DNA content of solid tumors necessitates tumor dispersal into single cell suspensions. TPB, a potassium-complexing agent, was utilized as an agent to aid dispersal of solid murine tumors into single cells. TPB-dispersed S102F tumor cells yield superior DNA distributions than those obtained by a previously reported mechanical dispersal technique (105).

The TPB dispersal technique was utilized to compare the in vivo cell cycle effects of FT and FU on the S102F tumor. FT (100 mg/kg) induced small but statistically significant increases in the fraction of cells in G₁ phase up to 8 hours after injection (Table 3). At 24 hours after treatment, the cell cycle age distributions appeared to have returned to control values. Since dramatic antitumor effects were not observed with a single injection of FT (100 mg/kg)

(Figure 4), it is perhaps not surprising that marked cell cycle perturbations were not observed. FT administered at a dose of 300 mg/kg exerted more dramatic effects on tumor growth (Figure 8) and on the age distribution of S102F tumor cells (Table 4). For example, a one and one-half-fold increase in the percent of cells in S phase was noted at 12 hours after injection of the drug. This possibly may be indicative of a drug-induced decrease in the rate of transit of cells through this phase of the proliferating cycle. The decreased percentage of cells in $G_2 + M$ at this time is consistent with this possibility. At 24 hours after treatment, an increase in the percent of cells in G_1 and a corresponding decrease in the percent of cells in S phase were observed. These results suggest that a synchronized cohort of cells arrested in early S phase at 12 hours had progressed through S, G_2 , and M (total duration in unperturbed tumors, 12 hours) and into G_1 . The fact that the phase distribution at 36 hours was almost identical to that observed at 24 hours suggests that the synchronization induced by FT treatment was maintained, at least, for a duration approximately equivalent to two cell cycles. Since the FCM analysis does not provide any information about dead or dying cells, or about changes in cell cycle phase durations, i.e., transit

times, a more detailed understanding of the mechanism of FT-induced cell cycle perturbations will be attained only after evaluation by other experimental techniques, such as percent labeled mitoses analysis and autoradiography. Limited autoradiographic studies were performed at selected intervals after drug treatment to verify that changes in the S phase populations did represent actual cell cycle perturbations and were not merely artifacts of the FCM analysis. For example, FCM analysis indicated that the percent of cells in S phase at 24 and 36 hours after treatment with FT (300 mg/kg) was 7 and 8%, respectively (Table 4). This may be compared to a value of 17% in control tumors. Autoradiography also indicated a significant decrease in the labeling index of S102F tissue sections prepared at those same time points (Table 6). These data indicate that FCM analysis accurately reflected in vivo cell cycle perturbations.

The effects of FU (65 mg/kg) on S102F tumor DNA distributions were also examined. FCM analysis revealed that there was a marked increase in the fraction of the tumor cell population in S phase between 2 and 16 hours after drug injection (Table 5). Studies at later intervals indicated that cells which had accumulated in S phase were released shortly thereafter. Thus, the

increased percent of cells in G_1 phase at 28 hours might be interpreted as having resulted from the progression of a cohort of cells released from an S phase block sometime between 14 and 24 hours. However, the fact that the proportion of cells in G_1 phase remained elevated 36 hours after treatment might also suggest the possibility of a G_1/S block. These data are consistent with the hypothesis that FU initially induced an accumulation of cells in S phase and then at 24-28 hours after drug injection prevented cells from making the G_1 to S phase transition. A G_1/S block following treatment with FU was also reported by Kovacs et al. (4) in studies on the rat hepatoma 3924A.

FU, after conversion to FUdRP, is believed to exert its antitumor and toxic effects through inhibition of thymidylate synthetase (27, 28). Since FT is believed to be a depot form of FU, it was of interest to compare the effects of equimolar doses of FT and FU on thymidylate synthetase activity in the S102F and Slow tumors and in the small intestine. In both tumors, $^3\text{H-UdR}$ incorporation was depressed to one-third of control levels within 24 hours. $^3\text{H-UdR}$ incorporation was depressed by 90% at 1 hour after FU (65 mg/kg) and only began to recover 48-72 hours later. Therefore, in both tumors, FU was a more potent inhibitor of thymidylate synthetase than an equimolar dose of FT. Similar

results were obtained in the small intestine of both S102F and Slow tumor-bearing animals. These data are in agreement with those of Cohen (106), who reported less inhibition and faster recovery of $^3\text{H-UdR}$ incorporation into DNA of rat small intestine after FT than FU, in equimolar doses. In previously reported studies (106), neither FT or FU inhibited thymidine incorporation into DNA, another indication that both drugs acted on thymidylate synthetase.

As discussed above, FCM analysis of FT and FU-treated S102F tumors indicated that cells were moving in and out of S phase during the 24-36 hour period studied. However, $^3\text{H-UdR}$ incorporation into DNA of the S102F tumor was depressed for at least 24 hours after both FU (65 mg/kg) and FT (300 mg/kg). Therefore, in order to resolve this apparent contradiction, the incorporation of $\text{Na}_2\text{H}^{32}\text{PO}_4$ into tumor cell DNA was utilized as an index of overall DNA synthesis. The results obtained from studies of ^{32}P incorporation (Table 7) in mice treated with FU (65 mg/kg) correlated with FCM analysis of tumor DNA distributions (Table 5). It was assumed that such a correlation would also be found for FT-treated tumors. These data suggest that results obtained from in vivo $^3\text{H-UdR}$ incorporation studies in animals treated with fluorinated pyrimidines provide an

indication of drug effects on thymidylate synthetase activity but do not accurately reflect ongoing DNA synthesis. Therefore, previously reported studies in which $^3\text{H-UdR}$ incorporation was utilized as an index of the rate of DNA synthesis (4, 107), should be re-evaluated in the light of this finding. Thus, even in the presence of an almost complete inhibition of thymidylate synthetase, tumor cells may utilize salvage pathways to generate thymidine triphosphate (108). The data obtained in the studies with ^{32}P indicate that mouse mammary tumor cells can use these pathways to maintain moderate rates of DNA synthesis after treatment with fluorinated pyrimidines.

In order to utilize FCM for analysis of the age distribution of the proliferating crypts, it is necessary to obtain a pure crypt cell suspension. Several procedures have been described for obtaining "crypt" preparations from the small intestine of the rat (94, 109, 110). In this study, modifications of published procedures were utilized to obtain crypt epithelial cells from the small intestine of mice. Although most of these techniques did yield enriched crypt cell populations, the final preparations were always contaminated by variable amounts of villus epithelium. In addition, cell clumping was a common problem in all the preparations.

The protocol described by Weiser (94) for isolating epithelial cells was modified and optimized for the mouse small intestine. The modified technique yielded a suspension of intact epithelial cells. Experiments in which ^3H -TdR was injected prior to crypt isolation indicated a six-fold increase in the specific activity of the crypt preparation as compared to that in the initial villus fraction (Table 8).

Cells obtained by this technique were primarily single, although some clumping did occur. Microscopic examination indicated the clumps were due to fragments of crypt and villus epithelia which had not been separated and to contaminating mucus which tended to aggregate the single cells. Undispersed epithelial fragments were separated by passage of the suspension through needles of successively smaller diameter and subsequent filtration through 37 μm nylon mesh. Mucus originating from the intestinal goblet cells and the ground substance of the submucosa (111) posed a more difficult problem. Several mucolytic agents, such as N-acetyl-l-cysteine and dithiothreitol were utilized with moderate success. The most effective mucolytic procedure involved incubation of the isolated epithelial cells in a solution containing ascorbic acid, hydrogen peroxide, and copper sulfate. This combination was

originally described for use in bronchial inhalers (112) and was reported to irreversibly cleave mucoprotein bonds (95). It did not appear to affect epithelial cell viability, as measured by trypan blue exclusion, or cell morphology.

It is known that crypt and villus cells differ both morphologically and biochemically. Villus cells are highly specialized for digestive and absorptive functions, whereas the crypt cells are proliferating and nondifferentiated. It has been shown with both tissue sections and fractionated epithelial cell homogenates that specific enzymes are localized primarily in villus epithelia (108, 113-115). Nonspecific esterases, alkaline phosphatase, lactate dehydrogenase, leucine aminopeptidase, and a variety of other enzymes are found to increase in activity as the crypt cell migrates onto the villus. Several of these enzymes, including leucine aminopeptidase and alkaline phosphatase, are associated with microvilli (108, 113, 116-119). Crypt cells contain very few microvilli, which only begin to appear in great numbers as these cells migrate onto the villus.

Fluorescent enzyme histochemical reactions were utilized in combination with the FCM to separate the crypt and villus populations. Leucine aminopeptidase (LAP) acts to split off the terminal amino acids from

proteins and polypeptides (120). It reacts most rapidly with leucine-containing compounds. Since this enzyme exhibits high activity in epithelial cell brush borders (e.g., microvilli), it was reasoned that a fluorescent enzyme product should be preferentially localized in villus cells. L-leucyl-4-methoxy- β -naphthylamide is hydrolyzed to LAP to yield a free naphthylamine (96). This product exhibits a blue fluorescence but is extremely soluble and will easily diffuse out of the area of enzyme activity. Therefore, a coupling agent, NSA, was utilized to precipitate the reaction product in situ. NSA is nonfluorescent. However, when NSA is coupled to naphthylamines by a Schiff-base reaction, the fluorescence of the naphthylamine shifts to longer wavelengths, and the resulting complex has a yellow-orange fluorescence.

FCM analysis and subsequent cell sorting of enzymatically-stained cells indicated that crypt and villus cells could be separated on the basis of LAP activity (Figures 23-26). Autoradiographic studies on unsorted and sorted epithelial cells indicated that all of the radioactive label was associated with crypt cells.

Attempts to restrain the sorted crypt and villus populations with a DNA-specific dye met with minimal success. The NSA-LAP product complex remained inside

the cell and could not be removed either by alkali treatment or by solvent extraction. Thus, restaining the sorted LAP-stained cells with a DNA-specific dye necessitated the use of a dye with a different emission spectrum than that of the enzyme product complex. Spectral analysis of the NSA-enzyme product indicated that the complex could be excited between 340 and 460 nm and that the emission spectrum was between 480 and 615 nm, with peaks at 530 and 595 nm (data not shown). Therefore, a DNA-specific dye with minimal green-red fluorescence was needed. Spectral analysis of several of the commonly available stains (chromomycin, propidium iodide, etc.) indicated that Hoechst 33258 was one of the few DNA stains which fulfilled this criterion. Hoechst 33258 is maximally excited in the ultraviolet region and has a maximum emission wavelength of 460 nm. With appropriate filters in the photomultipliers of the FCM, it was possible to block out the enzyme product fluorescence and detect only the DNA-specific Hoechst fluorescence. Although an acceptable DNA distribution of the sorted villus cells was obtained, Hoechst 33258-stained crypts yielded uninterpretable DNA distributions. The S and $G_2 + M$ phases were not discernible, whereas a peak which might have represented G_1 cells was unusually broad. Part of the problem encountered in restaining

the sorted cells may have resulted from the choice of the DNA-specific dye, Hoechst 33258. In order to obtain nuclear fluorescence with minimal cytoplasmic fluorescence, the concentration of the dye was fifty-fold lower than that used in previously reported protocols with Chinese hamster ovary cells (98). Although only the nucleus appeared to fluoresce under these conditions, it is possible that the fluorescence of the crypt nucleus was not stoichiometrically related to DNA. It has been shown with particular stains that the characteristics of DNA-staining may vary from one cell type to another (121-124). The fact that it was necessary to drastically reduce the Hoechst 33258 concentration might also indicate that the intestinal crypt cells stain differently than other cell types.

Additional studies are needed to resolve the problems observed in obtaining a DNA distribution of the intestinal crypt cells. For example, individual measurements of the amount of DNA in Hoechst 33258-stained cells should be correlated with their location in the DNA distribution obtained by FCM. Such a study would confirm the possibility that crypt nuclear fluorescence was not stoichiometrically related to DNA. If this were the case, further modifications of the DNA-staining protocol could then be made. The use of NSA as a coupling

reagent in the enzyme reaction may also contribute to the problem of obtaining interpretable crypt DNA distributions. Aromatic aldehydes react with proteins containing either aromatic amines or primary aliphatic amino groups, e.g., γ - or ϵ -amino groups. NSA, like formaldehyde and ethanol, is bound to cell proteins, producing a weak, greenish background fluorescence. The possibility exists that NSA may bind to the nuclear histones involved in maintaining DNA structure and, hence, affect the stoichiometry of a DNA-specific dye.

Since an adequate DNA distribution of Hoechst-stained cells was not obtained, the effects of FU and FT on the age distribution of the proliferating crypts were not evaluated. Although further development of the DNA staining procedure is needed, the separation of enzymatically-stained crypt and villus cells by the FCM was successful.

REFERENCES

1. C. Heidelberger, L. Greisbach, C. Cruz, R.J. Schnitzer, and E. Grunberg. Fluorinated pyrimidines VI. Effects of 5-fluorouridine and 5-fluoro-2'-deoxyuridine on transplantable tumors. Proc. Soc. Exptl. Biol. Med. 97, 470-473 (1958).
2. C. Heidelberger and F.J. Ansfield. Experimental and clinical use of fluorinated pyrimidines in cancer chemotherapy. Cancer Res. 23, 1226-1243 (1960).
3. D. Kessel, T.C. Hall, and I. Wodinsky. Nucleotide formation as a determinant of 5-fluorouracil response in mouse leukemias. Science 154, 911-913 (1966).
4. C.J. Kovacs, H.H. Hopkins, R.M. Simon, and W.B. Looney. Effects of fluorouracil on the cell kinetic and growth parameters of hepatoma 3924A. Br. J. Cancer 32, 42-50 (1975).
5. M. Umeda and C. Heidelberger. Comparative studies of fluorinated pyrimidines with various cell lines. Cancer Res. 28, 2529-2538 (1968).
6. R.G. Hahn, C.G. Moertel, A.J. Schutt, and H.W. Bruckner. A double-blind comparison of intensive course 5-fluorouracil by oral vs. intravenous route in the treatment of colorectal carcinoma. Cancer 4, 1031-1036 (1975).
7. R.B. Livingston and S.K. Carter. Single Agents in Cancer Chemotherapy, pp. 195-226. IFI/Plenum, New York, 1970.
8. F.J. Ansfield, J.M. Schroeder, and A.R. Curreri. Five year's clinical experience with 5-fluorouracil. JAMA 181, 295-299 (1962).
9. H.L. Davis, Jr., G. Ramirez, and F.J. Ansfield. Adenocarcinomas of stomach, pancreas, liver and biliary tracts. Cancer 33, 193-197 (1974).

10. B.L. Tranum, R.L. Stephens, D.E. Lehane, B. Hoogstraten, M. Lane, and A. Hout. Adriamycin (NSC-123127) Plus 5-Fluorouracil (NSC-19893): A Phase I Study. Cancer Chemotherapy Report, Part I, 59, 1163-1165 (1975).
11. P.T. Otis and S.A. Armentrout. Combination chemotherapy in metastatic carcinoma of the breast. Cancer 36, 311-317 (1975).
12. R.H. Creech, R.B. Catalano, M.J. Mastrangelo, and P.F. Engstrom. An effective low-dose intermittent cyclophosphamide, methotrexate, and 5-fluorouracil treatment regimen for metastatic breast cancer. Cancer 35, 1101-1107 (1975).
13. H.B. Muss, J.J. Lokich, and E. Frei. 5-Fluorouracil with cytosine arabinoside in metastatic gastrointestinal cancer. Clin. Pharmacol. and Therap. 18, 234-237 (1975).
14. R.J. Rutman, W. Cantarow, and K.E. Paschkus. Studies in 2-acetylaminofluorene carcinogenesis III. Utilization of uracil-2-C¹⁴ by preneoplastic rat liver and hepatoma. Cancer Res. 14, 119-123 (1954).
15. R. Duschinsky, E. Plevan, and C. Heidelberger. The synthesis of 5-fluoropyrimidines. J. Am. Chem. Soc. 79, 4559-4560 (1957).
16. T.C. Hsu, R.M. Humphrey, and C.E. Sommers. Responses of Chinese hamster and L cells to 2'-deoxy-5-fluoro-uridine and thymidine. J. Natl. Canc. Inst. 32, 839-855 (1964).
17. S.S. Cohen, J.G. Flaks, H.P. Barner, M.R. Loeb, and J. Lichtenstein. The mode of action of 5-fluorouracil and its derivatives. Proc. Natl. Acad. Sci. 44, 1004 (1958).
18. W.R. Bruce and B.E. Meeker. Comparison of the sensitivity of hematopoietic colony-forming cells in different proliferative states to 5-fluorouracil. J. Natl. Cancer Inst. 38, 401-405 (1967).
19. P.B. Danneberg, B.J. Montag, and C. Heidelberger. Studies on fluorinated pyrimidines. IV. Effects on nucleic acid metabolism in vivo. Cancer Res. 18, 328-334 (1958).

20. N.K. Chaudhuri, B.J. Montag, and C. Heidelberger. Studies on fluorinated pyrimidines. III. The metabolism of 5-fluorouracil-2-C¹⁴ and 5-fluorourotic-2-C¹⁴ acid in vivo. Cancer Res. 18, 318-328 (1958).
21. L. Bosch, E. Harbers, and C. Heidelberger. Studies on fluorinated pyrimidines V. Effects on nucleic acid metabolism in vitro. Cancer Res. 18, 335-343 (1958).
22. M.K. Gleason and H. Fraenkel-Conrat. Biological consequences of incorporation of 5-fluorocytidine in RNA of 5-fluorouracil-treated eukaryotic cells. Proc. Natl. Acad. Sci. U.S.A. 73, 1528-1531 (1976).
23. K.U. Hartman and C. Heidelberger. Studies on fluorinated pyrimidines XIII. Inhibition of thymidylate synthetase. J. Biol. Chem. 263, 3006-3013 (1961).
24. C. Heidelberger, "Fluorinated pyrimidines," in, Progress in Nucleic Acid Research and Molecular Biology (J.N. Davidson and W.I. Cohn, eds.), pp. 1-50. Academic Press, New York, 1965.
25. D.S. Wilkinson, T.D. Tlsty, and R.J. Hanas. The inhibition of ribosomal RNA synthesis and maturation in Novikoff hepatoma cells by 5-fluorouridine. Cancer Res. 35, 3014-3020 (1975).
26. D.S. Wilkinson and J. Crumley. The mechanism of 5-fluorouridine toxicity in Novikoff hepatoma cells. Cancer Res. 36, 4032-4038 (1976).
27. C. Heidelberger, A. Ghobar, R.K. Barker, and K.L. Mukherjee. Studies of fluorinated pyrimidines. X. In vivo studies on tumor resistance. Cancer Res. 20, 897-902 (1960).
28. R.J. Langenbach, P.V. Dannenberg, and C. Heidelberger. Thymidylate synthetase: Mechanism of inhibition by 5-fluoro-2'-deoxyuridylate. Biochem. Biophys. Res. Commun. 48, 1565-1571 (1972).
29. N.K. Chaudhuri, K.L. Murkerjee, and C. Heidelberger. Studies on fluorinated pyrimidines. IV. The degradative pathway. Biochem. Pharmacol. 1, 328-341 (1958).

30. B. Clarkson, A. O'Connor, L. Winston, and D. Hutchison. The physiologic disposition of 5-fluorouracil and 5-fluoro-2'-deoxyuridine in man. Clin. Pharmacol. Therap. 5, 581-610 (1964).
31. K.L. Mukherjee, J. Boohar, D. Wentland, F.J. Ansfield, and C. Heidelberger. Studies on fluorinated pyrimidines. XVI. Metabolism of 5-fluorouracil-2-C¹⁴ in cancer patients. Cancer Res. 23, 49-77 (1963).
32. K.L. Mukherjee and C. Heidelberger. Studies on fluorinated pyrimidines. IX. The degradation of 5-fluorouracil-6-C¹⁴. J. Biol. Chem. 235, 433-437 (1960).
33. H.R. Nitze, K. Vosteen, and U. Ganzer. Radiation treatment of human tumors following the in vivo synchronization of the cell cycle. Acta Otolaryng. 71, 227-231 (1971).
34. J.M. Venditti. Treatment schedule dependency of experimentally active antileukemic (L1210) drugs. Cancer Chemother. Rep. 2, 35-59 (1971).
35. B.D. Clarkson. Acute myelocytic leukemia in adults. Cancer 30, 1572-1582 (1972).
36. M.D. Dowling, T.S. Gee, B.J. Lee, B.D. Clarkson, and J.H. Burchenal. Treatment of acute non-lymphoblastic leukemia with arabinosylcytosine (Ara C) and 6-thioguanine (TG) every 12 hours. Proc. Am. Assn. Cancer Res. 13, 21 (1972).
37. A. Howard and S.R. Pelc. Synthesis of Desoxyribonucleic acid in normal and irradiated cells and its relation to chromosome breakage. Heredity Suppl. 6, 261 (1953).
38. H. Quastler and F.G. Sherman. Cell population kinetics in the intestinal epithelium of the mouse. Exp. Cell Res. 17, 420-438 (1959).
39. R. Baserga, R.D. Estensen, and R.D. Petersen. Inhibition of DNA synthesis in Ehrlich Ascites cells by Actinomycin D. II. The presynthetic block in the cell cycle. Proc. Natl. Acad. Sci. U.S.A. 54, 1141-1148 (1965).

40. S. Kishimoto and I. Lieberman. Synthesis of RNA and protein required for the mitosis of mammalian cells. Exptl. Cell Res. 36, 92-101 (1964).
41. T.P. Brent, J.A.V. Butler, A.A. Crathorn. Variations in phosphokinase activities during the cell cycle in synchronous populations of HeLa cells. Nature (London) 207, 176-177 (1965).
42. I.L. Cameron and R.C. Greulich. Evidence for an essentially constant duration of DNA synthesis in renewing epithelia of the adult mouse. J. Cell Biol. 18, 31-40 (1963).
43. K.G. Lark. Regulation of chromosome replication and segregation in bacteria. Bacteriol. Rev. 30, 3-32 (1966).
44. S.A. Muphree, E. Stubblefield, and E.C. Moore. Synchronized mammalian cell cultures III. Variation of ribonucleotide reductase during the replication cycle of Chinese hamster fibroblasts. Exp. Cell Res. 58, 118-124 (1969).
45. D.M. Prescott and M.A. Bender. Synthesis of RNA and protein during mitosis in mammalian tissue culture cells. Exp. Cell Res. 26, 260 (1962).
46. J.H. Taylor. Nucleic acid synthesis in relation to the cell cycle division. Ann. N.Y. Acad. Sci. 90, 409-421 (1960).
47. M.L. Mendelsohn. The growth fraction: A new concept applied to tumors. Science 132, 1496 (1960).
48. W.R. Bruce and H.A. Van der Gaag. Quantitative assay for the number of murine lymphoma cells capable of proliferation in vivo. Nature (London) 199, 79-80 (1963).
49. F. Valeriote and L. Van Putten. Proliferation-dependent cytotoxicity of anticancer agents: A review. Cancer Res. 35, 2619-2630 (1975).
50. A.F. Hermens and G.W. Barendsen. Changes of cell proliferation kinetics in rat rhabdomyosarcoma before and after X-irradiation. Eur. J. Can. 5, 173-189 (1973).

51. W.S. Wilcox, D.P. Griswold, W.R. Laster, Jr., F.M. Schabel, Jr., and H.E. Skipper. Experimental evaluation of potential anticancer agents XVII Kinetics of growth and regression after treatment of solid tumors. Cancer Chemother. Rep. 47, 27-39 (1965).
52. M. Omine and S. Perry. Cytokinetic characterization of small cells in spontaneous AKR leukemia. Blood 40, 952 (1972).
53. F.M. Schabel, Jr. The use of tumor growth kinetics in planning "curative" chemotherapy of advanced solid tumors. Cancer Res. 29, 2384-2389 (1969).
54. W.R. Bruce, B.E. Meeker, and F.A. Valeriote. Comparison of the sensitivity of normal hematopoietic and transplanted lymphoma colony-forming cells to chemotherapeutic agents administered in vivo. J. Natl. Cancer. Inst. 37, 233-245 (1966).
55. H. Madoc-Jones and W.R. Bruce. On the mechanism of the lethal action of 5-fluorouracil on mouse L cells. Cancer Res. 28, 1976-1981 (1968).
56. B.K. Bhuyan, L.G. Scheidt, and T.J. Fraser. Cell cycle phase specificity of antitumor agents. Cancer Res. 32, 398-407 (1972).
57. C.B. Lozzio. Lethal effects of fluorodeoxyuridine on cultured mammalian cells at various stages of the cell cycle. Cell Physiol. 74, 57-62 (1969).
58. S.S. Milles, A.L. Muggia, and H.M. Spiro. Colonic histologic changes induced by 5-fluorouracil. Gastroenterology 43, 391-399 (1962).
59. R.C. Stalzer, J.M. Kiely, G.L. Pease, and A.L. Brown, Jr. Effects of 5-fluorouracil on human hematopoiesis. Cancer 18, 1071-1078 (1965).
60. V.K. Vaitkevicius, M.J. Brennan, V.L. Beckett, J.E. Kelley, and R.W. Talley. Clinical evaluation of cancer chemotherapy with 5-fluorouracil. Cancer 14, 131-152 (1961).
61. P. Seifert, L.H. Baker, M.L. Reed, and V.K. Vaitkevicius. Comparison of continuously infused 5-fluorouracil with bolus injection in treatment of patients with colorectal adenocarcinoma. Cancer 36, 123-128 (1975).

62. M.J. Brennan, V.K. Vaitkevicius, and J.W. Rebeck. Megaloblastic anemia associated with inhibition of thymine synthesis (Observations during 5-fluorouracil treatment). Blood 16, 1535-1545 (1960).
63. S.A. Hiller, R.A. Zhuk, and M.Y. Lidak. Analogs of pyrimidine nucleosides. I. N₁-(α -tetrahydrofuryl) derivatives of natural pyrimidine bases and their antimetabolites. Dokl. Acad. Nauk SSSR 176, 332-335 (1967).
64. N.G. Blokhina, E.K. Vozny, and A.M. Garin. Results of treatment of malignant tumors with Ftorafur. Cancer 30, 390-392 (1972).
65. A. Cichy, L. Jurga, and M. Klvana. Experience with furanidyl-fluorouracil in advanced tumors of the breast. Neoplasma 21, 723-732 (1974).
66. Russian Ftorafur brochure.
67. I.M. Kravenki and A.A. Zidermane. Antineoplastic activity of Ftorafur [N₃-(2'-furanidyl)5-fluorouracil] in experimental animals. Presented at the First All-Union Conference on the Chemotherapy of Malignant Tumors. Riga, October 7-11, 1968, pp. 214-225.
68. R.A. Earl and L.B. Townsend. The synthesis of 1-(tetrahydro-2-furanyl)-5-fluorouracil (Ftorafur) via direct fluorination (I.) J. Heterocyclic Chem. 9, 1141-1143 (1972).
69. I. Hrsak and S. Pavicic. Comparison of the effects of 5-fluorouracil and Ftorafur on the haematopoiesis in mice. Biomed. 21, 164-167 (1974).
70. R.K. Johnson, B.T. Garibjanian, D.P. Houchens, I. Kline, M.R. Gaston, A.B. Syrkin, and A. Goldin. Comparison of 5-fluorouracil and Ftorafur. I. Quantitative and qualitative differences in toxicity to mice. Cancer Treatment Reports 60, 1335-1345 (1976).
71. C. Konda, H. Nithani, N. Sakauchi, et al. Chemotherapy of cancer with oral administration of N₁-(2'-furanidyl)-5-fluorouracil (FT-207). Jpn. J. Cancer Clin. 19, 495-499 (1973).

72. N. Karev, N. Blokhina, E.K. Vozny, et al. Comparative evaluation of the efficacy of Ftorafur and 5-fluorouracil in the treatment of breast cancer. Minerva Med. 65, 2811-2814 (1974).
73. N.I. Karev, N.G. Blokhina, E.K. Vozny, et al. Experience with Ftorafur treatment in breast cancer. Neoplasma 19, 347-350 (1972).
74. T. Hattori, H. Furure, and K. Furukawa. Clinical experiences with FT-207. Jpn. J. Cancer Clin. 19, 50-53 (1973).
75. M. Valdivieso, G.P. Bodey, J.A. Gottlieb, and E.J. Freireich. Clinical evaluation of Ftorafur (pyrimidine-deoxyribose N,-2'-furanidyl-5-fluorouracil). Cancer Res. 36, 1821-1824 (1976).
76. B.T. Garibjanian, R.K. Johnson, I. Kline, S. Vadlamudi, M. Gang, J.M. Venditti, and A. Goldin. Comparison of 5-fluorouracil and Ftorafur. II. Therapeutic response and development of resistance in murine tumors. Cancer Treatment Reports 60, 1347-1361 (1976).
77. A.Z. Smolyanskya and D.A. Tugarinov. To biological activity of antitumor antimetabolite "Ftorafur." Neoplasma 19, 341-346 (1972).
78. J.P. Horwitz, J.J. McCormick, K.D. Philips, et al. In vitro biological evaluation of the R and S isomers of 1-(tetrahydrofuran-2-yl)-5-fluorouracil. Cancer Res. 35, 1301-1304 (1974).
79. A.M. Cohen. The disposition of Ftorafur in rats after intravenous administration. Drug Metab. Disp. 3, 303-308 (1975).
80. D.V. Meiren and A.K. Belousova. On the mechanism of action of Ftorafur, a new antitumor agent. Vopr. Med. Khim. 18, 288-293 (1972).
81. S. Fujii, H. Okuda, H. Toide, et al. Fate of 1-(2-tetrahydro-furyl)-5-fluorouracil (FT-207), an anti-tumor agent. I. Absorption, tissue distribution and excretion. Oyo Uakuri 8, 597-604 (1974).
82. H. Fujita, K. Ogawa, T. Sawabe, et al. In vivo distribution of N₁-(2'-tetrahydrofuryl)-5-fluorouracil (FT-207). Jpn. J. Cancer Clin. 18, 911-916 (1972).

83. R.A. Tobey and H.A. Crissman. Use of flow micro-fluorometry in detailed analysis of effects of chemical agents on cell cycle progression. Cancer Res. 32, 2726-2732 (1972).
84. R.A. Tobey and H.A. Crissman. Comparative effects of three nitrosourea derivatives on mammalian cell cycle progression. Cancer Res. 35, 460-470 (1975).
85. C. Rappaport and G.B. Howze. Dissociation of adult mouse liver by sodium tetraphenylboron, a potassium complexing reagent. Proc. Soc. Exptl. Biol. Med. 121, 1010-1025 (1966).
86. M.G. Pallavicini, A.M. Cohen, L.A. Dethlefsen, and J.W. Gray, "Dispersal of solid tumors for flow cytometer (FCM) analysis," in Pulse-Cytophotometry Proceedings of the Third International Symposium on Pulse Cytophotometry (D. Lutz, ed.). European Press, Ghent, Belgium (In press, 1977).
87. M. L. Mendelsohn and L.A. Dethlefsen, in "Cell kinetics in breast cancer: The turnover of non-proliferating cells." Recent Results in Cancer Research (M.L. Griem, E.V. Jensen, J.E. Ultmann, and R.W. Wissler (eds.)), Vol. 42 pp. 73-86. Springer, New York, 1973.
88. M.L. Mendelsohn and L.A. Dethlefsen. Effects of selection and passage on volumetric growth rate of mouse mammary tumors. Lawrence Livermore Laboratory Report UCRL-51798 (1975).
89. L.A. Dethlefsen, J.M.S. Prewitt, and M.L. Mendelsohn. The analysis of tumor growth curves. J. Natl. Cancer Inst. 40, 389-405 (1968).
90. C.G. Morley and H.S. Kingdon. Use of ³H-thymidine for measurement of DNA synthesis in rat liver--A warning. Analyt. Biochem. 45, 298-305 (1972).
91. K. Burton. A study of the conditions and mechanism of the diphenylamine reaction for the colorimetric estimation of deoxyribonucleic acid. Biochem. J. 62, 315-323 (1956).
92. W.C. Schneider. Determination of nucleic acids in tissues by Pentose Analysis. Methods Enzymol. 3, 680-684 (1957).

93. J.E. Gill and M.M. Jotz. Deoxyribonucleic acid cytochemistry for automated cytology. J. Histochem. Cytochem. 22, 470-477 (1974).
94. M.M. Weiser. Intestinal epithelial cell surface membrane glycoprotein synthesis. I. An indicator of cellular differentiation. J. Biol. Chem. 248, 2536-2541 (1973).
95. W.V. Robertson, M.W. Ropes, and W. Beaver. Degradation of mucins and polysaccharides by ascorbic acid and hydrogen peroxide. Biochem. J. 35, 903-908 (1941).
96. F.A. Dolbeare and R.E. Smith. The flow cytometric measurement of peptidases with 5-nitrosalicylaldehyde and 4-methoxy- β -naphthylamine derivatives. Clin. Chem. (In press, 1977).
97. H.A. Crissman and R.A. Robey. Cell cycle analysis in 20 minutes. Science 184, 1297-1298 (1974).
98. S.A. Latt, Y.S. George, and J.W. Gray. Flow cytometric analysis of BRDU substituted cells stained with 33258 Hoechst. J. Histochem. Cytochem. (In press, 1977).
99. M. van Dilla, L. Steinmetz, D. Davis, R. Calvert, and J.W. Gray. High speed cell analysis and sorting with flow systems: Biological applications and new approaches. IEE. Trans. Nucl. Sci.: NS-21, 714-720 (1974).
100. P.N. Dean and J.J. Jett. Mathematical analysis of DNA distributions derived from flow microfluorometry. J. Cell Biol. 60, 523-527 (1974).
101. N. Unemi, K. Itarima, Y. Daidai, et al. Experimental studies on antineoplastic action of N₁-(2'-tetrahydrofuryl)-5-fluorouracil (FT-207) - Effect on experimental tumors. Jpn. J. Cancer Clin. 17, 731-742 (1971).
102. S. Fujii, S. Watanabe, Y. Yasuda, et al. Experimental studies of N₁-(2'-tetrahydrofuryl)-5-fluorouracil (FT-207). Antitumor activity after oral administration. Oyo Yakuri 7, 1277-1292 (1973).

103. L.M. van Putten, L.K.J. Kram-Idsenga, and M. Pijbers-Debruin. A comparison of the cell killing in the mouse after exposure to Ftorafur and 5-fluorouracil (Abstr.) Br. J. Cancer 30, 179-180 (1974).
104. C.R. Smart, L.B. Townsend, W.J. Rusho, H.J. Eyre, J.M. Quagliana, M.L. Wilson, C.B. Edwards, and S. J. Manning. Phase I study of Ftorafur, an analog of 5-fluorouracil. Cancer 36, 103-106 (1975).
105. L.A. Dethlefsen, J.W. Gray, Y.S. George, S. Johnson. "Flow cytometric analysis of the perturbed cellular kinetics of solid tumors: problems and promises," in, Pulse-Cytophotometry, Proceedings of the Second International Symposium on Pulse Cytophotometry (Th. Buchner, W. Gohde, and J. Schumann eds.), pp. 188-200. European Press, Ghent, Belgium.
106. A.M. Cohen. Comparative effects of Ftorafur and 5-fluorouracil on DNA synthesis in rat small intestine. Life Sci. 17, 1363-1368 (1975).
107. H.A. Hopkins and J.A. Wakefield. Utilization of ³H from deoxyuridine and thymidine for synthesis of DNA and other macromolecules in various organs of the rat. Biochem. Pharmacol. 26, 59-61 (1977).
108. D. Kessel and I. Wodinsky. Thymidine kinase as a determinant of the response to 5-fluoro-2'-deoxyuridine in transplantable, murine leukemias. Molec. Pharmacol. 6, 251-254 (1969).
109. D.D. Harrison and H.L. Webster. The preparation of isolated intestinal crypt cells. Exptl. Cell Res. 55, 257-260 (1969).
110. H.L. Webster and D.D. Harrison. Enzyme activities during the transformation of crypt to columnar intestinal cells. Exptl. Cell Res. 56, 245-253 (1969).
111. F.S. Sjöstrand. A simple and rapid method to prepare dispersions of columnar epithelial cells from the rat intestine. J. Ultrastruct. Res. 22, 424-442 (1968).
112. M.J. Dulfano and P. Glass. An effective mucolytic aerosol in chronic bronchitis. JAMA 207, 1310-1314 (1969).

113. R. Fortin-Magana, R. Hurwitz, J.J. Herbst, and N. Kretchmer. Intestinal enzymes: Indicators of proliferation and differentiation in the jejunum. Science 167, 1627-1628 (1969).
114. B. Friedman, D.S. Strachan, and M.M. Dewey. Histochemical and biochemical analysis of the non-specific esterases of the small intestine of the rat. J. Histochem. Cytochem. 14, 560-566 (1966).
115. H.R. Jarvis. Enzymes in the mucosa of the small intestine of the rat, the guinea pig and the rabbit. J. Histochem. Cytochem. 11, 692 (1963).
116. H.A. Padykula. Recent functional interpretations of intestinal morphology. Fed. Proc. 21, 873-879 (1962).
117. F. Moog and R.D. Grey. Spatial and temporal differentiation of alkaline phosphatase on intestinal villi of the mouse. J. Cell Biol. 32, 61-65 (1967).
118. E.D. Waschsmuth and A. Torhorst. Possible precursors of aminopeptidase and alkaline phosphatase in the proximal tubules of kidney and the crypts of small intestine of mice. Histochem. 38, 43-56 (1974).
119. E. D. Wachsmuth. Differentiation of epithelial cells in human jejunum: Localization and quantification of amino peptidase, alkaline phosphatase and aldolase isozymes in tissue sections. Histochem. 48, 101-109 (1976).
120. V.K. Hopsu-Havu, P. Rintola, and G.G. Glenner. A hog kidney aminopeptidase liberating N-terminal dipeptides. Partial purification and characteristics. Acta Chem. Scand. 22, 299 (1968).
121. N.B. Atkin and B.M. Richards. Deoxyribonucleic acid in human tumors as measured by microspectrophotometry of feulgen stain: A comparison of tumors arising at different sites. Br. J. Cancer 10, 769-786 (1956).
122. B.H. Mayall. Deoxyribonucleic acid cytophotometry of stained human leukocytes. I. Differences among cell types. J. Histochem. Cytochem. 17, 249-257 (1969).

123. K. Noeske. Discrepancy between cytophotometric feulgen values and deoxyribonucleic acid content. J. Histochem. Cytochem. 19, 169-173 (1971).

FIGURES

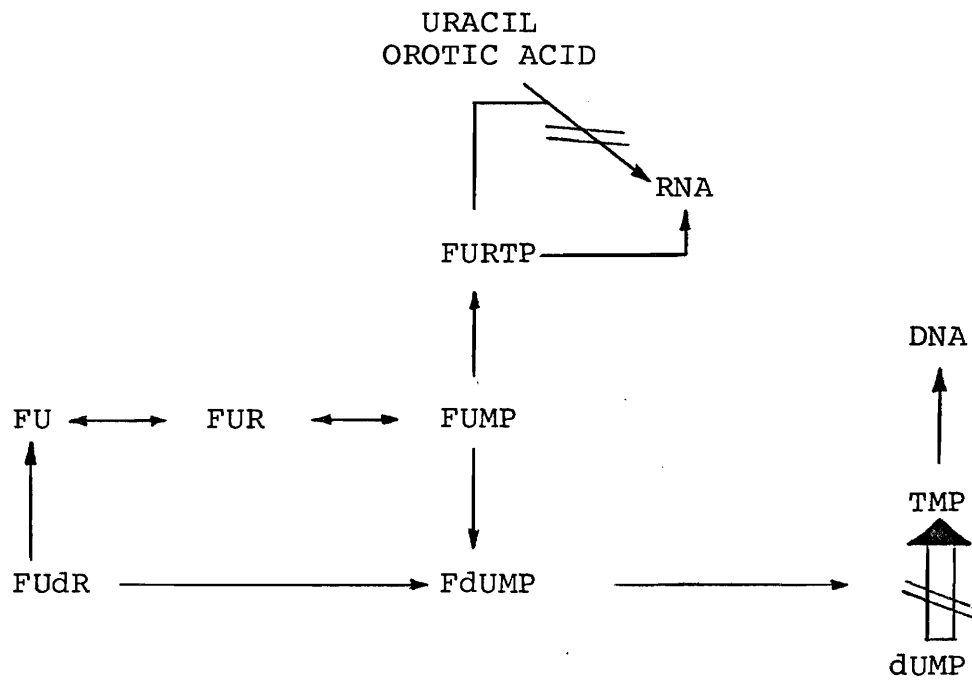


Figure 1. Anabolism of 5-Fluorouracil. 5-Fluorouracil (FU), 5-fluoro-2'-deoxyuridine (FUdR), 5-fluoro-2'-deoxyuridine 5'-monophosphate (FdUMP), 5-fluoro-uridine 5'-monophosphate (FUMP), deoxyuridylate (dUMP), thymidylate (TMP), 5-fluorouridine (FUR), 5-fluorouridine 5'-triphosphate (FURTP).

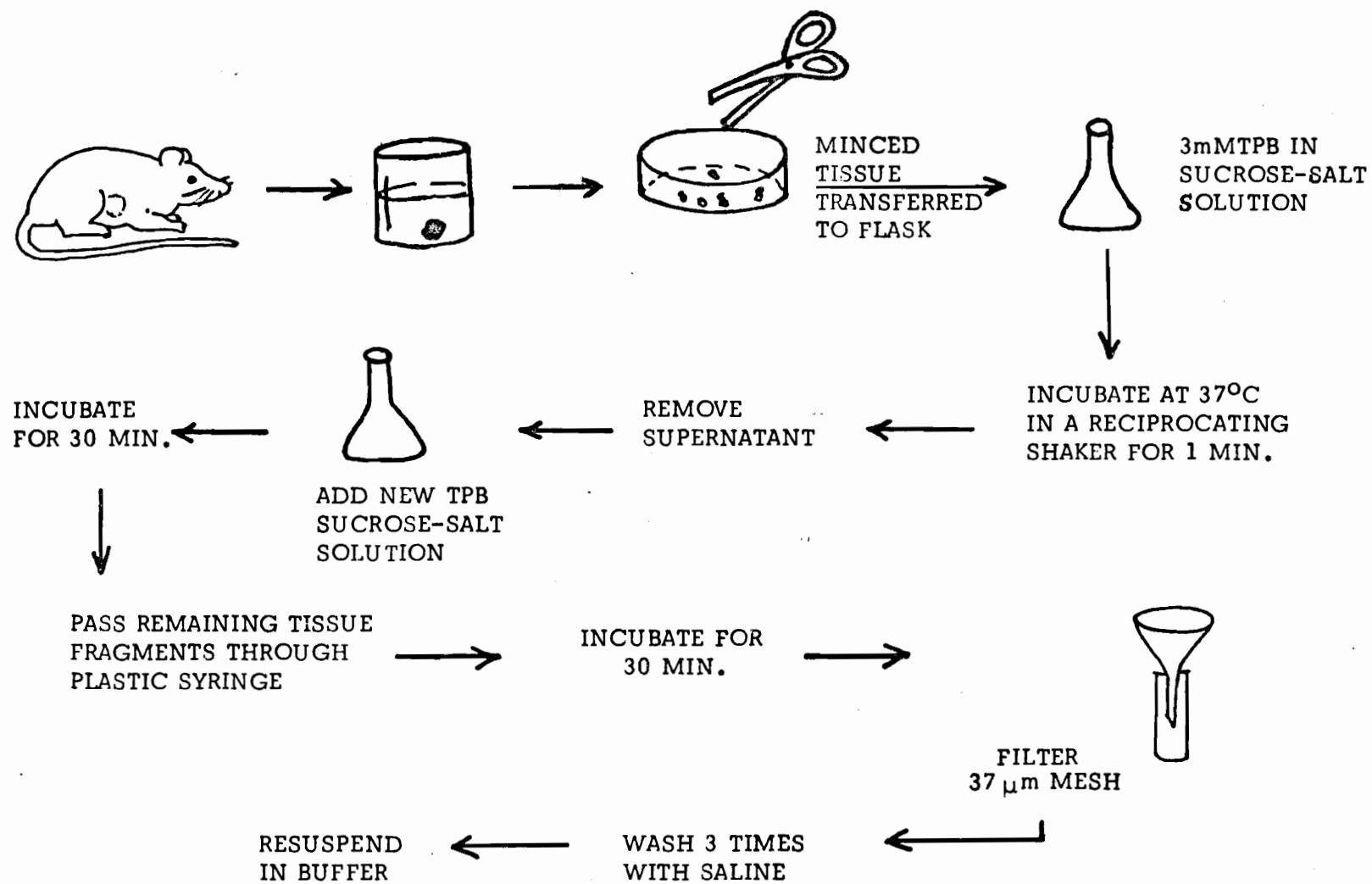


Figure 2. TPB Tumor Dispersal Procedure

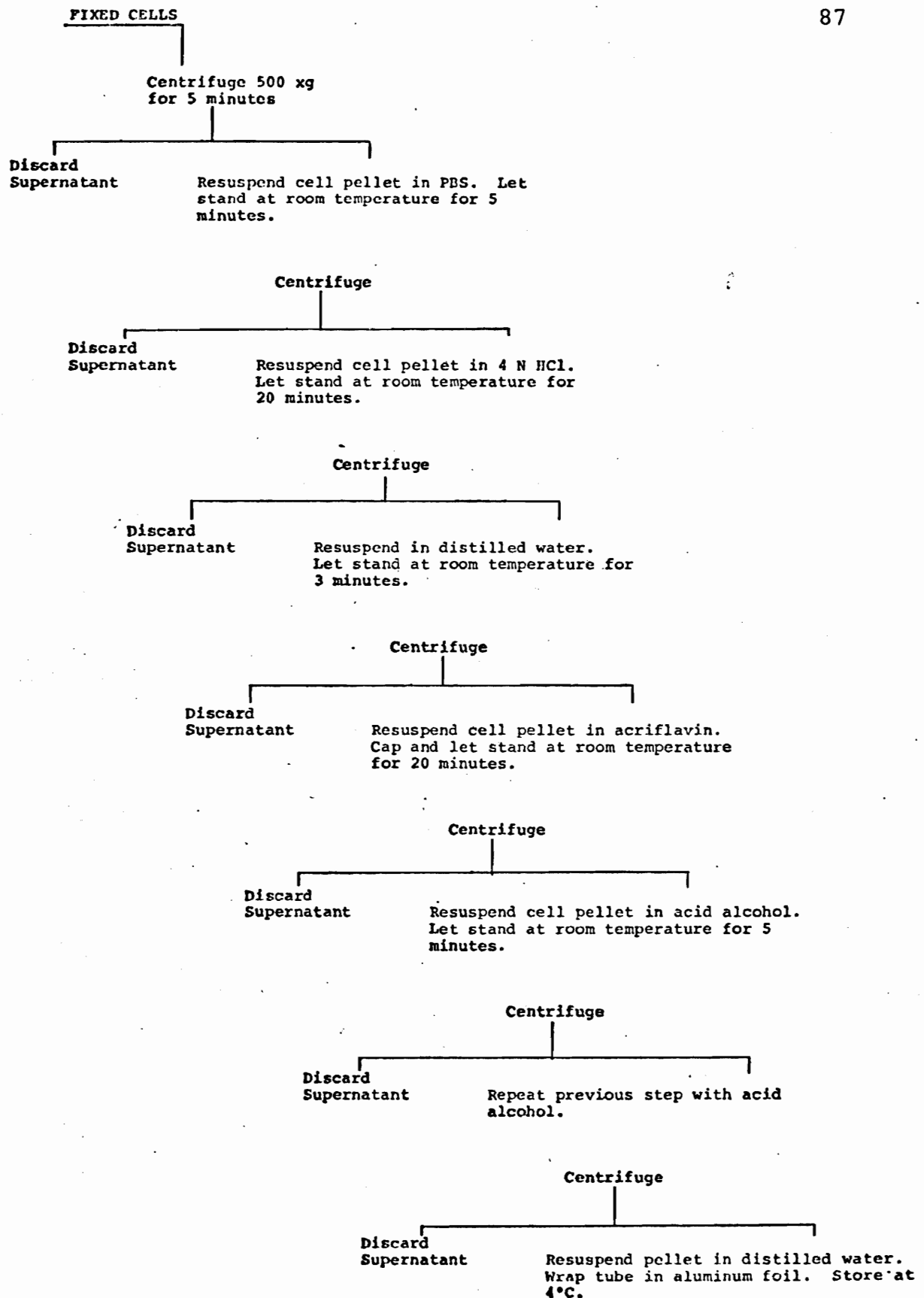

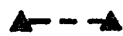



Figure 3. Acriflavin-Feulgen Staining Protocol

Figure 4. Inhibition of growth of S102F tumors by multiple injections of FT and FU. The lines in this figure and all following figures were fitted by eye. Each data point represents the mean of 8-12 tumors. The vertical bars show one S.E. of the mean. For clarity, only half of the error bar is shown. Drug treatment was initiated on Day 0 and continued for 9 days thereafter.

	Control
	FT (100 mg/kg)
	FU (20 mg/kg)

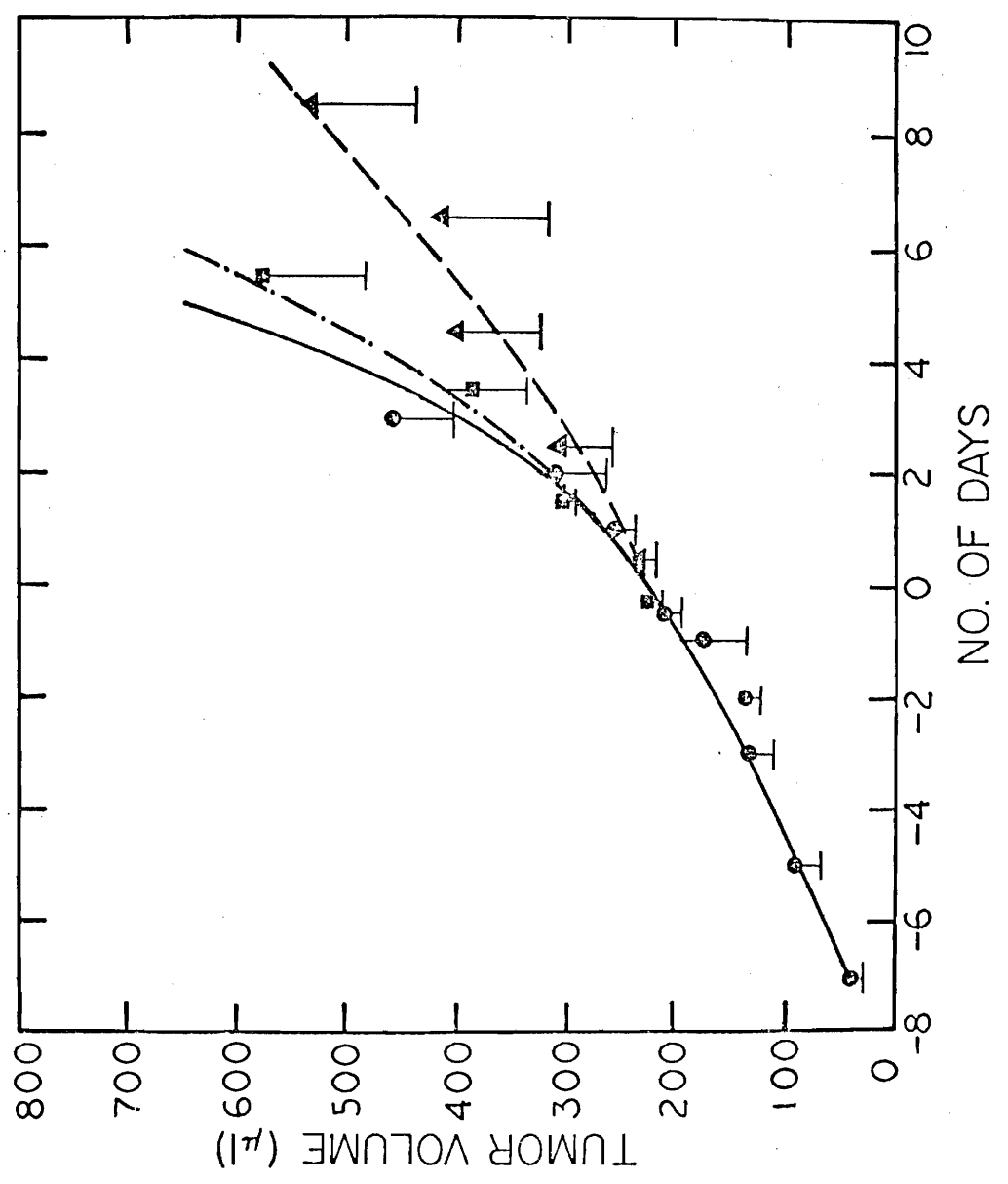
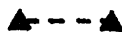


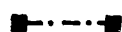
Figure 5. Host toxicity of multiple injections of FT and FU in mice bearing S102F tumors. Each data point represents the mean body weight change of mice bearing the S102F tumor. These are the same mice whose tumor growth is shown in Figure 4. The vertical bars show the S.E. of the mean of 8-10 mice. Drug injections began on day 0 when the tumor volume was approximately 200 μl and continued for 9 days thereafter. The pre-treatment weight of the mice was between 22 and 28 g.



Control



FT (100 mg/kg)



FU (20 mg/kg)

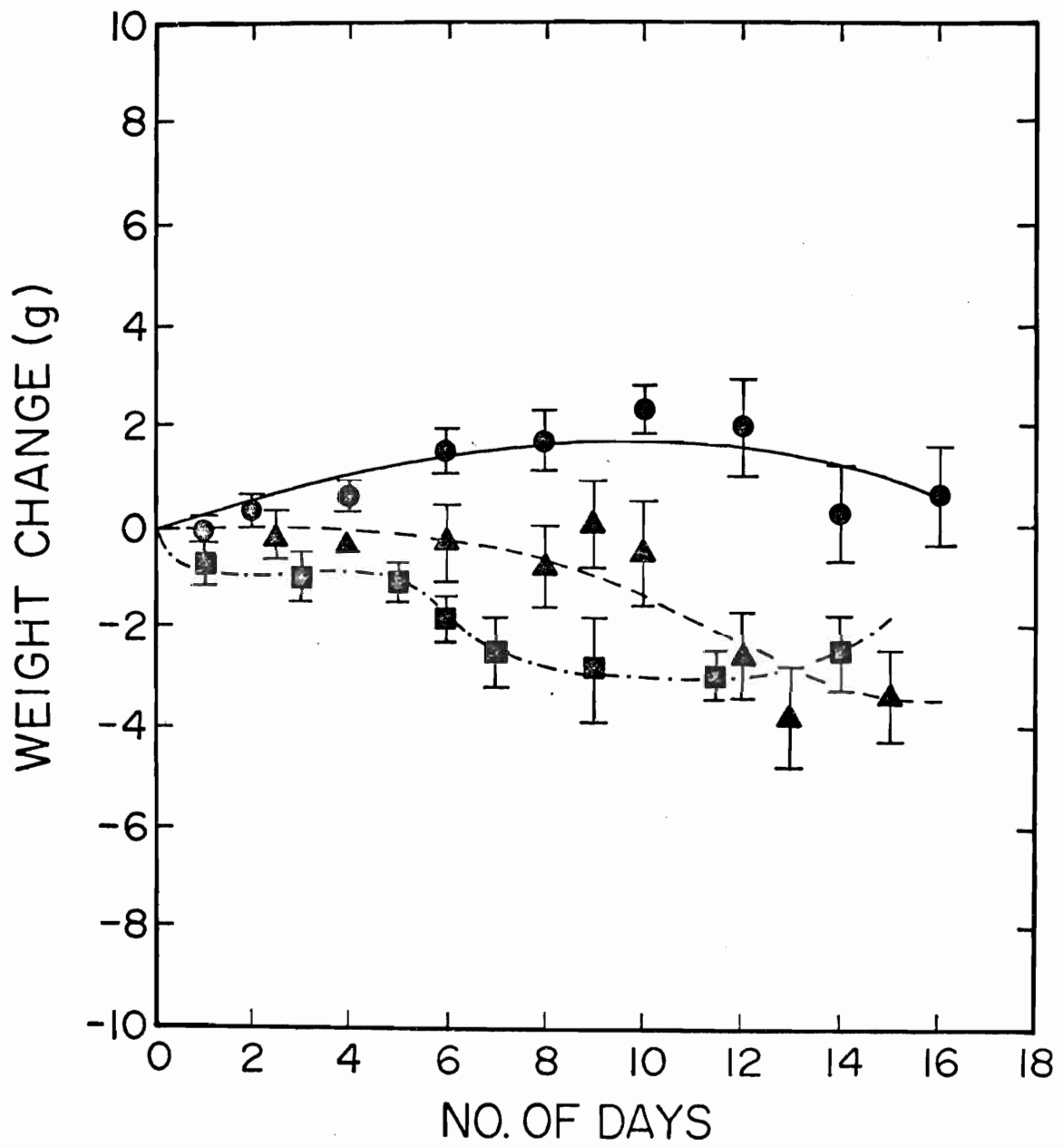


Figure 6. Inhibition of growth of Slow tumors by multiple injections of FT and FU. Each data point represents the mean of 8-12 tumors. The vertical bars show one S.E. of the mean. Drug treatment was initiated on Day 0 and continued for 9 days thereafter.

●—●	Control
▲- -▲	FT (100 mg/kg)
■· · ·■	FU (20 mg/kg)

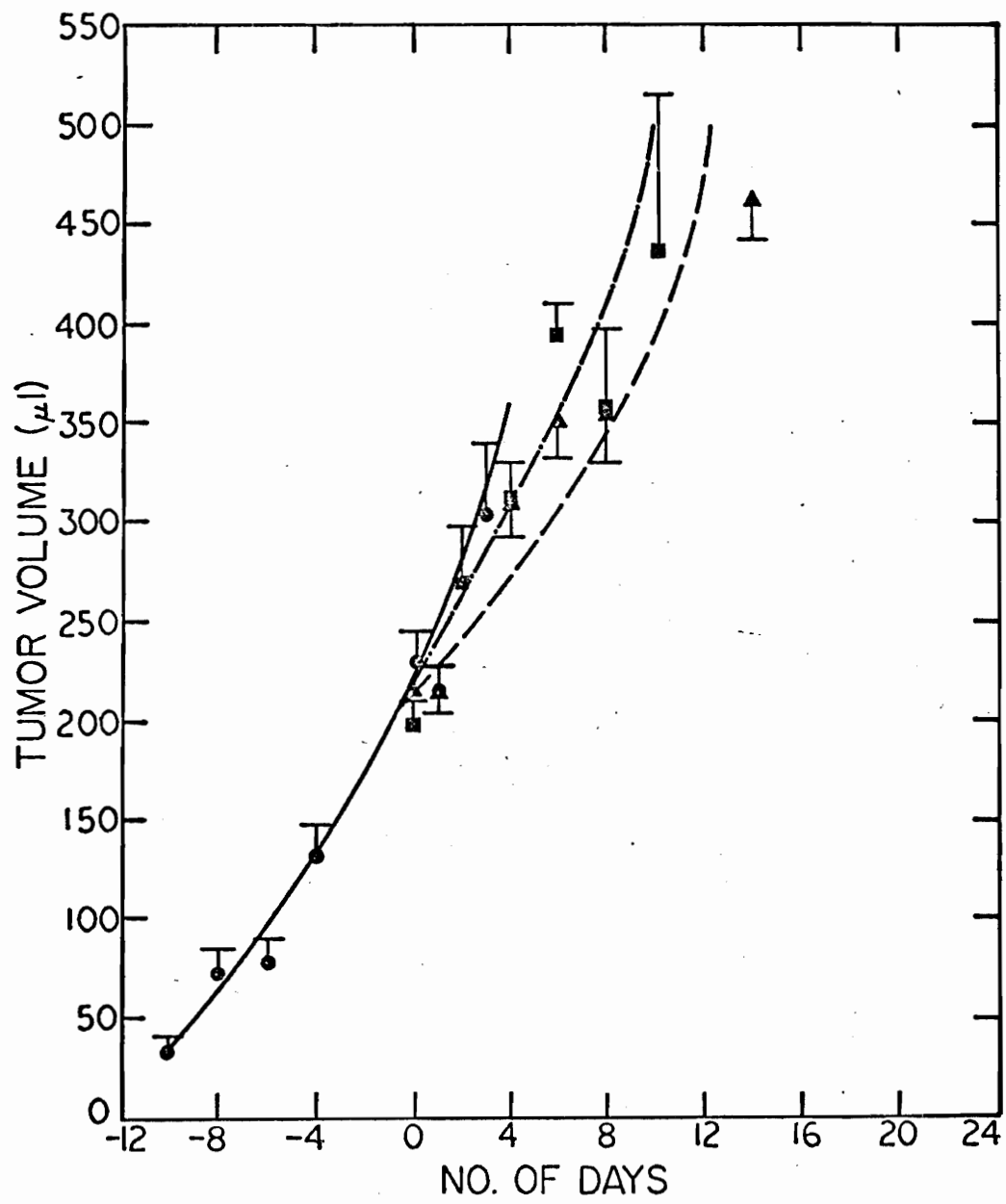
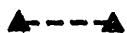


Figure 7. Host toxicity of multiple injections of FT and FU in mice bearing Slow tumors. Each data point represents the mean body weight change of 8-10 mice. These are the same mice whose tumor growth is shown in Figure 6. The vertical bars show the S.E. of the mean. Drug injections began on Day 0 when the tumor volume was approximately 200 μl and continued for 9 days thereafter. The pretreatment weight of the mice was between 22 and 28 g.



Control



FT (100 mg/kg)



FU (20 mg/kg)

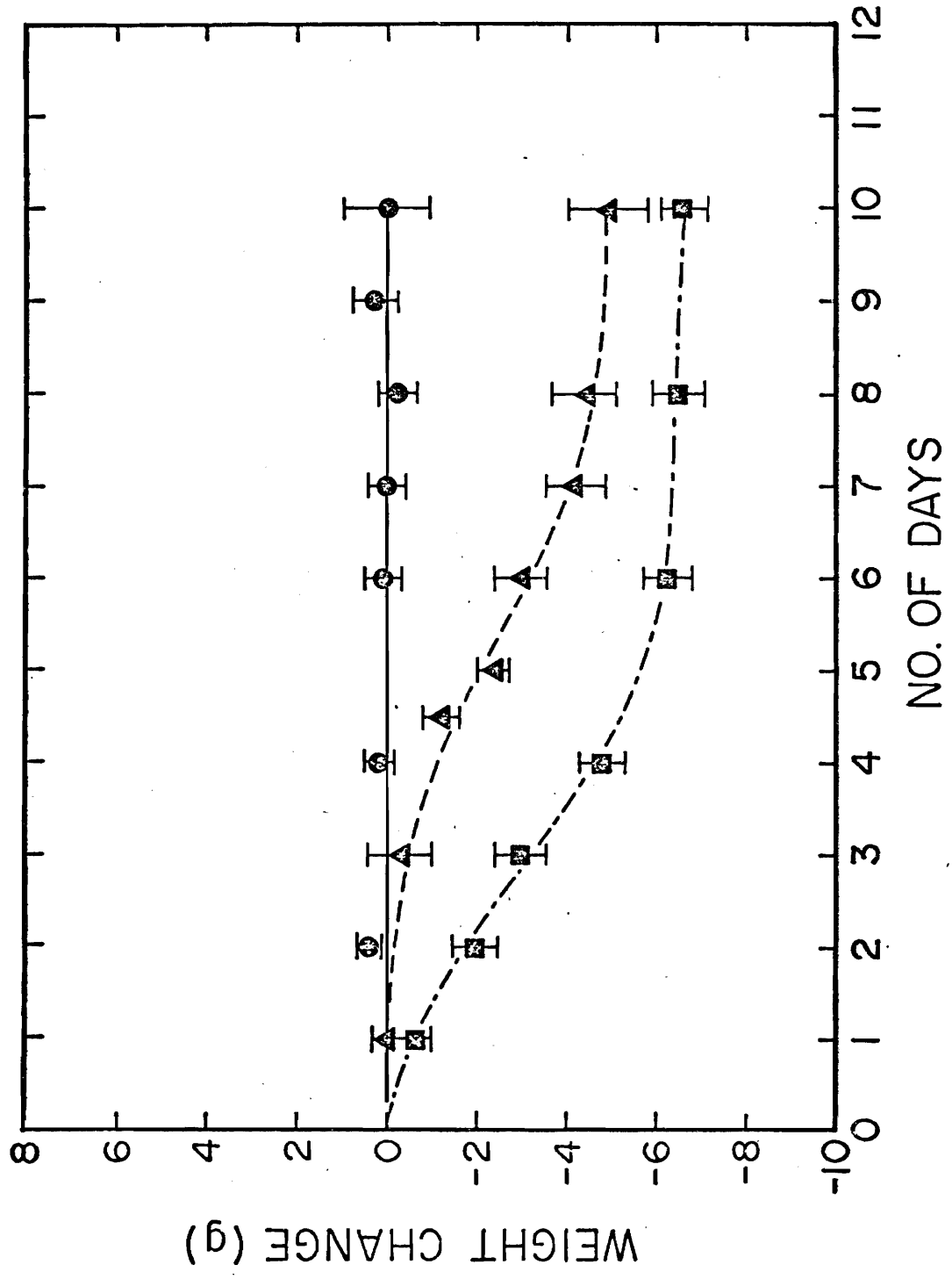
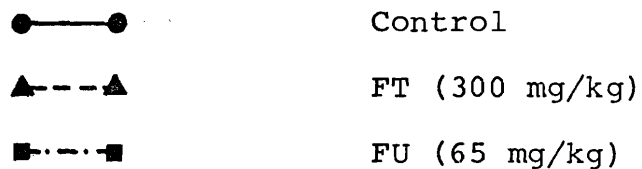


Figure 8. Inhibition of the growth of S102F tumors by a single injection of FT or FU. Each data point represents the mean tumor volume of 9-10 tumors. The vertical bars show the S.E. of the mean. A single injection of either drug was given on Day 0.



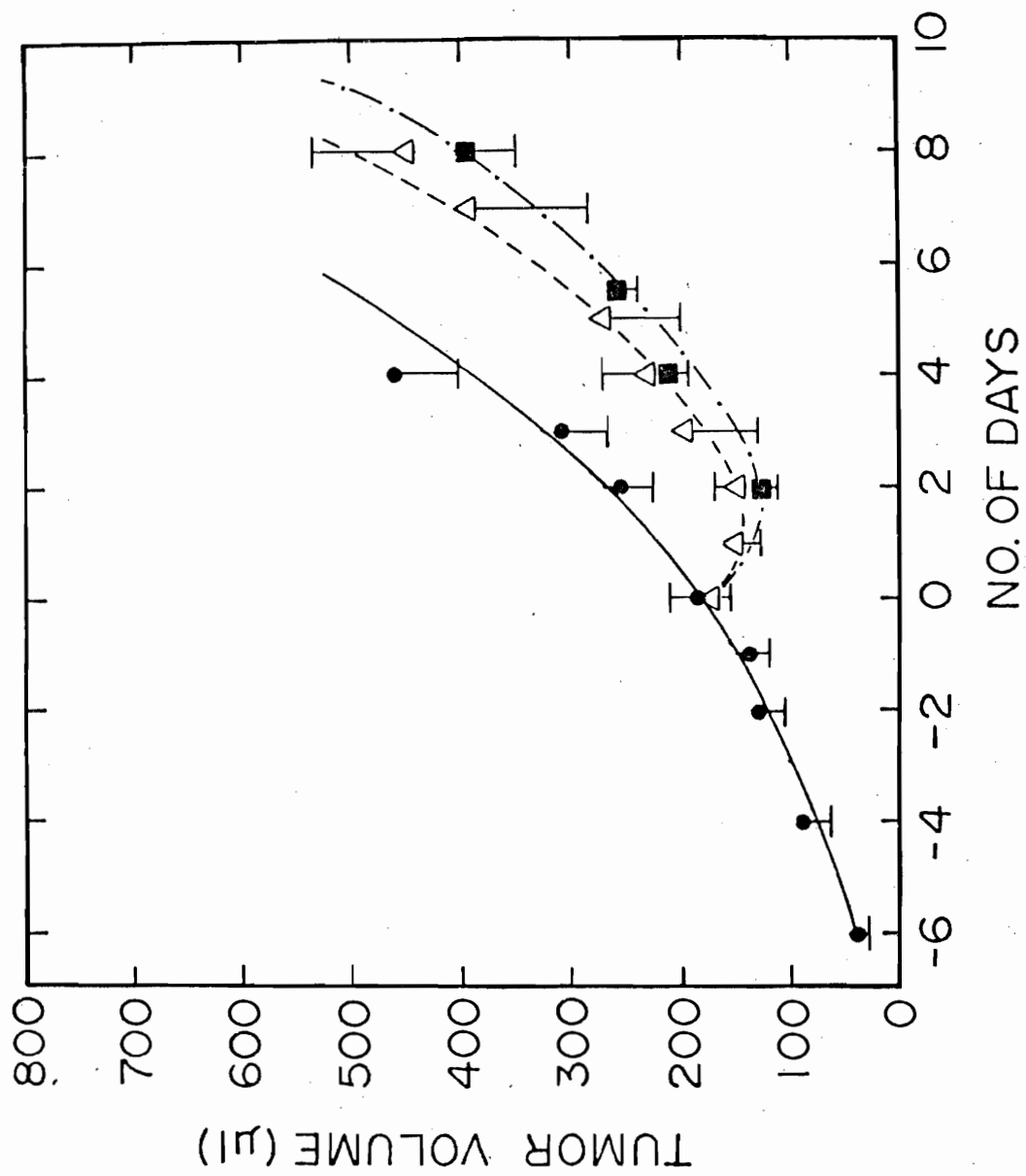


Figure 9. Host toxicity of a single injection of FT or FU in mice bearing the S102F tumor. Each data point represents the mean body weight change of 9-10 mice bearing the S102F tumor. These are the same mice whose tumor growth is shown in Figure 8. The vertical bars show the S.E. of the mean. Drugs were administered on Day 0 when the tumor volume was approximately 200 μl . The pretreatment weight of the mice was between 22 and 28 g.

●—●	Control
▲---▲	FT (300 mg/kg)
■-.-■	FU (65 mg/kg)

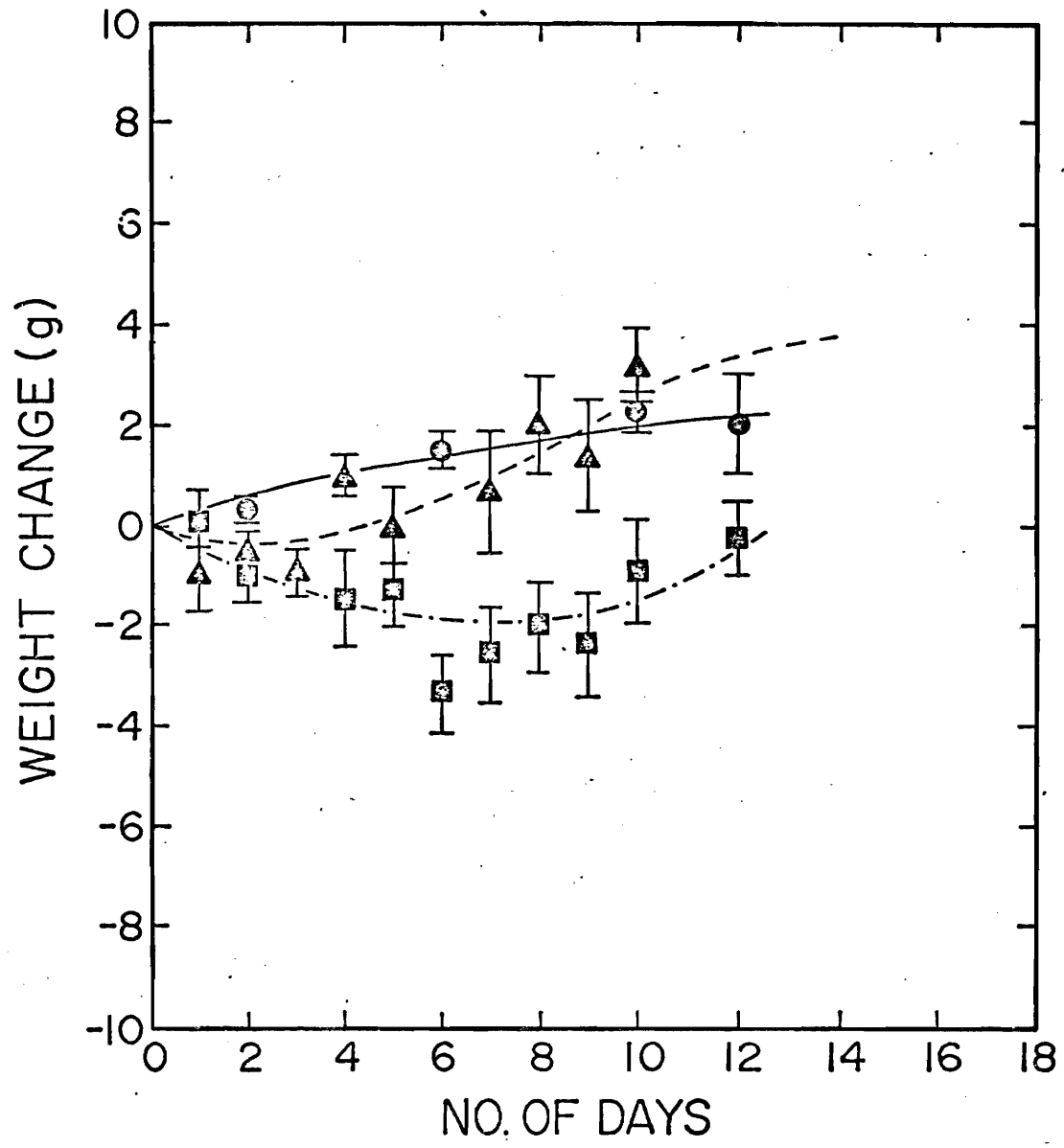


Figure 10. Inhibition of the growth of the Slow tumor by a single injection of FT or FU. Each data point represents the mean tumor volume. The vertical bars show the S.E. of the mean of 10-15 tumors. Day 0 represents the first day of tumor measurements. FT was administered as a single dose on Day 8 and FU on Day 10.



Control



FT (300 mg/kg)



FU (65 mg/kg)

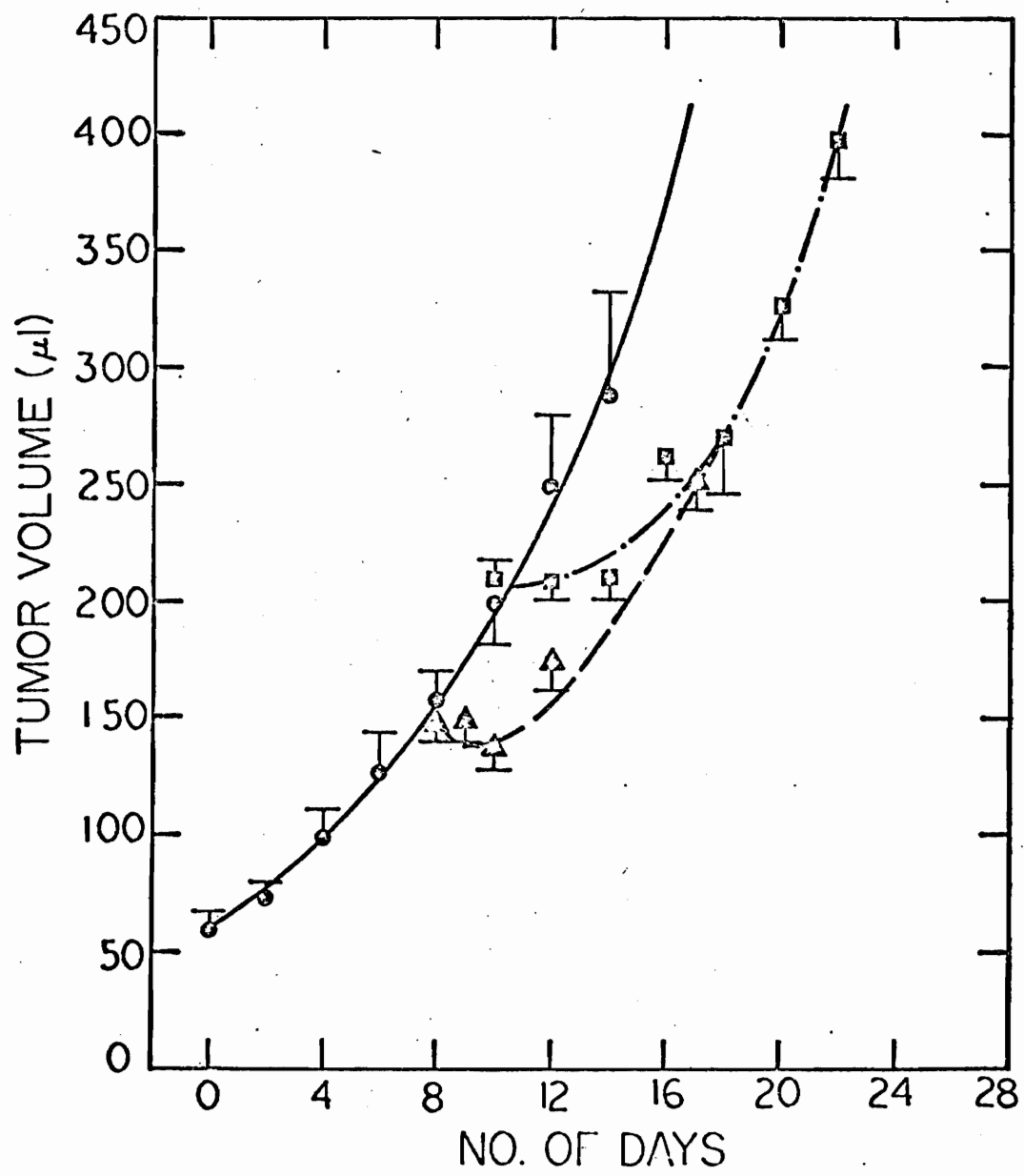
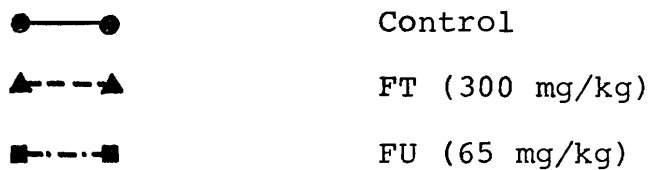


Figure 11. Host toxicity of a single injection of FT or FU in mice bearing the Slow tumor. Each data point is the mean body weight change of 10-15 mice. These are the same mice whose tumor growth is shown in Figure 10. The vertical bars show the S.E. of the mean. Day 0 represents the day of drug administration. The pretreatment weight of the mice was between 22 and 28 g.



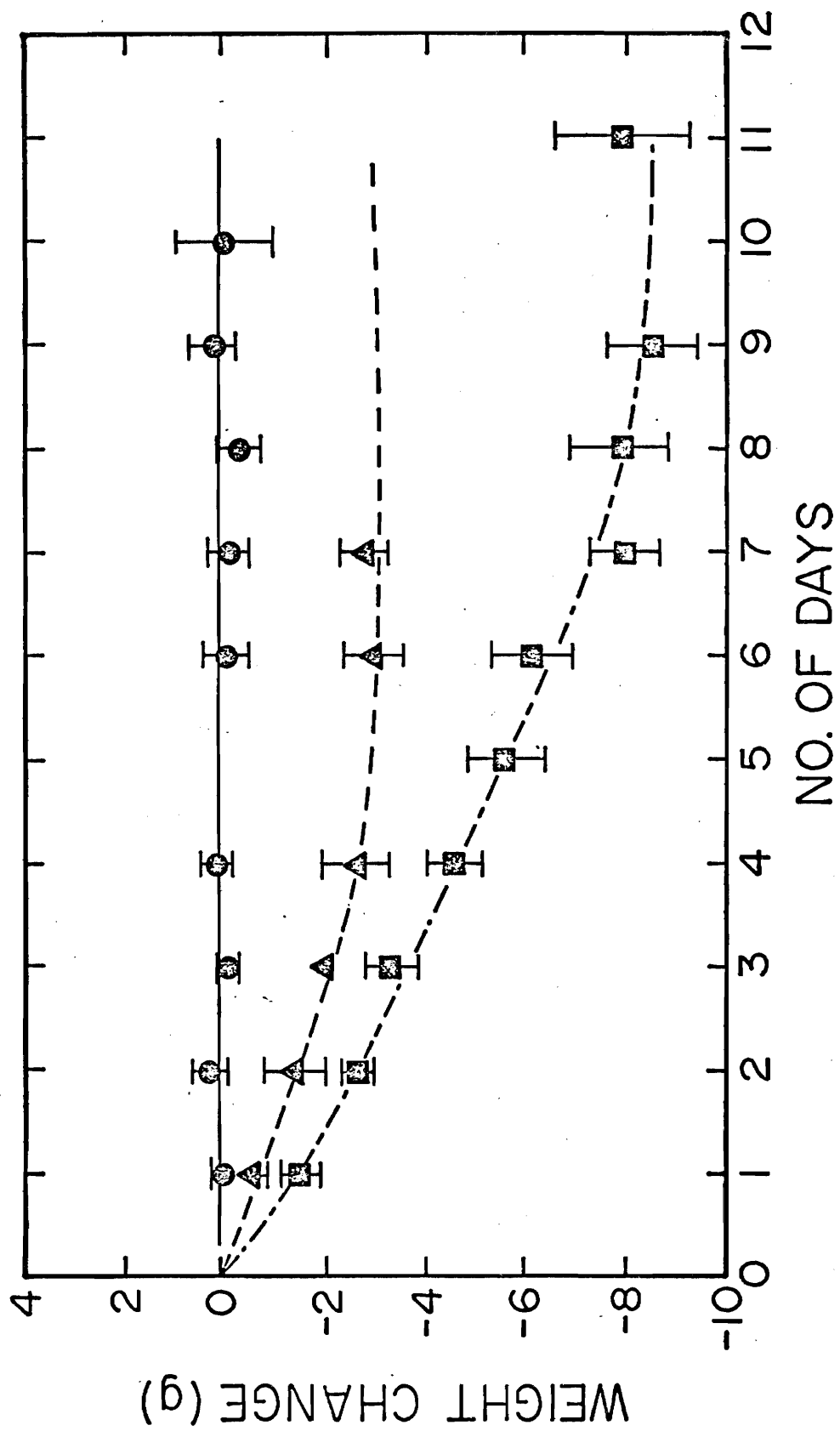
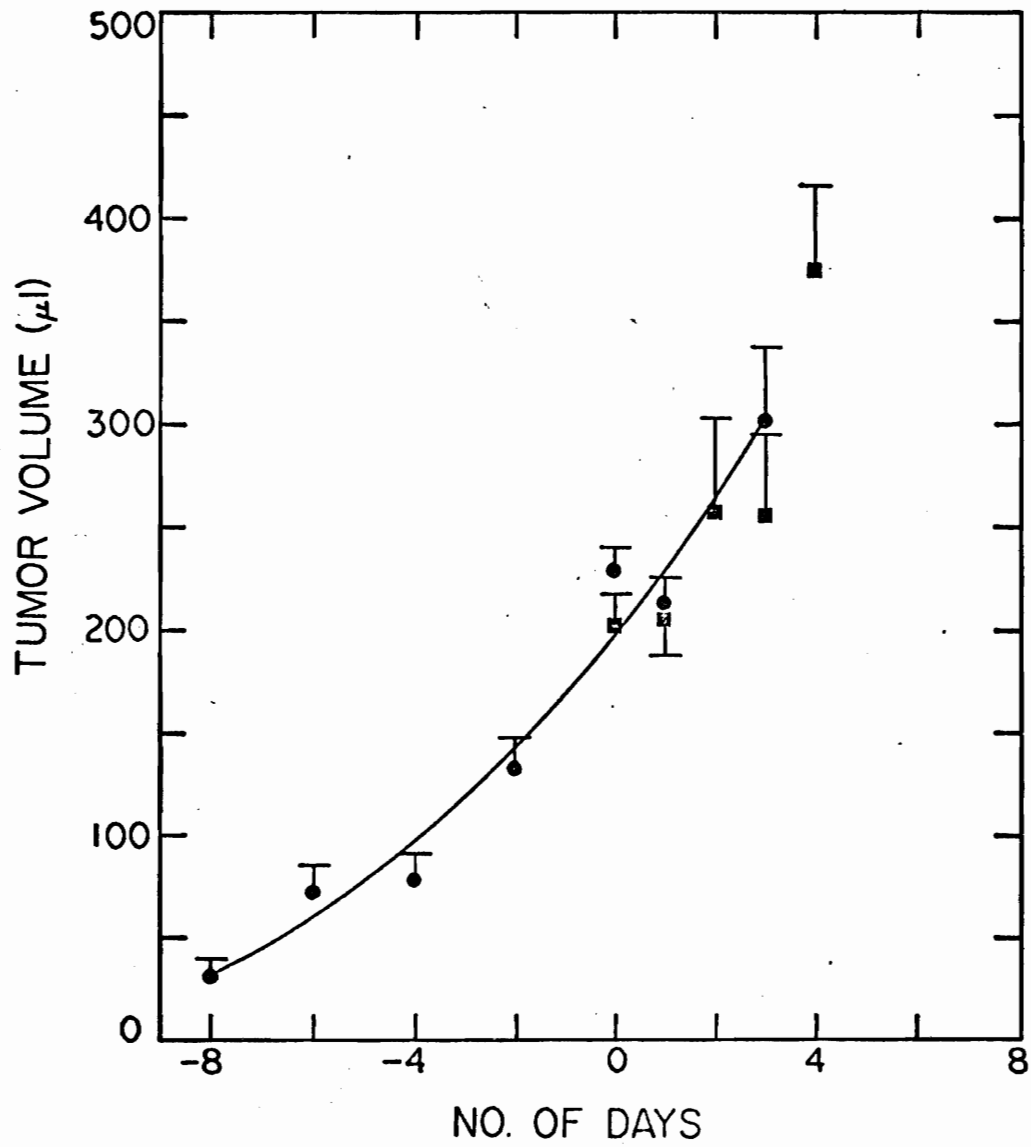


Figure 12. Effect of body weight loss on the growth of the Slow tumor. Each data point represents the mean volume of 9-12 tumors. Food was withheld on Day 0 and for 2-3 days thereafter. The mean \pm S.E. weight loss was 5.5 ± 0.1 g.

● Control
■ Treated



- Figure 13. (a) Histological section of the S102F tumor. Stained with hematoxylin and eosin.
- (b) Single cell suspension of the S102F tumor prepared with TPB. Stained with hematoxylin and eosin.

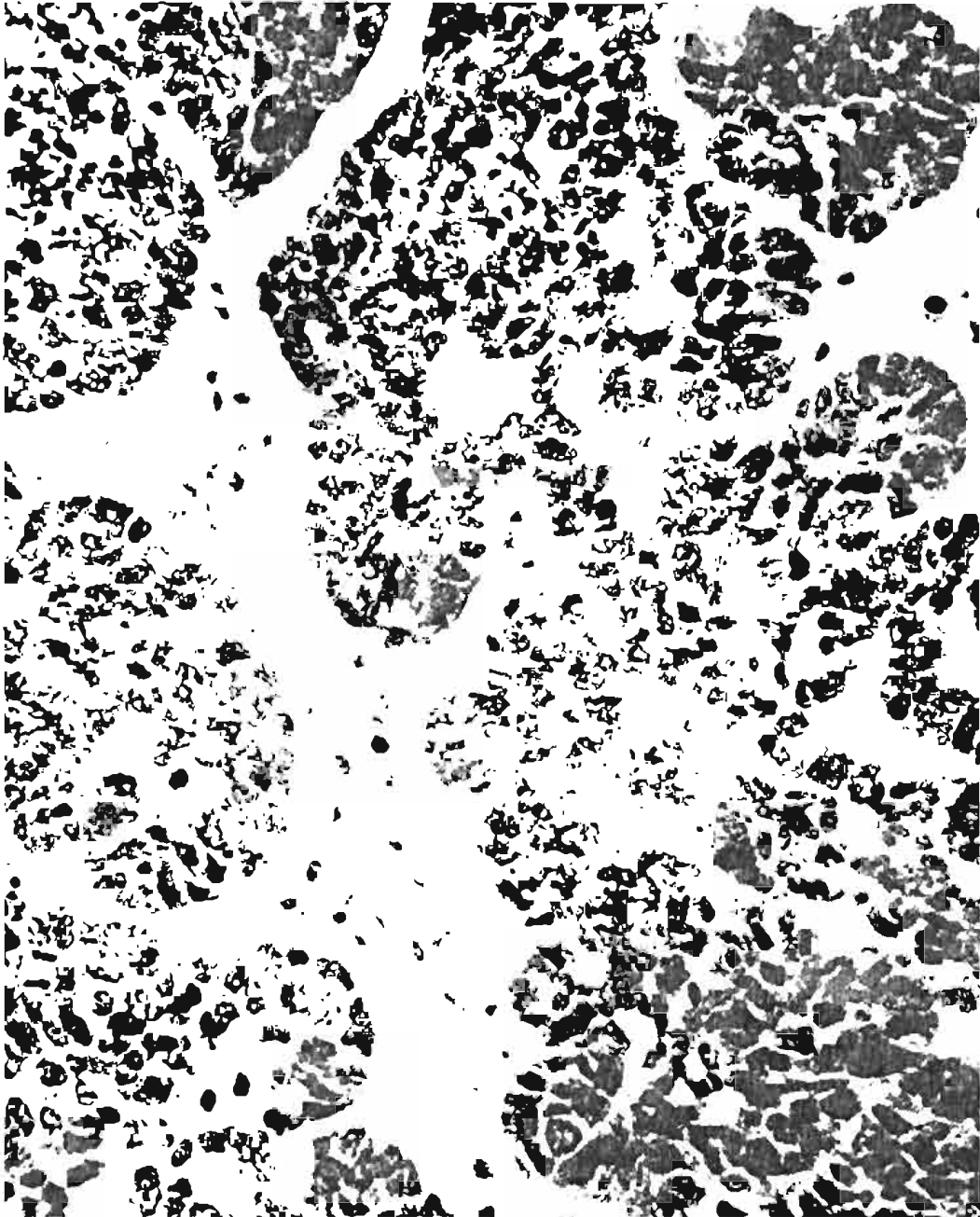




Figure 14. An uncorrected DNA distribution of an acriflavin-stained S102F single cell suspension prepared with TPB. Note the low level of background fluorescence and minimal cell clumping.

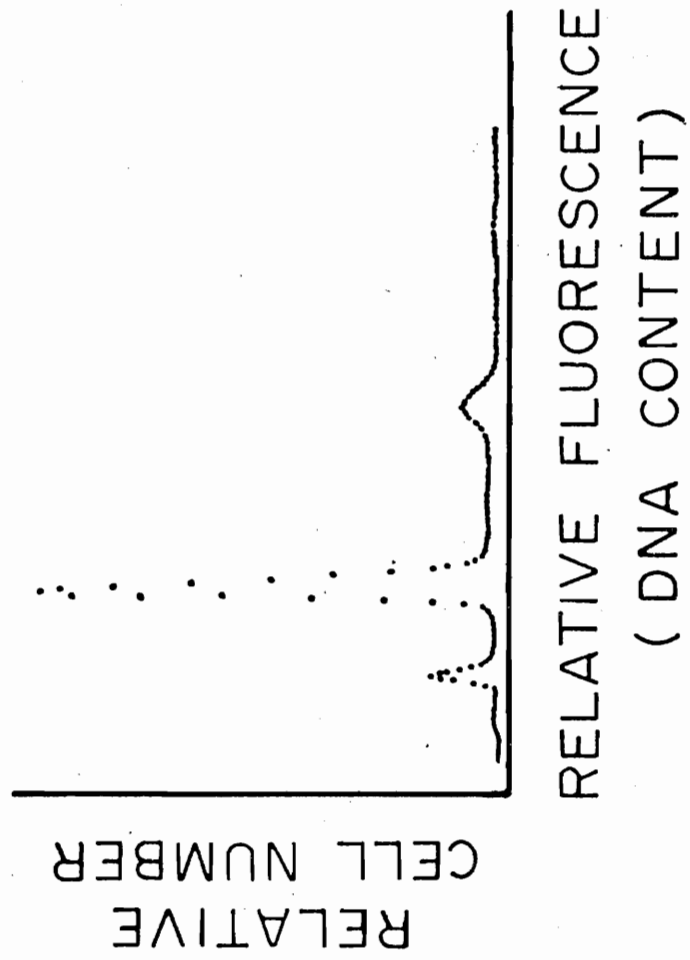


Figure 15. Computer analysis of a DNA distribution of TPB-dispersed S102F tumor cells. The solid lines represent computer drawn fits to the G_1 peak, $G_2 + M$ peak, and S phase portion of the histogram. The fraction of the tumor cell population in G_1 , S, and $G_2 + M$ is shown in the upper right-hand corner. The modal channel number and coefficient of variation (C.V.) for the G_1 and $G_2 + M$ peaks are also listed.

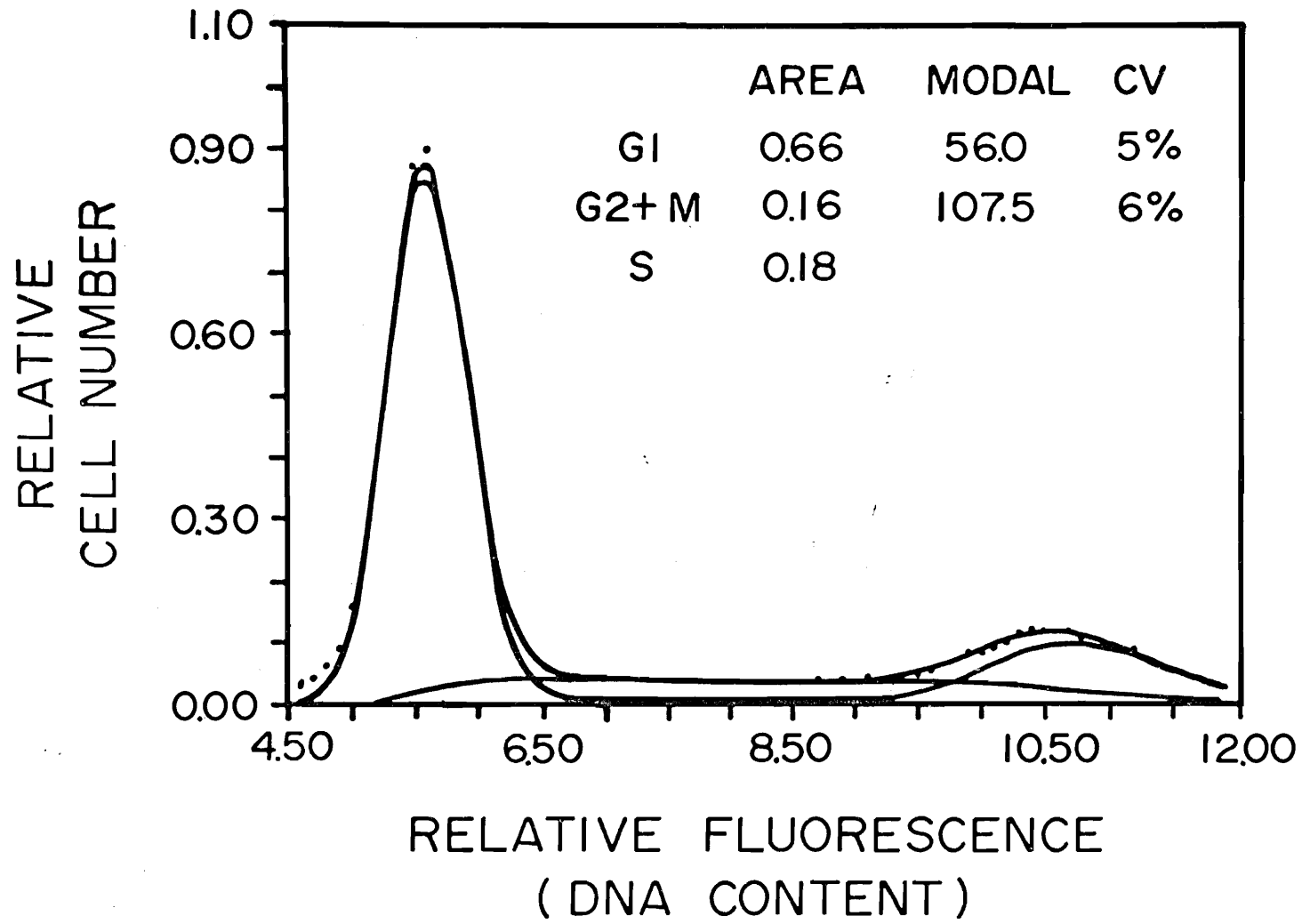


Figure 16. Inhibition of deoxyuridine incorporation into the DNA of S102F tumors by FT and FU. Each data point and vertical bar represents the mean \pm S.E. of 15-20 samples obtained from treated animals. The area enclosed by the dashed lines indicates the mean \pm S.E. of 15-20 control animals.

▲ FT (100 mg/kg)
■ FU (65 mg/kg)

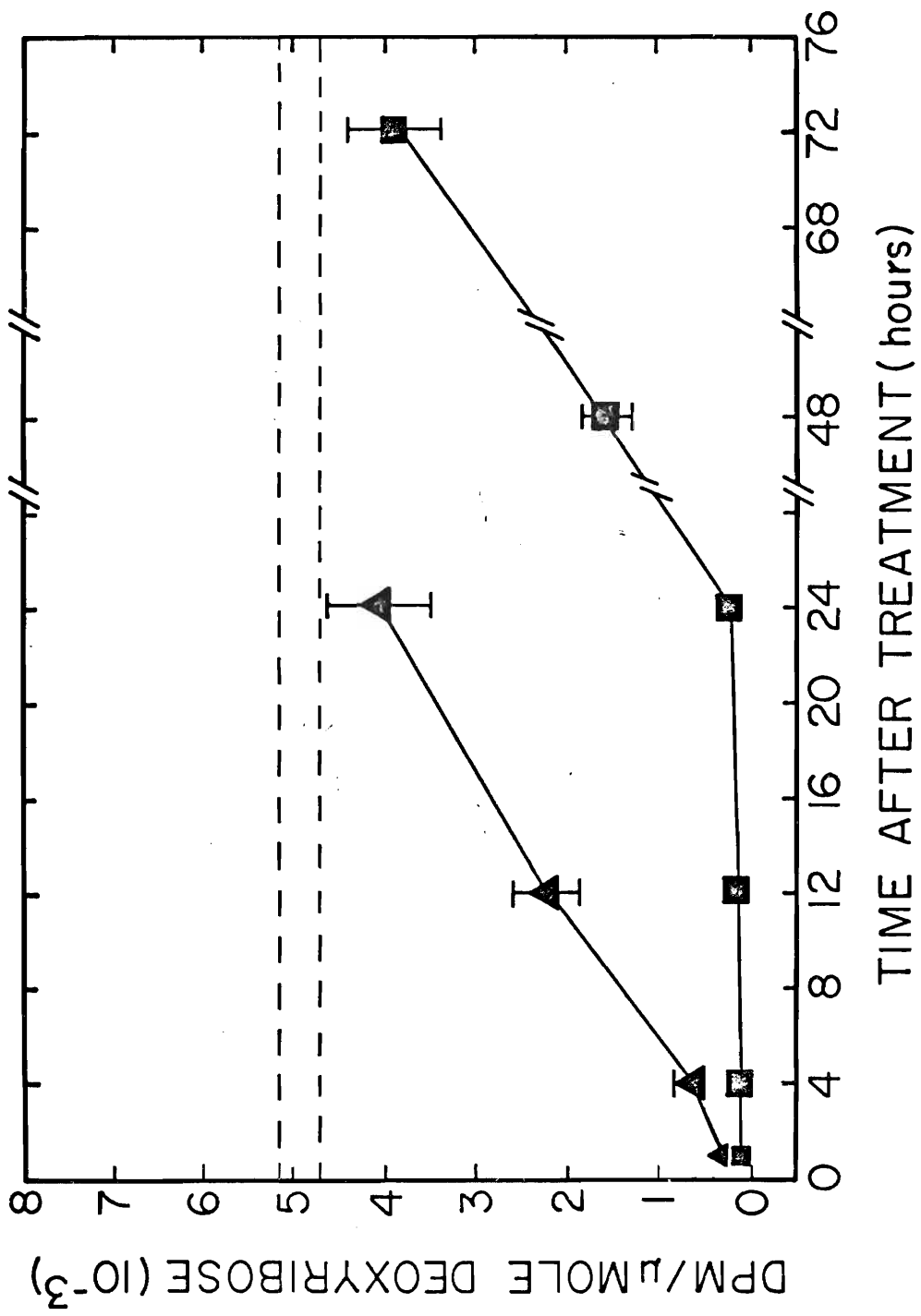


Figure 17. Inhibition of ^3H -deoxyuridine incorporation into the DNA of the small intestine of S101F tumor-bearing animals. The intestine were taken from mice bearing the S102F tumors represented in Figure 16. Each data point represents the mean \pm S.E. of 15-20 samples obtained from treated animals. The area bordered by the dashed lines encloses the mean \pm S.E. of 15-20 control animals.



FT (100 mg/kg)



FU (65 mg/kg)

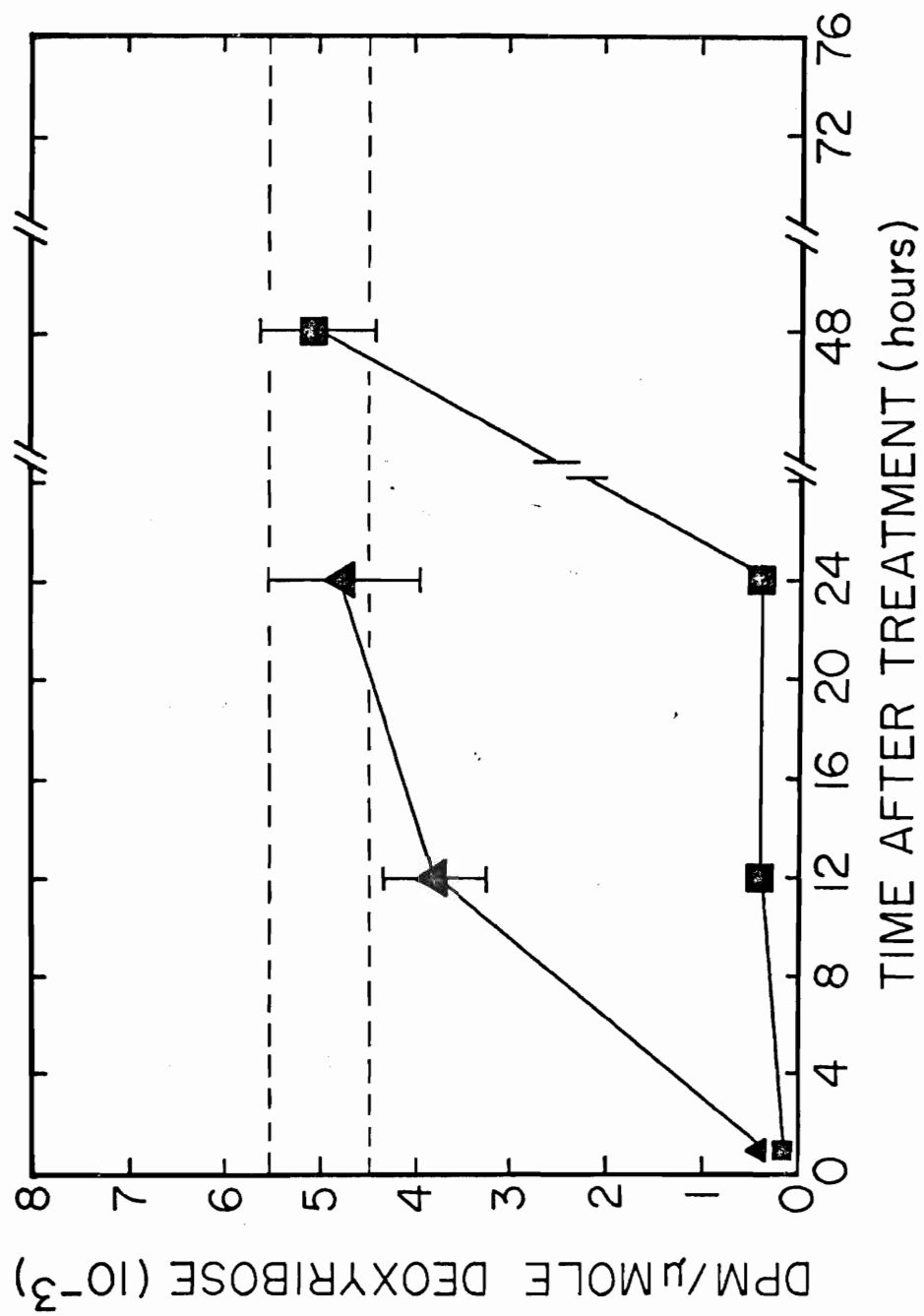


Figure 18. Inhibition of ^3H -deoxyuridine incorporation into the DNA of Slow tumors by FT and FU. Each data point and vertical bar represents the mean \pm S.E. of 15-20 samples obtained from treated animals. The area bordered by the dashed lines encloses the mean \pm S.E. of 15-20 control samples.

▲	FT (100 mg/kg)
■	FU (65 mg/kg)

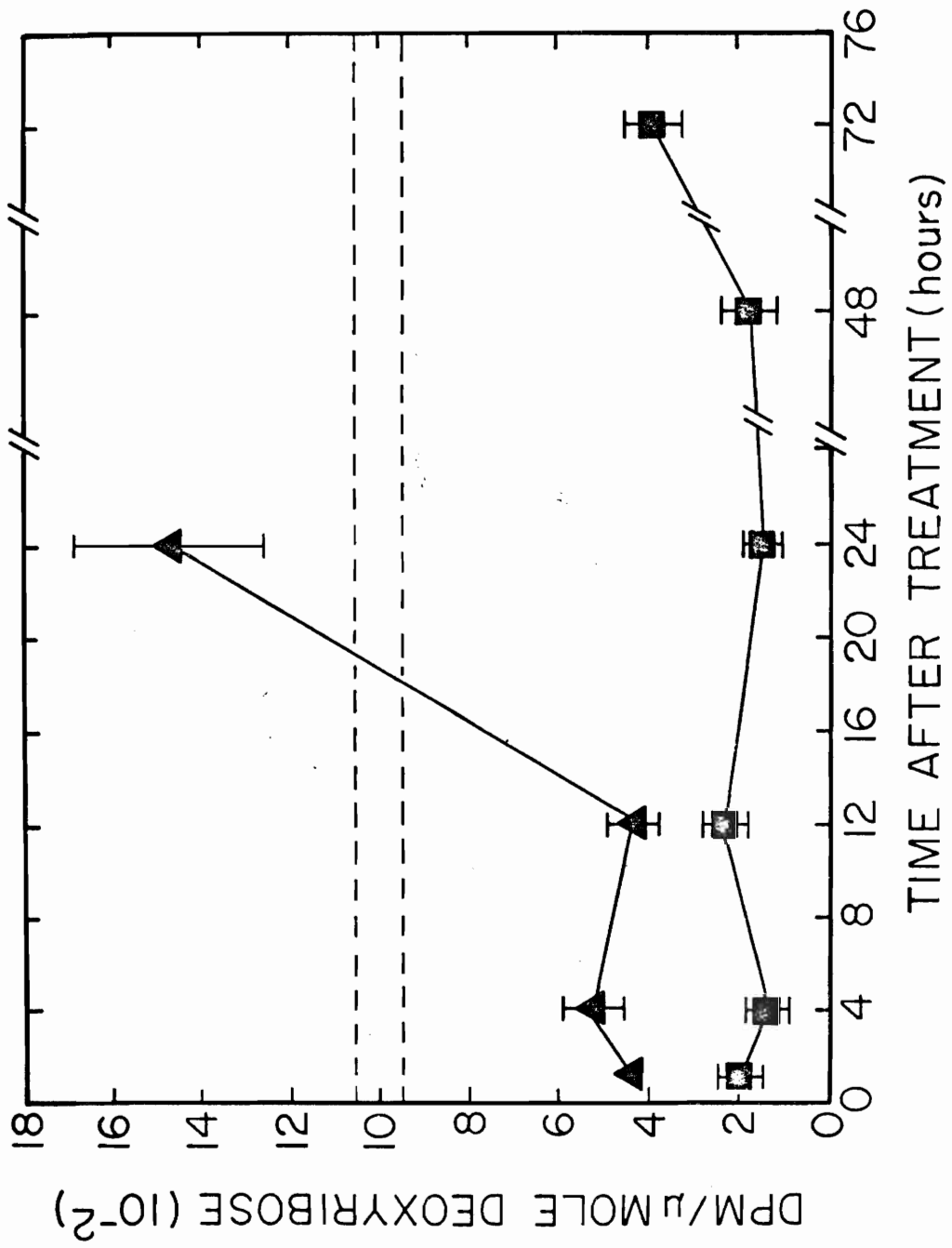


Figure 19. Inhibition of ^3H -deoxyuridine incorporation into the DNA of the small intestine of Slow tumor-bearing animals. The intestines were taken from mice bearing the tumors shown in Figure 18. Each data point represents the mean \pm S.E. of 15-20 samples obtained from treated animals. The area bordered by the dashed lines encloses the mean \pm S.E. of 15-20 control samples.

▲ FT (100 mg/kg)
■ FU (65 mg/kg)

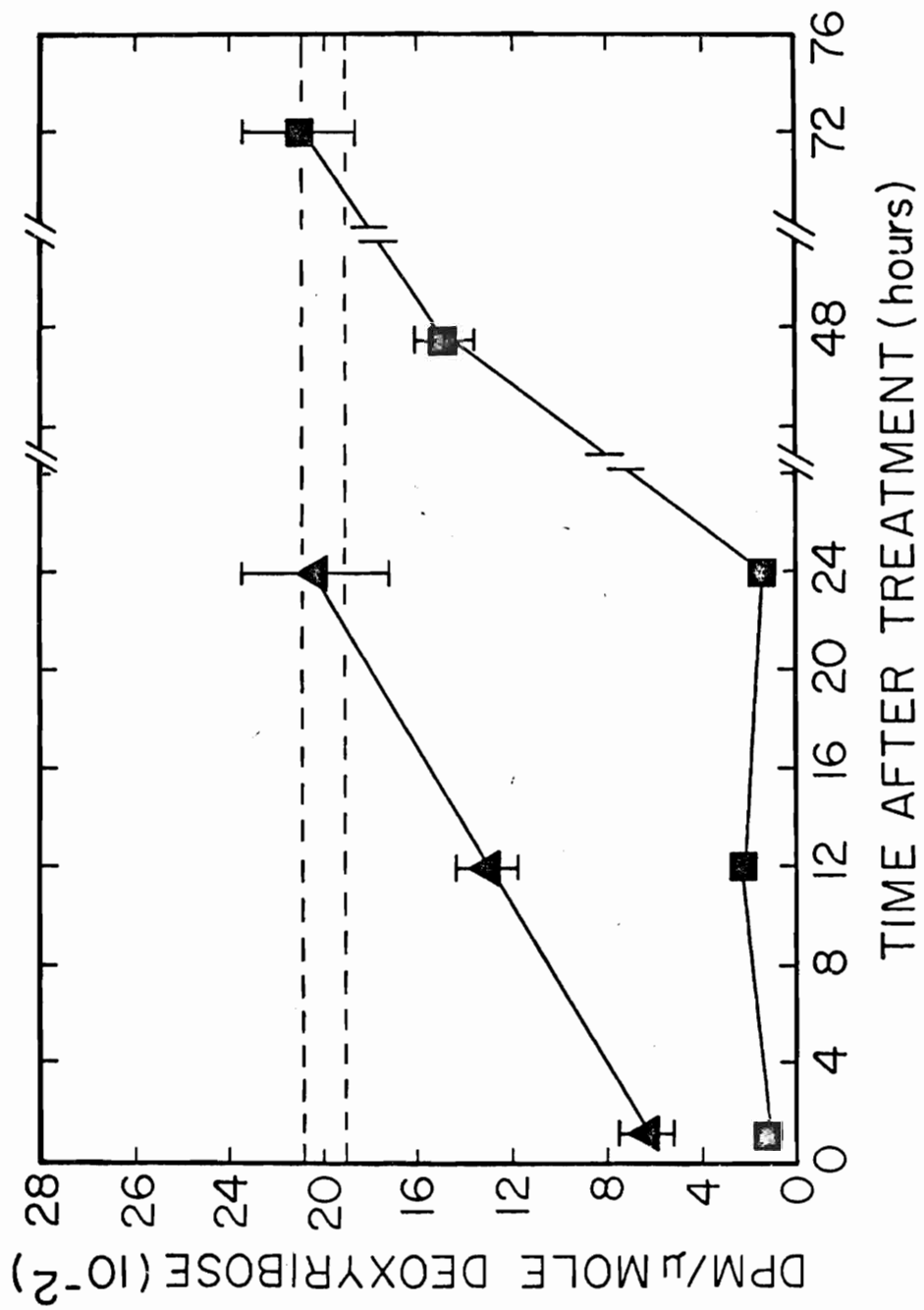


Figure 20. Inhibition of ^3H -deoxyuridine incorporation into the DNA of S102F tumors by large doses of FT and FU. Each data point represents the mean \pm S.E. of 12-18 samples. The area bordered by the dashed lines encloses the mean \pm S.E. of 15-20 control samples.

▲ FT (300 mg/kg)
■ FU (65 mg/kg)

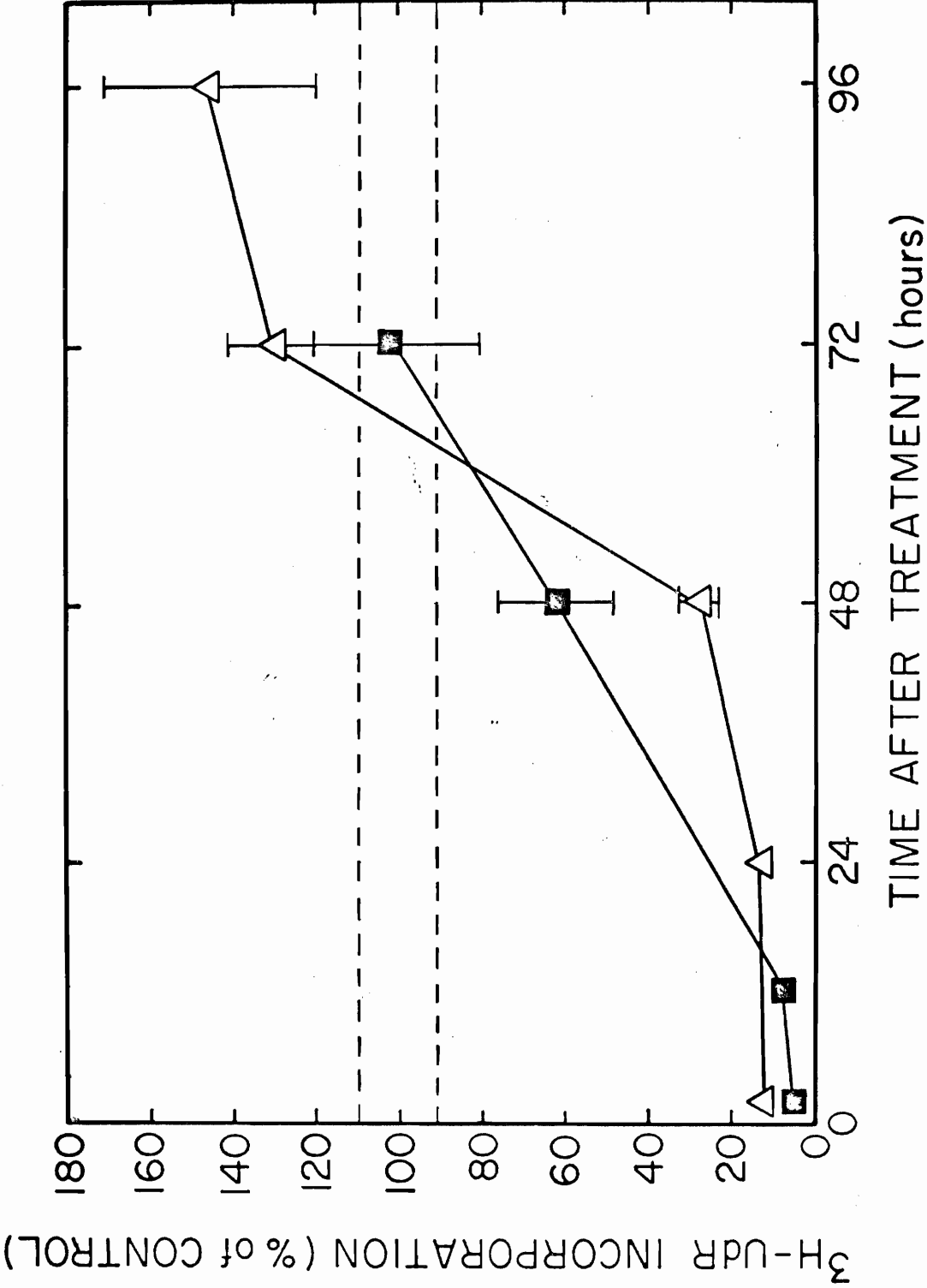
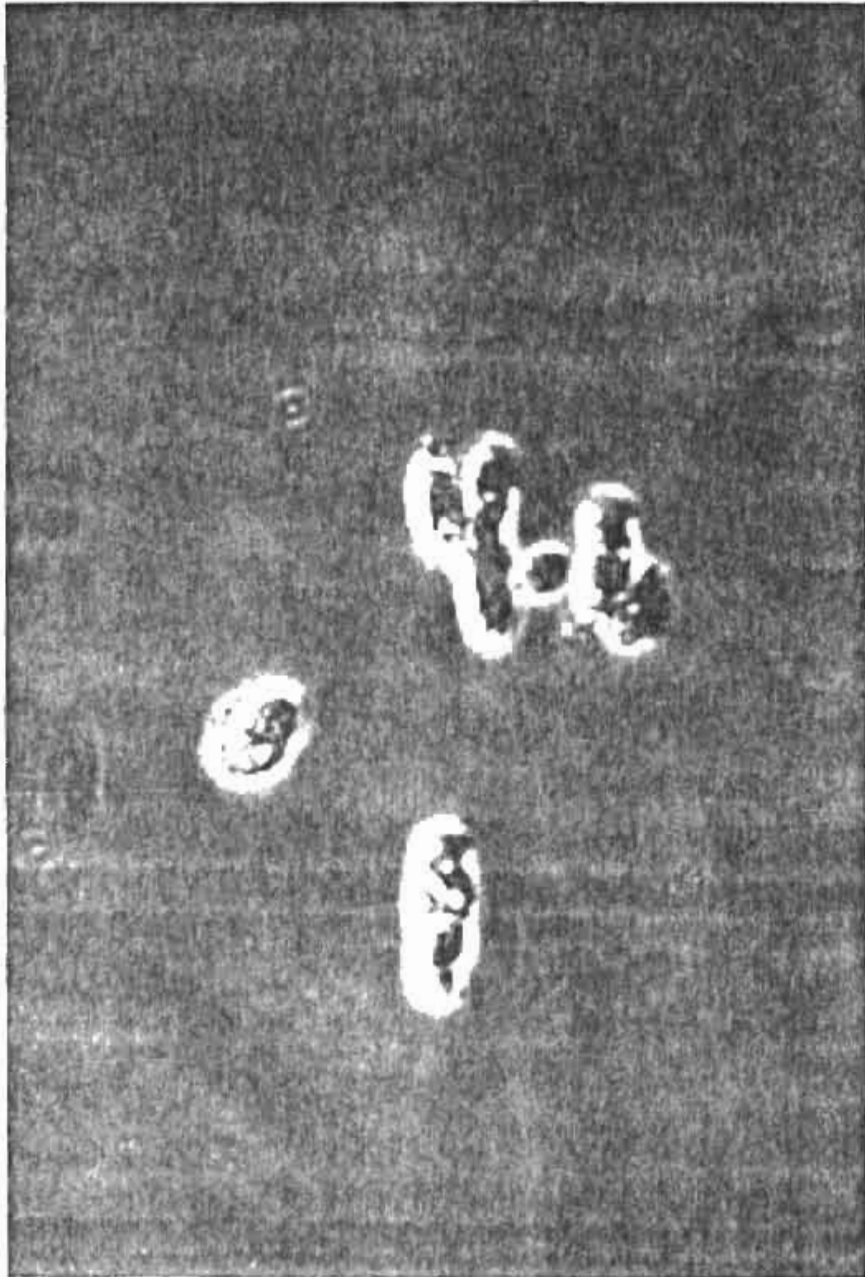


Figure 21. Phase contrast photomicrograph of an unstained intestinal epithelial cell suspension. Villus cells are distinguished by their distinct brush borders. Crypt cells lack microvilli and show a high nuclear to cytoplasmic ratio.

Figure 22. Phase contrast photomicrograph of an epithelial cell suspension stained for leucine aminopeptidase activity.

- (a) Cell preparation as viewed under the light microscope. A round crypt cell is located between several hemi-ellipsoid villus cells.
- (b) Same cells viewed under fluorescent illumination. The villus cells are seen to fluoresce brightly, whereas the crypt cell exhibits minimal fluorescence.



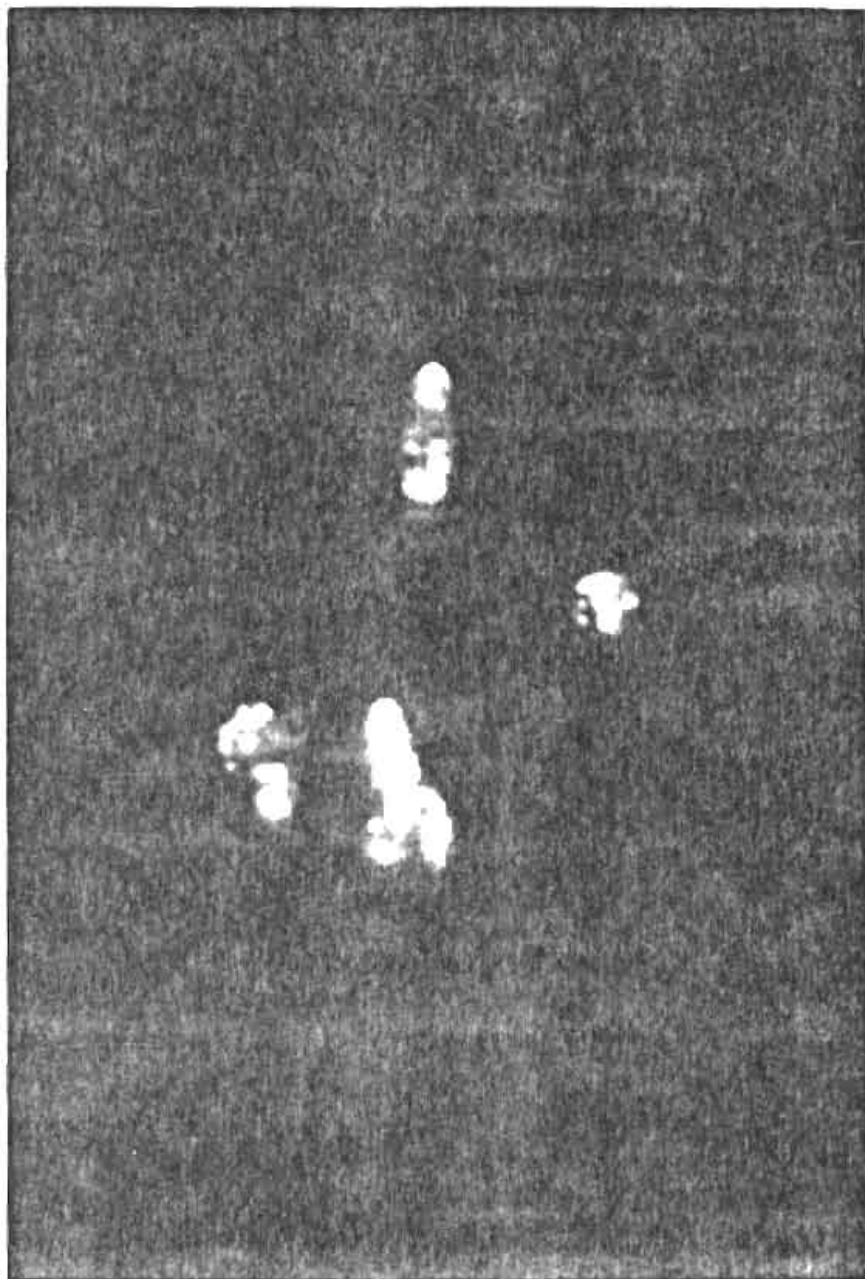
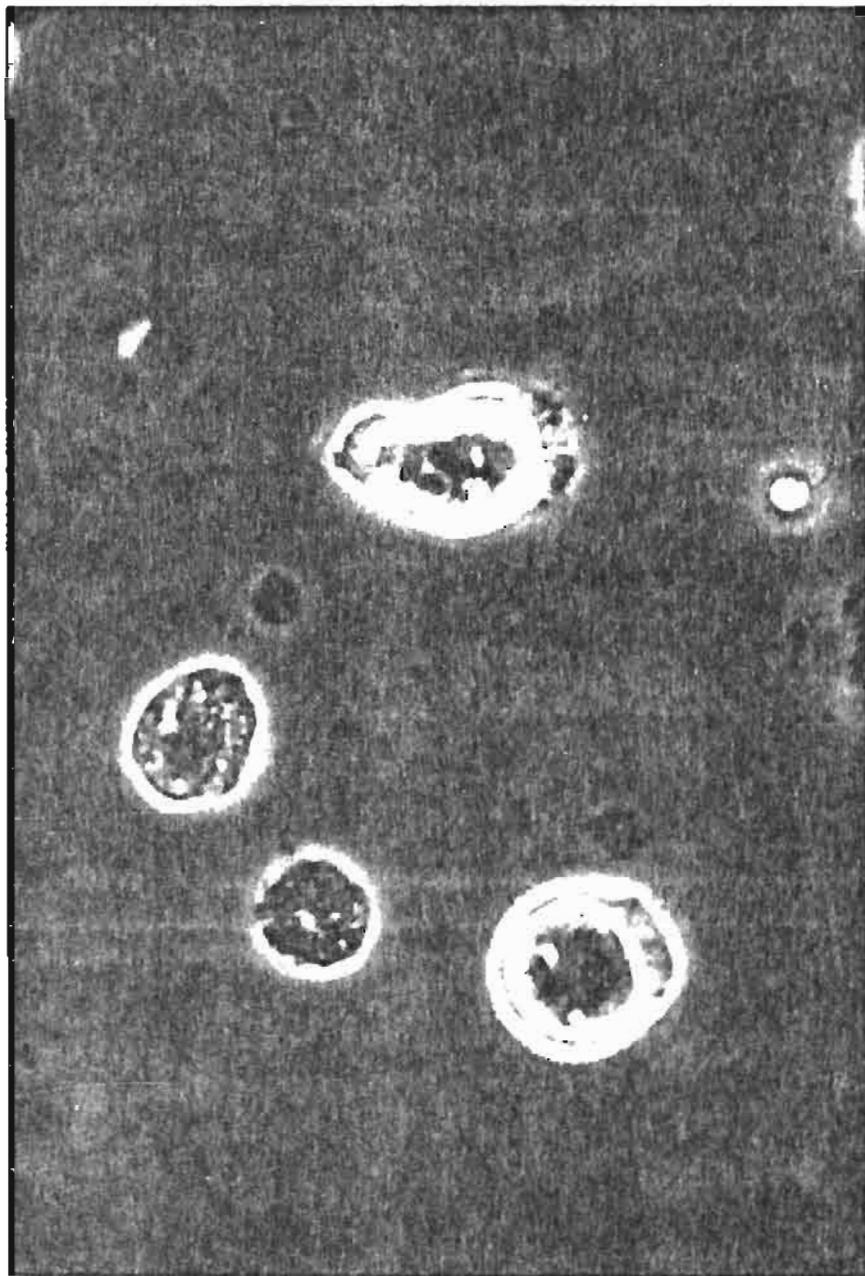
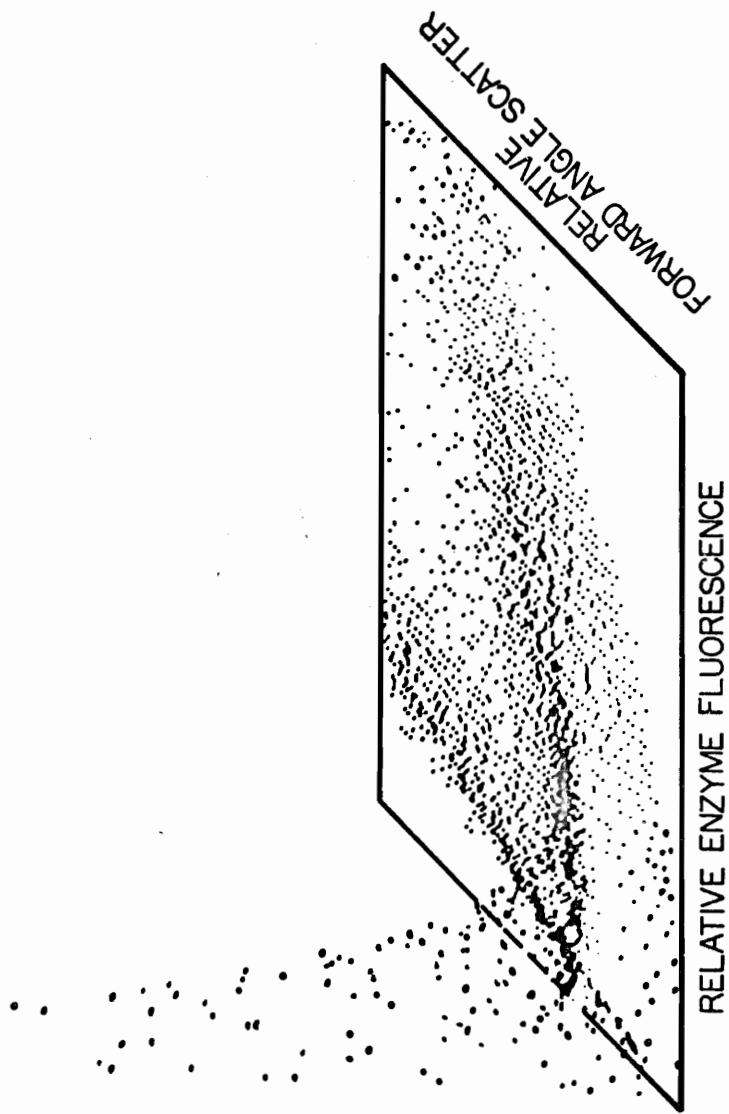


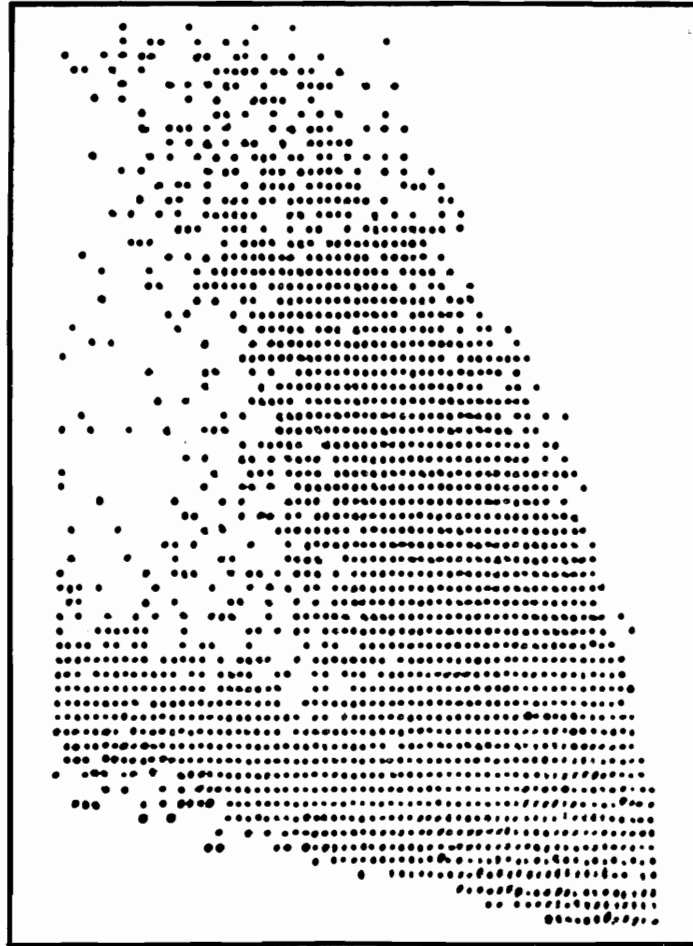
Figure 23. Two variable FCM analysis of an epithelial cell suspension stained for leucine aminopeptidase activity. Linear amplification of enzyme fluorescence is represented on the x-axis, low-angle (0-7°) forward scatter on the y-axis, and cell counts on the z-axis.

(a) Isometric plot

(b) Contour plot







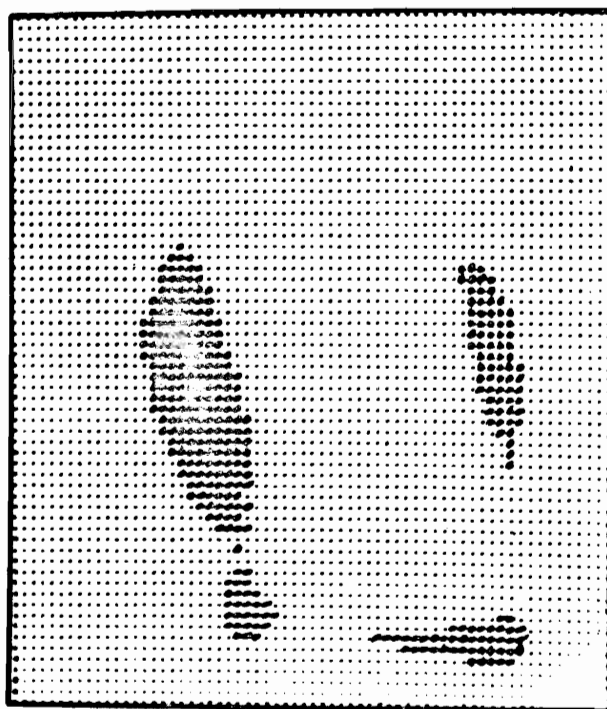
RELATIVE ENZYME FLUORESCENCE

RELATIVE ANGLE SCATTER

Figure 24. Two variable analysis by the FCM of a leucine aminopeptidase-stained intestinal epithelial cell suspension. Logarithmic amplification was utilized to view enzyme fluorescence (x-axis) and low-angle ($0-7^\circ$) forward scatter (y-axis). Cell counts (linear amplification) are represented on the z-axis.

(a) Isometric plot

(b) Contour plot



RELATIVE
FORWARD ANGLE SCATTER

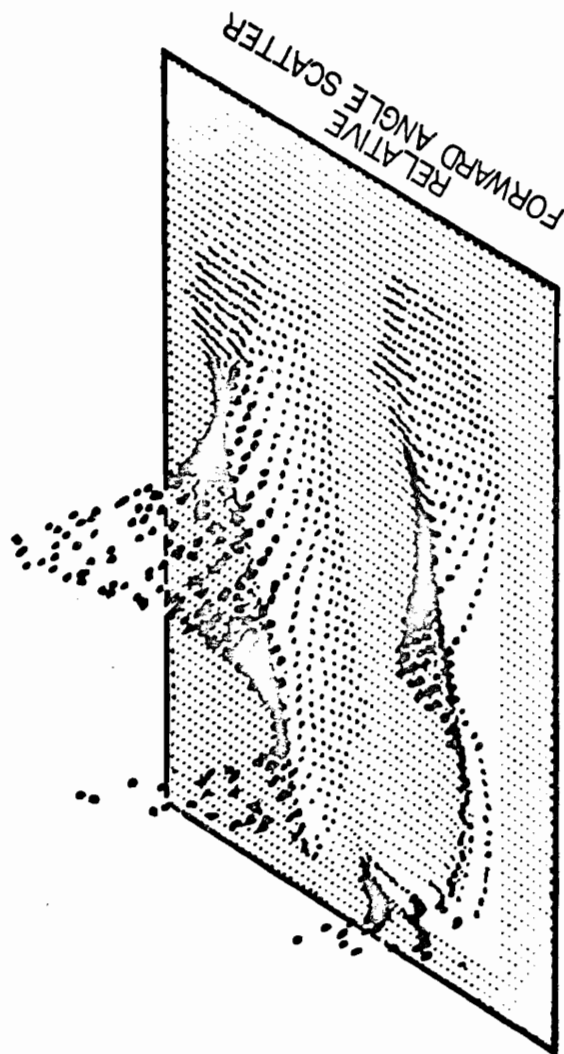
RELATIVE ENZYME FLUORESCENCE

Figure 25. Photomicrographs of sorted crypt and villus populations. Crypt and villus cells were separated on the basis of leucine aminopeptidase activity as described in the text. Electronic cell sorting was performed on cells comprising the histogram shown in Figure 24. Prior to cell isolation, the mice received a 30 minute pulse of ^3H -TdR to label the proliferating cells in S phase.

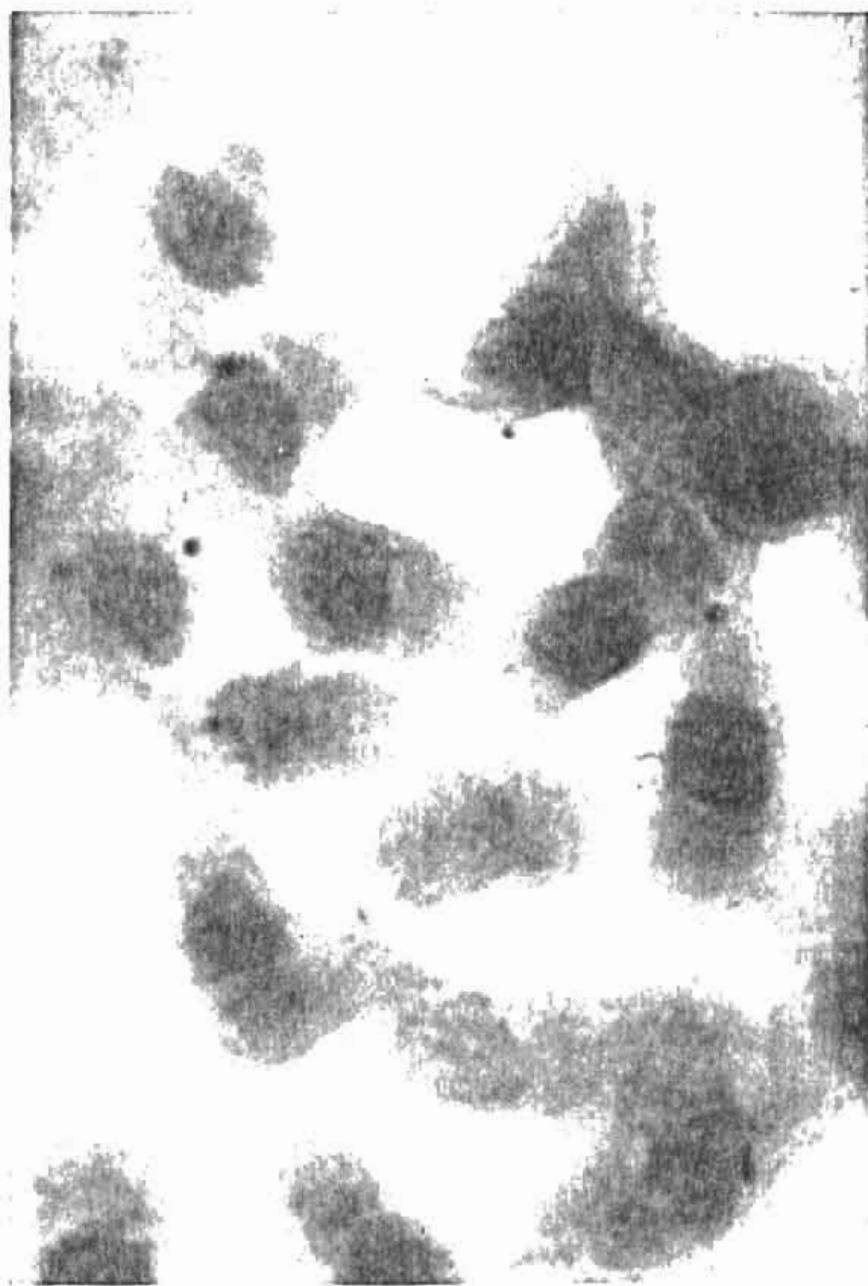
(a) Hematoxylin- and eosin-stained villus cells.

(b) Hematoxylin- and eosin-stained crypt cells.

Labeled cells are seen in the center of the field. No labeled cells were found in the sorted villus populations.



RELATIVE ENZYME FLUORESCENCE



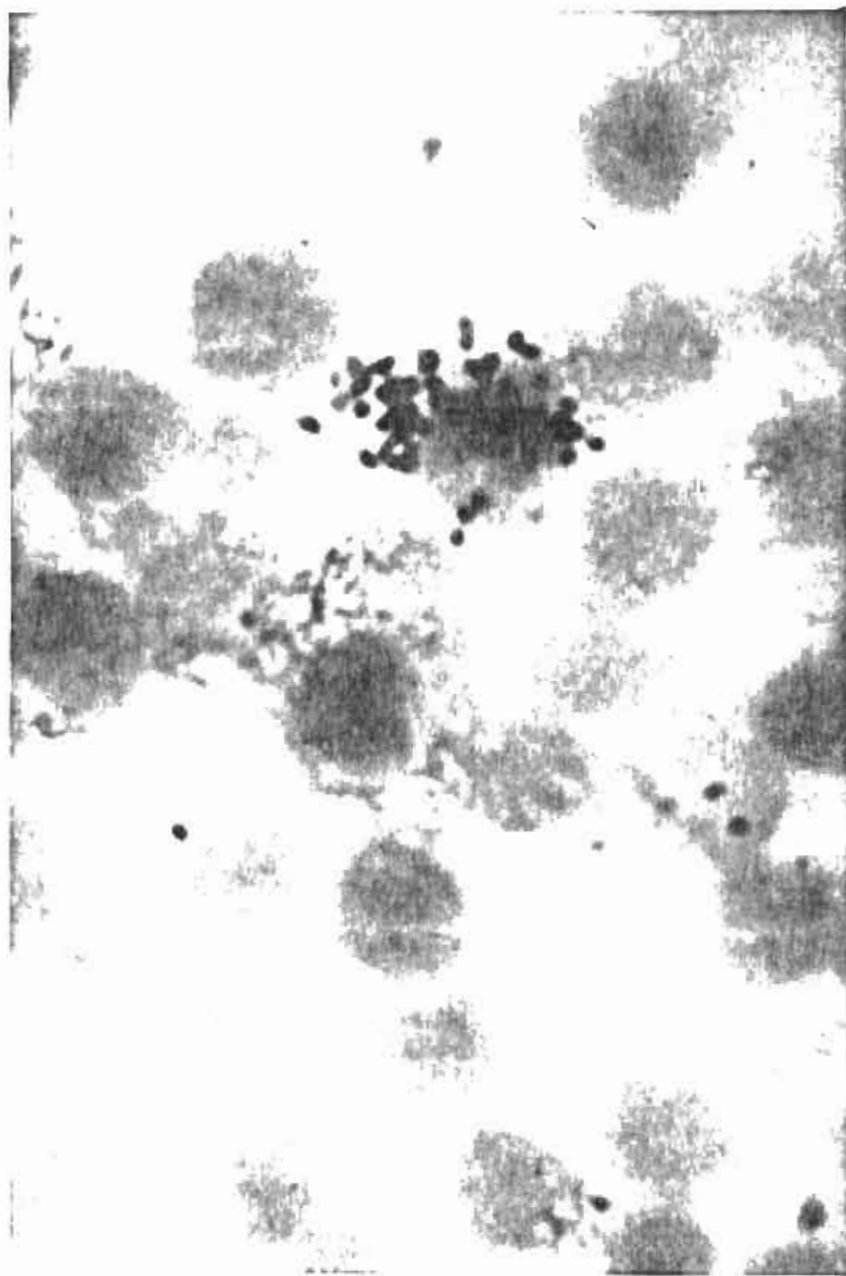
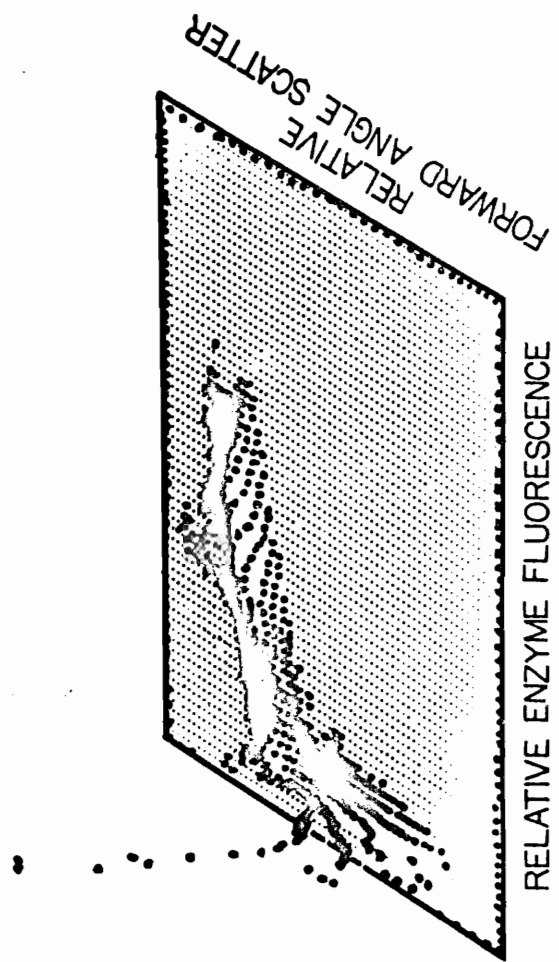
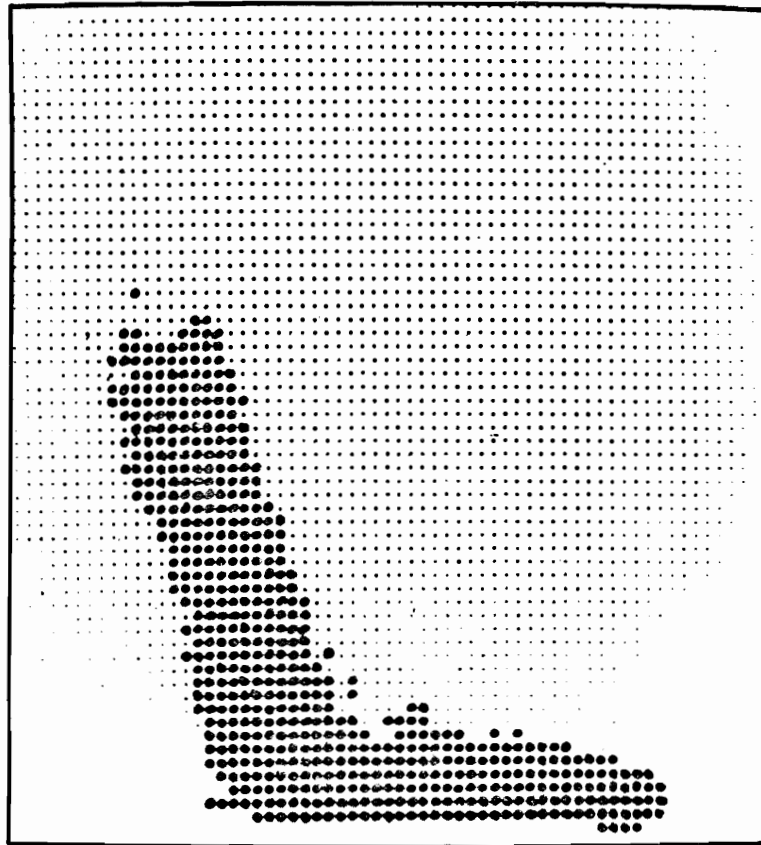


Figure 26. Two-variable analysis of an epithelial cell suspension stained under more optimal reaction conditions (as described in Methods section) for leucine aminopeptidase activity. Logarithmic amplification of enzyme fluorescence and low-angle ($0-7^\circ$) forward scatter are represented on the x- and y-axis, respectively. Cell counts are shown on the z-axis.

(a) Isometric plot.

(b) Contour plot.





RELATIVE
ANGLE SCATTER

RELATIVE ENZYME FLUORESCENCE

VITA

NAME: Maria Georgina Pallavicini

BIRTH: September 20, 1952
San Francisco, California

MARITAL STATUS: Single

EDUCATION: Ygnacio Valley High School
Concord, California, 1970

University of California at
Berkeley--Biochemistry (B.A.)
1973

HONORS AND AWARDS: Recipient of Honors Scholarship,
1970-1972

Rho Chi (Honorary Pharmacy
Society)

Sigma Xi

PUBLICATIONS:

- Pallavicini, M.G. and Nichols, W.K. Inhibition of lymphocyte blastogenesis by factor(s) in alloxan-diabetic rat plasma, Diabetes 25:614-622 (1976).
- Pallavicini, M.G., Cohen, A.M., Dethlefsen, L.A., and Gray, J.W. Dispersal of solid tumors for flow cytometer (FCM) analysis, in, Pulse-Cytophotometry Proceedings of the Third International Symposium on Pulse Cytophotometry. (Th. Buchner, W. Gohde, J. Schuman, eds.) Ghent, Belgium: European Press (in press, 1977).
- Pallavicini, M.G. and Nichols, W.K. Inhibition of lymphocyte blastogenesis by plasma from alloxan-diabetic rats, Fed. Proc. 34:760 (1975).

Publications (continued):

- Nichols, W.K. and Pallavicini, M.G. Insulin stimulation of lymphocyte blastogenesis. The Pharmacologist 17: 243 (1975).
- Pallavicini, M.G. and Cohen, A.M. The anti-tumor activity of Ftorafur against leukemias and mammary tumors in mice, The Pharmacologist 17:202 (1975).
- Pallavicini, M.G., Cohen, A.M., Dethlefsen, L.A. and Gray, J.W. Dispersal of solid tumors for flow cytometric analysis, Cell Kinetics Society, March 11-14 (1977).
- Pallavicini, M.G., Dolbeare, F., Gray, J.W., Cohen, A.M. and Dethlefsen, L.A. Separation of crypt and villus cell populations by flow cytometry, Cell Kinetics Society, March 11-14 (1977).
- Pallavicini, M.G., Cohen, A.M., Dethlefsen, L.A., and Gray, J.W. Flow cytophotometric analysis of DNA content of perturbed C3H mouse mammary tumors. AACR May (1977).